Broadband Teleportation and Entanglement in Cascaded Open Quantum Systems

Changsuk Noh

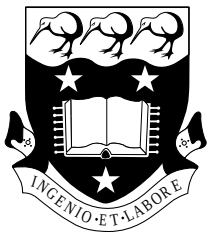

A thesis submitted
in partial fulfillment of the
requirements for the degree of
Doctor of Philosophy
in
Physics

The University of Auckland
August 2009

Abstract

Quantum optics provides powerful means to probe quantum mechanics. In this thesis, we study various aspects of quantum phenomena arising in quantum optical systems. Part I studies broadband quantum teleportation. After presenting three different methods of analyzing the standard teleportation protocol, we study the interplay between various bandwidths in determining the fidelity of a broadband quantum field teleportation. Explicit formulae for the degrees of first- and second-order coherence for the teleportation of resonance fluorescence are derived for this purpose. Part II studies entanglement arising in cascaded open quantum (optical) systems. First, a detailed laser model is produced within quantum trajectory theory to study the total decoherence rate of a laser-driven qubit. Second, using this model, we address the issue of laser quantum state, viewed in connection with separability of the laser-driven-qubit system. Third, a measure of entanglement within quantum trajectory theory called 'Contextual Entanglement' is calculated for a few simple systems and compared with the 'Entanglement of Formation'. Lastly, we introduce a method to quantify entanglement (based on the contextual entanglement) between a source and the field it emits, which we call the 'Entanglement Spectrum'. It is applied to study the entanglement between a laser-driven qubit and the field the qubit scatters.

Acknowledgements

I owe my deepest gratitude to my supervisor, Howard Carmichael, whose insight always pointed me in the right direction whenever I hit a wall. This thesis could not have started nor finished without his guidance. 'We' in this thesis refers to him and me, for this work is as much his as it is mine, except the errors which are all mine.

I am indebted to Hyunchul Nha for his friendship and guidance. His thoughtful comments on the first draft of the laser quantum state paper has been a great help, and the discussions I have had with him on our work on teleportation has helped me deepen my understanding.

I would also like to thank Scott Parkins for his help whenever I knocked on his door throughout the last 4 years. My thanks also goes to Matthew Collett, Paul Barker, David Krofcheck, and Alan Stamp for their enjoyable lectures and friendly discussions.

Last but not least, I would like to express sincere gratitude to my friends and family, for their support outside work.

Changsuk Noh
August 14th 2009

List of abbreviations

Stochastic electrodynamics (SED)
Einstein, Podolsky, and Rosen (EPR)
Quantum trajectory theory (QTT)
Gea-Banacloche (GB)
van Enk and Kimble (vEK)
Entropy of Entanglement (EE)
Local operations and classical communications (LOCC)
Entanglement of formation (EF)
Distillable entanglement (DE)
Relative entropy of entanglement (REE)
Contextual entanglement (CE)
Entanglement spectrum (ES)

Contents

List of Figures

Chapter 1

Introduction

Quantum optics has proven to be an ideal testbed for a variety of quantum mechanical phenomena due to its technical maturity and the experimental sensitivity it provides. For example, Bell inequality violations [2] have been verified successfully with optical setups [3, 4] (using polarization states of photons instead of spin 1/2 particles), and realizations of quantum information protocols often employ optical apparatus. Perhaps the most famous quantum information protocol is that of quantum teleportation [5–7], where either a polarization state of photons [8] or the quadrature amplitudes of a laser beam are teleported [1]. The subject has attracted a vast number of papers over the last 15 years or so. Nowadays the majority of teleportation devices are optical ones [1, 8, 9].

The main goal of this thesis is to investigate various aspects of quantum systems within quantum optics, with the recurring topics of resonance fluorescence—a qubit (2-level atom) driven by a laser—and quantum trajectory theory. Special emphasis is placed on problems involving cascaded open systems. Those readers not familiar with resonance fluorescence are referred to excellent textbooks on quantum optics such as [10–12]. Quantum trajectory theory is a theory of continuous monitoring for open Markovian systems [13], and is also known by the name Monte-Carlo wavefunction method [14–16]. Chapters 17-19 of [17] contain a good introduction to the topic.

This thesis is divided into two principal parts. In the first part we propose, and study the implications of, teleporting a quantum field, rather than a quantum state. By this we mean that all statistical properties of the input field, across its entire bandwidth, are to be reproduced by the teleported field. Specifically, for optical fields, all orders of correlation functions must be reproduced. By considering

the first- and second-order correlation functions explicitly, we determine restrictions on the various bandwidths (input field bandwidth, squeezing bandwidth, Alice's measurement bandwidth, Bob's filter bandwidth) required to teleport a beam of light (a quantum field) successfully, where the teleportation protocol is the optical one of Furusawa *et al.* [1], with an added filter cavity at the output port.

The second part, divided into two sections, is concerned with quantum entanglement. Quantum entanglement has played a very special role in quantum mechanics (and continues to do so). It provided the inspiration for Bell to come up with a testable prediction which differentiates quantum mechanics from local realistic (so called hidden variable) theories [2], thus promoting what had hitherto been lurking in the realm of natural philosophy to the realm of experimental physics, and furthermore putting an end to the desperate search initiated by Einstein, Podolsky, and Rosen [18] for a local hidden variable theory. Over the last couple of decades, the pioneering works of Bennett and others have renewed the interest in quantum entanglement, perhaps creating an even bigger stir than before. These authors discovered that quantum entanglement can be a *useful resource* in quantum information processing and quantum computing. Examples include quantum cryptography [19], super-dense coding [20], fast quantum computations [21,22], and quantum teleportation [5]. Part II of this thesis investigates quantum entanglement arising in cascaded open systems (within quantum optics). The first half looks at the resonance fluorescence system, addressing the issue of whether there is decoherence due to entanglement between the laser and the qubit and the related issue of assigning a quantum state to the laser field. The second half investigates a quantitative measure of entanglement defined within quantum trajectory theory [23]. More precisely, we ask the question of how one can quantify entanglement between a source and its radiated field in open systems.

1.1 Outline

A brief outline of each chapter follows, stating the aim and providing quick surveys of the main topics. A detailed introduction to each topic is given at the start of each chapter.

Chapter 2 and Appendices A-D comprise the first part of this thesis. The aim there is to study the limitations on the 'fidelity' of continuous variable quantum teleportation imposed by various experimental parameters such as the degree of squeezing, squeezing bandwidth, detection bandwidths, etc..., by studying the cor-

relation functions of the teleported field of resonance fluorescence. The chapter starts with a brief introduction to quantum teleportation, then introduces the quantum trajectory and stochastic electrodynamics description of broadband quantum teleportation. Another method, more suitable for evaluations of the correlation functions, is then introduced, based on the Heisenberg picture. This method is subsequently applied in a study of the teleportation of resonance fluorescence, where the optical spectrum and intensity correlation function are used to characterize the input and output fields.

Chapters 3 and 4 comprise the second part of this thesis. Chapter 3 engages the issue of decoherence (hence entanglement) in the laser-qubit interaction system introduced there. A birth-death model developed within quantum trajectory theory is applied to describe the laser-qubit interaction within the framework of cascaded open quantum systems. It is found that the laser and qubit can be described by separable states in the appropriate limit explained in Ch. 3. As a consequence, the total decoherence rate can be accounted for by spontaneous emission of the qubit alone. With the vantage point provided by this finding (the separability of states), we are able to address the issue of the quantum state of a laser, giving a criterion which argues in favour of the coherent state description. Chapter 4 investigates quantitative measures of quantum entanglement in cascaded open systems, with the aim of understanding the entanglement between a source and its scattered field. To start with, a conventional (quantum information theoretical) measure of entanglement, the 'Entanglement of Formation' and a measure of entanglement defined within quantum trajectory theory introduced by Nha and Carmiael [23], the 'Contextual Entanglement', are defined. Using these two measures, the entanglement between a laser and a two-level atom driven by the laser is computed, then the entanglement between a free-standing qubit and its spontaneous emission field is discussed. At this point we introduce a measure we call 'Entanglement Spectrum', which measures, within the framework of quantum trajectory theory, entanglement between a source and its radiated broadband field. As an extension of the spontaneous emission case, photon transfer in an N-cavity-linear-array is considered. Finally, preliminary calculations of the ES of a driven qubit are presented.

Chapter 5 presents the conclusions and possible avenues for further investigation.

Part I

Broadband quantum teleportation of optical fields

Chapter 2

Quantum teleportation

As we show below, quantum teleportation was first proposed as a 'disembodied transportation' of a qubit quantum state [5]. This view (of quantum state teleportation) continues to hold even for continuous variable teleportation [6, 7], where in the latter reference teleportation of the quantum state of a single mode of light is considered. A broadband theory has been developed [24] and demonstrated [25], but these works do not fully explore what it means to teleport a quantum field. We propose that successful teleportation of a quantum field—specifically a beam of light—requires the emerging quantum field to be identical (with added noise of course) to the input field. In the specific case of a light beam we require all statistical properties of the field to be reproduced at the output—i.e. all orders of correlation functions to be reproduced[1]—and this requires a filtering cavity to be attached to a conventional teleporter. There is an infinite number of correlation functions, however; furthermore, high order correlation functions can be very hard to compute. We need something more manageable. Our more limited goal is to carry out a calculation which enables efficient evaluations of the first- and second-order correlation functions of teleported fields, including their dependence on experimental parameters, such as the degree of squeezing and filter bandwidths. We thus work out the requirements, in the form of inequalities satisfied by the bandwidths, for the successful teleportation of a beam of light (quantum field) including its temporal correlations. From the works in this chapter it seems plausible that teleportation will work to all orders of correlation functions, once the requirements are met and

[1]Existing experiments do not quite conform to this view. The output beams contain a vast amount of noise that is filtered in detection, where the measurements are restricted to quadrature measurements.

if the squeezing is strong enough.

This chapter starts with a brief introduction to quantum teleportation and gives a survey of methods for analyzing the continuous variable version of it. First we show how continuous variable teleportation of an optical field can be naturally described within quantum trajectory theory. The concept of stochastic electrodynamics (SED) is then introduced and applied to describe the teleportation process for a limited class of input fields and measurements made at the output. SED has its limitations, not being a quantum theory, but it has the advantage of giving a clear intuitive picture of how teleportation works. It is also adequate to describe teleportation of classical fields (those possessing a positive definite Wigner function), which generalizes naturally to teleportation of quantum fields. After these introductory sections, we go over to the Heisenberg picture description, noting its close connection with the SED approach. This description is subsequently applied to calculations of the first- and second-order correlation functions of a teleported field. Teleportation of the vacuum and the scattered field of resonance fluorescence are used as examples to investigate the 'fidelity' of teleportation and its dependence on experimental parameters, thus deriving the conditions required for successful teleportation. Some of the work in this chapter has been published in [26].

2.1 Basics

Quantum teleportation was first introduced by Bennett *et al.* [5] in the context of quantum information theory. They showed that with the aid of perfect entanglement an arbitrary unknown state of a qubit can be 'teleported' to another qubit (initially one of a pair of entangled qubits). Vaidman extended their analysis to continuous variables [6], and Braunstein and Kimble came up with a realistic proposal for continuous variable teleportation utilizing squeezed states [7]. We now go over each of these proposals briefly.

Consider Alice and Bob at two different locations. The qubit teleportation of Bennett *et al.* can be summarized in the following steps [5]:

1. Alice and Bob initially share a maximally entangled pair of particles, usually taken to be in the singlet state.

2. Alice gets a qubit whose unknown state she is asked to teleport.

3. Alice performs a joint measurement (called a Bell-state measurement) on the

qubit and her half of the entangled pair.

4. Alice sends the measurement result to Bob over a classical channel.

5. Bob performs a particular unitary operation on his share of the entangled pair dependent upon the measurement result he receives from Alice.

Vaidman's proposal [6] was to replace the singlet state with the EPR state [18] and the Bell-state measurements by joint measurements of position and momentum. Of course, the unknown state is now described by continuous variables, which in this case are position and momentum.

The proposal of Braunstein and Kimble [7] was to realize this in a quantum optical setup with finite entanglement (often called a noisy channel in the literature). The continuous variables in the optical case are the x and y quadratures of an optical field mode. They are defined as $a_X = (a + a^\dagger)/\sqrt{2}$ and $a_Y = (a - a^\dagger)/\sqrt{2}i$, where a is the annihilation operator for the mode of light in question, which is described by a quantum mechanical harmonic oscillator. The Bell-state measurements are replaced by quadrature measurements, which can be performed efficiently with balanced homodyne detectors [11]. The steps of teleportation are now as follows:

1. Alice and Bob initially share two modes of light in a two-mode squeezed state.

2. Alice also gets the mode of light that she wants to teleport.

3. Alice mixes the input mode with her share of the two-mode squeezed state by passing the two modes through a 50/50 beam splitter. She then measures the x quadrature of one of the resulting modes and the y quadrature of the other, using two balanced homodyne detectors.

4. Alice sends the measurement results to Bob.

5. Bob displaces his share of the two-mode squeezed state by an amount that depends on the measurement results.

The beams in a two-mode squeezed state can be obtained by mixing two squeezed beams at a 50/50 beam splitter, where the squeezed quadratures of the two beams are orthogonal and their degrees of squeezing are the same.

The first experimental demonstration of continuous variable quantum teleportation was achieved by Furusawa *et al.* [1]. They succeeded in teleporting a modulated

beam of laser light (coherent state). Their procedure was essentially that of Braunstein and Kimble, but there was an important distinction: the input quantum field and squeezed light used were broadband. In fact, they ran their experiment continuously in time, meaning that the procedure was not divided into steps. Such broadband teleportation was later studied by van Loock *et al.* [24]. Figure 2.1 de-

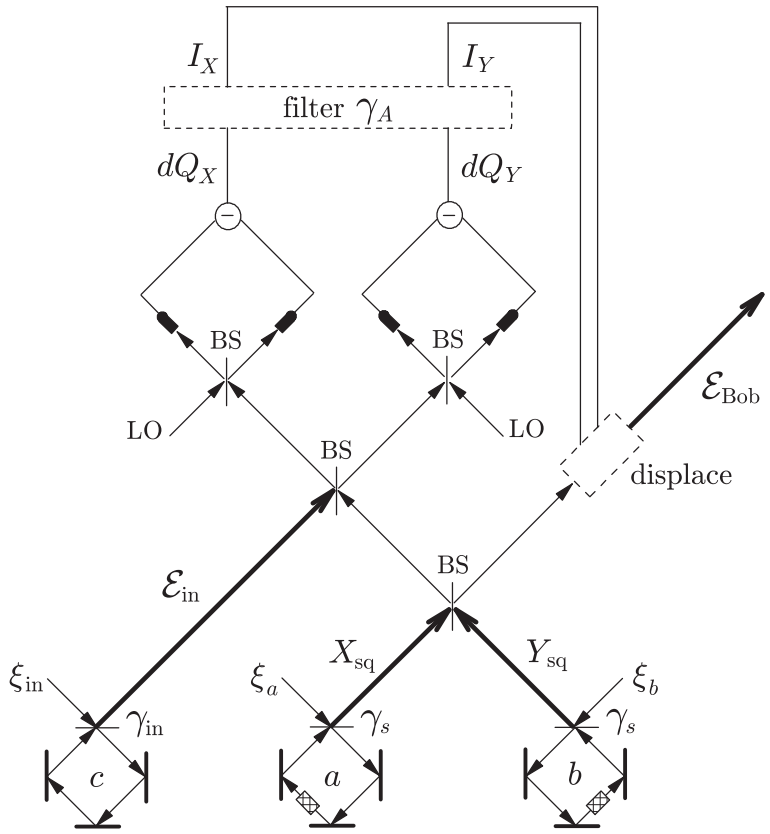

Figure 2.1: Schematic representation of the continuous variable teleportation protocol, as implemented in [1]. BS stands for 50/50 beam splitter and LO for local oscillator (high intensity laser).

picts the experiment schematically. Note that the input field and two squeezed fields now have bandwidths γ_{in} and γ_s respectively, and the balanced homodyne detectors both have a finite detection bandwidth γ_A. I_X and I_Y are continuous photocurrents representing continuous values of Alice's quadrature measurements.

The following section outlines a theoretical model, very suitable for this broadband, continuously monitored system.

2.2 Quantum trajectory theory

We give a brief introductory comment on what quantum trajectory theory is and show why it is suitable for describing the teleportation process. Explicit equations, though not derived, are given for completeness.

2.2.1 Basics

Quantum trajectory theory (QTT) can be defined as the quantum theory of continuous quantum measurements for Markovian optical systems (described by Lindblad master equations [27]).[2] Because the system is Markovian, measurements made on the reservoir fields do not change the dynamics of the system. Thus we can apply continuous measurements by placing (imaginary) detectors in the reservoir and infer the dynamics of the system from the measurement results. The resulting quantum states are *conditioned* on the measurement results, and will usually have stochastic components due to quantum fluctuations. QTT tells us how these conditional states are to be evolved for a given system—including a detection scheme. Different detection schemes allow us to infer different aspects of the dynamics (the principle of complementarity). In quantum optics, the basic building blocks of detectors are photon counters, which are described by quantum jumps within the framework of QTT.[3] When these jumps do not occur, the states evolve continuously, and this continuous evolution plus the quantum jumps map out a particular trajectory in Hilbert space. When averaged over all possible trajectories, QTT is equivalent to the master equation, i.e., quantum trajectories can be thought of as different unravellings of the density operator evolution. QTT is also called the Monte-Carlo wavefunction method [14–16] because one often has to resort to numerical Monte-Carlo simulations.

2.2.2 Teleportation within quantum trajectory theory

The continuous variable teleportation scheme of Fig. 2.1 can be readily implemented in quantum trajectory theory, as shown by Carmichael [28]. Because Alice's measurements only employ homodyne detectors, the conditioned state obeys a stochastic Schrödinger equation (see Ch. 18 of [17]) and the only jump operators one needs to

[2] See Ch. 17-19 of [17] and references therein for a detailed exposition on quantum trajectory theory.

[3] The conditioned state changes as our knowledge is modified, hence a 'sudden' gain of knowledge from photodetection results in a 'sudden' update of the state.

consider are those at the output. The results of Alice's quadrature measurements are generated within the simulation and the state is conditioned on them. The strength of QTT in describing teleportation is that one can simulate real experiments on a shot-to-shot basis, just as it would look in an ideal experiment with no loss and perfect detectors. The equation for the conditioned state is presented here as promised:

$$d|\bar{\bar{\psi}}_{\rm REC}\rangle = \Big\{ \Big(H_{\rm in}/i\hbar - \gamma_{\rm in}c^\dagger c\Big)\,dt - \gamma_s\left[\lambda(A^\dagger B^\dagger - AB) + A^\dagger A + B^\dagger B\right]dt \tag{2.1}$$

$$+ (dQ_X + i dQ_Y)\sqrt{\gamma_s}A + (dQ_X - i dQ_Y)\sqrt{\gamma_{\rm in}}c$$

$$- (I_x - iI_Y)\sqrt{\gamma_s}B dt + dU_{\rm Bob}\Big\}|\bar{\bar{\psi}}_{\rm REC}\rangle, \tag{2.2}$$

where $A \equiv (a+b)/\sqrt{2}$, $B \equiv (a-b)/\sqrt{2}$, and a, b, c are the annihilation operators for the modes shown in Fig. 2.1; λ is a parameter that controls the degree of squeezing, and ranges from 0 to 1, and $dU_{\rm Bob}$ accounts for the backaction produced by whatever measurement Bob performs on the output field. Incremental charges corresponding to Alice's measurements are given by

$$\begin{aligned} dQ_X &= 2\left[\sqrt{\gamma_{\rm in}}\langle c_X\rangle_{\rm REC} + \sqrt{\gamma_s}\langle A_X\rangle_{\rm REC}\right]dt + dW_X, \\ dQ_Y &= 2\left[\sqrt{\gamma_{\rm in}}\langle c_Y\rangle_{\rm REC} + \sqrt{\gamma_s}\langle A_Y\rangle_{\rm REC}\right]dt + dW_Y, \end{aligned} \tag{2.3}$$

where the subscripts X and Y denote the x and y quadrature operators. The filtered currents obey the equations

$$dI_X = -\gamma_A(I_X dt - dQ_X), \qquad dI_Y = -\gamma_A(I_Y dt - dQ_Y) \tag{2.4}$$

assuming that the homodyne filters have Lorentzian profiles. The Furusawa experiment measured the quadrature fluctuations with a balanced homodyne detector at the output, but one can consider other types of measurements such as heterodyne detection or photon counting. These are described in [28] where they are applied to teleportation of the vacuum and the scattered field of resonance fluorescence. Later on (Sect. 2.6.1) we will plot optical spectra calculated from the equations of this section and compare them with the spectra calculated by an alternate method.

2.3 SED

2.3.1 Basics

Stochastic electrodynamics is a semi-classical theory of quantized electromagnetic waves [29]. It treats the vacuum fluctuations as a real stochastic phenomenon and is effectively a hidden-variable theory with a probability distribution for quadrature amplitudes of the field given by the Wigner function [30]. Because Wigner functions give symmetrically ordered operator averages, such as moments of the quadrature amplitudes, SED gives correct results as long as one measures symmetrically ordered operator averages only. Also, the Wigner function has to be non-negative for it to behave as a probability distribution, which puts a restriction on the class of states that may be described within SED. We use SED to describe the teleportation process, closely following the work of Carmichael and Nha [31]. Look also at [32] and references therein for more information.

It is possible to explain the experiment of Furusawa *et al.* entirely within SED because they only measure quadrature amplitudes and also because their input state is a coherent state, which has a positive Wigner function. Let us go back to Fig. 2.1 and describe the process in terms of classical stochastic field variables. In this section all the variables are classical stochastic variables. $\mathcal{E}_{\rm in}$ can be decomposed into a complex valued mean and fluctuations:

$$\mathcal{E}_{\rm in}(t) = \sqrt{\gamma_{\rm in}}c(t) + \xi^t_{\rm in}, \tag{2.5}$$

where we have introduced the superscript t to emphasize the stochastic nature of the fluctuation. $\xi^t_{\rm in}$ is a white noise process that has infinite energy, or in other words it is delta correlated, i.e., $\overline{\xi^{t'}_{\rm in}\xi^{t*}_{\rm in}} = \delta(t'-t)$, where the bar denotes averaging over time. Mathematically, it is better to use $\xi^t_{\rm in}dt = dW_{\rm in}(t)$, where $dW_{\rm in}(t)$ is the complex Wiener increment[4]:

$$\overline{dW_{\rm in}dW_{\rm in}} = \overline{dW^*_{\rm in}dW^*_{\rm in}} = 0 \tag{2.6a}$$

$$\overline{dW_{\rm in}dW^*_{\rm in}} = dt/2. \tag{2.6b}$$

[4]Delta function correlation is the limiting case as $dt \to 0$. See Ch. 4 of Gardiner [33].

2.3.2 Squeezing

Squeezing has a very intuitive explanation in terms of SED as we show in this subsection. Let a be the intracavity field which is squeezed in the x quadrature. The stochastic differential equation for a satisfies [31]

$$da = -\frac{\gamma_s}{2}(a + \lambda a^*)dt - \sqrt{\gamma_s}dW_{\text{in}}, \tag{2.7}$$

where λ is a parameter that controls the degree of squeezing. $\lambda = 0$ ($\lambda = 1$) gives no (perfect) squeezing in the x quadrature. Having said this, one cannot actually see squeezing in the intracavity field. It is dominated by the noise term ξ^t_{in}. It is in the output field described by the stochastic differential equation

$$d\mathcal{E}_{\text{out}} = \sqrt{\gamma_s}adt + dW_{\text{in}} \tag{2.8}$$

that one sees the effect of squeezing most readily. Remember, $dW_{\text{in}} = \mathcal{E}_{\text{in}}dt$. Figure 2.2 shows a filtered version of the output field,[5] where fluctuations in the x quadrature have been suppressed at the cost of enhanced fluctuations in the y quadrature.

Filtering is done with the equation

$$dF = -\gamma_f(F - d\mathcal{E}_{\text{out}})dt, \tag{2.9}$$

where F is the filtered output field and γ_f is the filter bandwidth. Basically what happens is that field a inside the cavity adjusts so that, over the finite bandwidth γ_s, it emerges out of phase with the input noise, W_{in}; thus, when the two fields are added, they interfere destructively (perfect squeezing of the input noise).

2.3.3 Teleportation

We now go on to an SED description of teleportation. We choose a to be squeezed in the x quadrature and b in the y quadrature. Then the fields out of the squeezing cavities are given by:

$$X_{\text{sq}} = \sqrt{\gamma_s}a + \xi^t_a, \qquad\qquad Y_{\text{sq}} = \sqrt{\gamma_s}b + \xi^t_b, \tag{2.10}$$

[5]Note that filtering is essential. The field generated by Eq. (2.8) has bandwidth dt^{-1}, and is dominated by the high frequency noise of the Wiener process W_{in} without filtering.

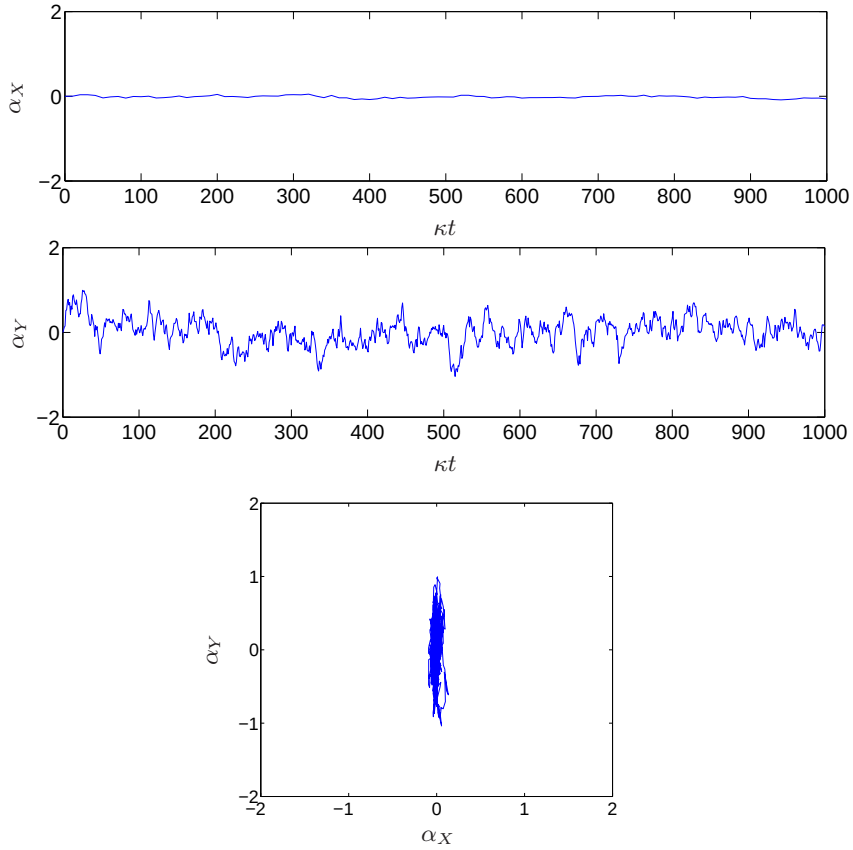

Figure 2.2: Fluctuations in the quadrature amplitudes of $\mathcal{E}_{\rm out}$ as a function of time (above) and as a phase space plot (below), for $\lambda = 0.5$ and filter bandwidth $0.1\gamma_s$.

where ξ_a^t and ξ_b^t are independent white noise terms like $\xi_{\rm in}^t$ introduced earlier. a obeys (2.7), whereas b obeys the same equation with $\lambda \to -\lambda$. Correlated ('entangled') fields are then created by passing $X_{\rm sq}$ and $Y_{\rm sq}$ through a 50/50 beam splitter. The fields at the output of the beam splitter can be written as

$$\mathcal{E}_A = \frac{1}{\sqrt{2}}(X_{\rm sq} + Y_{\rm sq}), \qquad \mathcal{E}_B = \frac{1}{\sqrt{2}}(X_{\rm sq} - Y_{\rm sq}). \tag{2.11}$$

Figure 2.3 shows filtered versions of $\mathcal{E}_A$ and $\mathcal{E}_B$. They merely look like noises at first sight, but in fact they are highly correlated, as shown in Fig. 2.4. Indeed if you look carefully you can see that the figure on the l.h.s of Fig. 2.3 is very closely the mirror reflection of the figure on the r.h.s. $\mathcal{E}_A$ is now mixed with $\mathcal{E}_{\rm in}$ at a 50/50

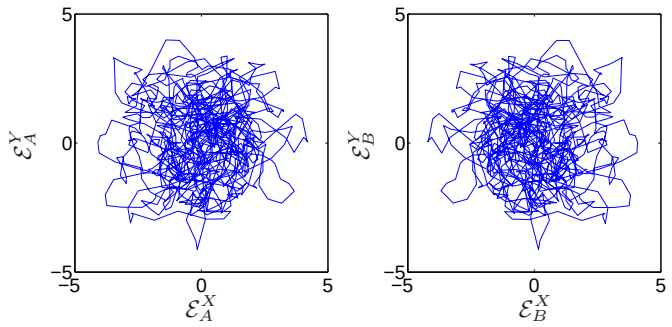

Figure 2.3: Phase space plots showing filtered versions of $\mathcal{E}_A$ and $\mathcal{E}_B$ for $\gamma_f = 0.01\gamma_s$ and $\lambda = 0.9$.

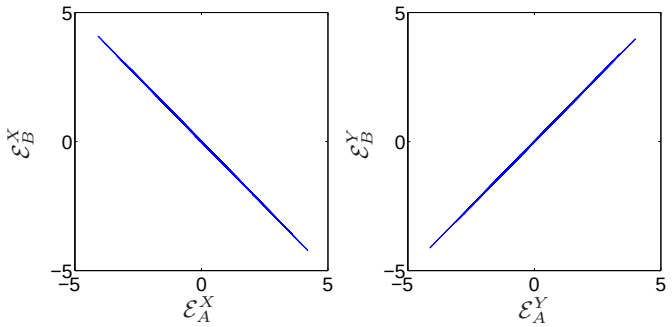

Figure 2.4: Phase space plots showing correlations between the filtered versions of $\mathcal{E}_A$ and $\mathcal{E}_B$.

beam splitter. The resulting fields are

$$\frac{1}{\sqrt{2}}(\mathcal{E}_{\text{in}} + \mathcal{E}_A), \qquad \frac{1}{\sqrt{2}}(\mathcal{E}_{\text{in}} - \mathcal{E}_A). \tag{2.12}$$

x and y quadrature measurements on these fields just return their corresponding quadrature values, which we denote by $\frac{1}{\sqrt{2}}(\mathcal{E}_{\text{in}}^X + \mathcal{E}_A^X)$ and $\frac{1}{\sqrt{2}}(\mathcal{E}_{\text{in}}^Y - \mathcal{E}_A^Y)$. These measured values then go through a filter, which can be represented mathematically by a convolution with an impulse response function F_A. Thus after the displacement of the squeezed field distributed to Bob one obtains

$$\mathcal{E}_{\text{Bob}} = \mathcal{E}_B + F_A * (\mathcal{E}_{\text{in}} + \mathcal{E}_A^*), \tag{2.13}$$

where Bob's field has been displaced by $F_A * \sqrt{2}\left[\frac{1}{\sqrt{2}}(\mathcal{E}_{\rm in}^X + \mathcal{E}_A^X) + i\frac{1}{\sqrt{2}}(\mathcal{E}_{\rm in}^Y - \mathcal{E}_A^Y)\right]$. In the limit $\gamma_A \to \infty$, i.e., no filtering, Bob's field becomes

$$\begin{aligned}\mathcal{E}_{\rm Bob} &= \mathcal{E}_{\rm in} + \mathcal{E}_B + \mathcal{E}_A^* \\ &= \mathcal{E}_{\rm in} + \frac{1}{\sqrt{2}}(X_{\rm sq} + X_{\rm sq}^*) - \frac{1}{\sqrt{2}}(Y_{\rm sq} - Y_{\rm sq}^*) \\ &= \mathcal{E}_{\rm in} + \sqrt{2}X_{\rm sq}^X - i\sqrt{2}Y_{\rm sq}^Y. \end{aligned} \tag{2.14}$$

One can easily see that $\mathcal{E}_{\rm Bob} \to \mathcal{E}_{\rm in}$ as the squeezing increases. It can also be deduced from Fig. 2.4 that in the limit of infinite squeezing, $\mathcal{E}_B^X = -\mathcal{E}_A^X$ and $\mathcal{E}_B^Y = \mathcal{E}_A^Y$, which is equivalent to saying $\mathcal{E}_B + \mathcal{E}_A^* = 0$. Figure 2.5 displays phase space plots of the filtered input and output fields. The input field is a coherent state of amplitude $5 + 5i$. We have assumed Alice's bandwidth broad enough to pass all the input and squeezed fields. The 'fidelity' of teleportation is quite good as can be seen from the fact that all the kinks are in the right places. The discrepancies are due to the limited amount of squeezing.

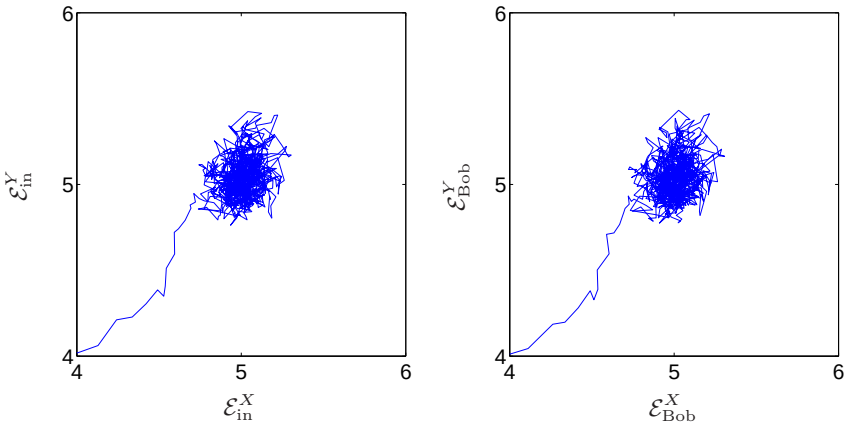

Figure 2.5: Filtered input and output fields for $\lambda = 0.9$.

2.3.4 Limitations

Thus far we have shown how a hidden variable account of continuous variable teleportation can be given. In this description detailed trajectories of quadrature amplitudes can be teleported across a finite bandwidth (much less than the squeezing bandwidth), to arbitrarily good accuracy, limited only by the degree of squeezing. However, thanks to Bell [2], we know that a local hidden variable theory such as SED

cannot reproduce all the details of nature. So where is the problem? The problem, mentioned at the start of this section, is that SED cannot describe input fields that have non-positive-definite Wigner functions. Light in a Schrödinger cat state, i.e., in a superposition of coherent states with opposite signs, provides an example, as such states have negative regions in their Wigner representations. Another limitation is that SED only gives expectation values of symmetrically ordered operators. It cannot account for photon counting experiments for example, as these are related to normally ordered operators.[6]

2.4 Heisenberg picture description

2.4.1 Operator treatment of Alice's measurements

For a quantum mechanical description of teleportation one can use quantum trajectory theory as described earlier. This method has its advantages, but is inappropriate for probing parameter dependencies of the correlation functions of the teleported field,[7] which is just what we want to do in the next section. For this purpose, we adopt a description based on the Heisenberg picture. Alice's measurement results are now formally treated as operators. Basically, the reason we can treat them as operators is because their operator characteristics do not show up; the operator notation is merely a bookkeeping device for calculating correlations. Let us show this explicitly. As before, the measurement results are

$$I_X = \frac{1}{\sqrt{2}}(\mathcal{E}^X_{\rm in} + \mathcal{E}^X_A), \qquad\qquad I_Y = \frac{1}{\sqrt{2}}(\mathcal{E}^Y_{\rm in} - \mathcal{E}^Y_A), \tag{2.15}$$

where the $\mathcal{E}$'s and I's are now operators and filtering has been ignored. $\mathcal{E}^X$ and $\mathcal{E}^Y$ are equivalent to position and momentum, x and p, and obey the same commutation relations up to a constant factor. Thus I_X and I_Y commute between themselves and their adjoints (because of the $-$ in I_Y), i.e., they are not field operators. Then it is not so strange that they are equivalent to measurement results. Moreover after the

[6] One can of course always calculate symmetrically ordered correlation functions and then use commutation relations to do the reordering by hand. Nevertheless, by doing this one gives up the realistic connection between measurement signals and the fluctuating fields in SED.

[7] This is because it takes a long time to compute the correlation functions, especially for extreme values of parameters such as a very small input bandwidth or a high degree of squeezing.

displacement of Bob's field one obtains

$$\mathcal{E}_{\text{Bob}} = \mathcal{E}_B + \mathcal{E}_{\text{in}} + \mathcal{E}_A^\dagger, \tag{2.16}$$

when filtering is ignored. The field operator $\mathcal{E}_{\text{in}} + \mathcal{E}_A^\dagger$ is supposed to be a number rather than an operator, but since this field commutes with itself and its adjoint as well as $\mathcal{E}_B$ it is again not so surprising that it can be treated formally as if it were an operator (or as if it were expressed in terms of operators). At any rate, one can always incorporate a larger part of the system into the quantum framework. In this vein one may treat the homodyne measurements and the classical channel quantum mechanically which amounts to treating the measurement results formally as operators, but in the classical limit—i.e. neglecting quantum fluctuations. This point of view is, in our opinion, essentially the same as that explained in Ralph's work on all-optical teleportation[8] which is summarized in Appendix A.

2.4.2 Filtering of the output field

Hopefully the reader is convinced by now that this method is legitimate. If not, just wait until Sect. 2.6.1 where we show quantitative agreements between the Heisenberg picture calculations and (more orthodox) quantum trajectory simulations. Note, also, the close resemblance between the SED and Heisenberg picture descriptions: in the Heisenberg picture description the output field is merely the operator version of (2.13). We have shown in the SED calculations, however, that only filtered fields are meaningful. High frequency noise dominates the signal otherwise. For this reason we consider placing a filter cavity, with bandwidth γ_B, at the output field as shown in Fig. 2.6. The output field can then be written as

$$\begin{aligned}\mathcal{E}_{\text{out}} &= F_B * (\mathcal{E}_{\text{Bob}} + \xi_{\text{out}}) - \xi_{\text{out}}, \\ &= F_B * (\mathcal{E}_B + F_A * (\mathcal{E}_{\text{in}} + \mathcal{E}_A^\dagger) + \xi_{\text{out}}) - \xi_{\text{out}},\end{aligned} \tag{2.17}$$

where $F_{(A,B)} * \cdot$ now represents

$$(\gamma_A, \gamma_B) \int_0^t dt' e^{-(\gamma_A,\gamma_B)(t-t')} \cdot . \tag{2.18}$$

In the frequency domain, this is equivalent to multiplication by a Lorentzian func-

[8] All-optical teleportation was introduced in [34]. See [35] for a discussion on treating the classical channel with Heisenberg operators; Ralph gives a short proof using the no-cloning theorem.

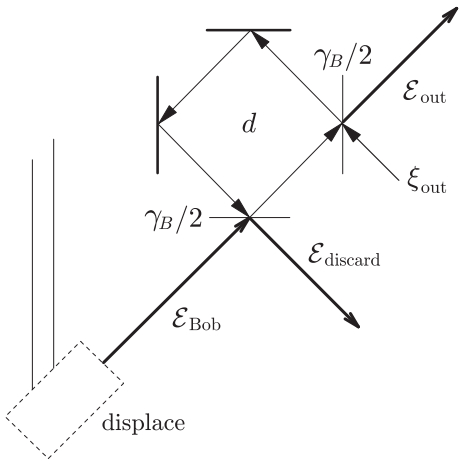

Figure 2.6: Filtering cavity placed in the path of $\mathcal{E}_{\rm Bob}$.

tion with full-width $2\gamma_A$ or $2\gamma_B$.

We now calculate the correlation functions of the output field. For this purpose it is convenient to rewrite (2.17) as

$$\mathcal{E}_{\rm out} = \mathcal{E}_{\rm in}^{ff'} + \mathcal{E}_A^{\dagger ff'} + \mathcal{E}_B^{f}. \tag{2.19}$$

We have dropped the free-field (vacuum) term $\xi_{\rm out}$ as it will not contribute to correlation functions that are normal-ordered. The superscripts f and f' refer to filtering by Bob and Alice respectively, i.e., they represent the convolutions in (2.18).

2.4.3 First-order correlation function

The normalized first-order correlation function is defined as

$$g^{(1)}_{\rm out}(\tau) = \frac{\lim_{t\to\infty}\langle \mathcal{E}^\dagger_{\rm out}(t+\tau)\mathcal{E}_{\rm out}(t)\rangle}{\lim_{t\to\infty}\langle \mathcal{E}^\dagger_{\rm out}(t)\mathcal{E}_{\rm out}(t)\rangle} \equiv \frac{\langle \mathcal{E}^\dagger_{\rm out}(\tau)\mathcal{E}_{\rm out}\rangle}{\langle \mathcal{E}^\dagger_{\rm out}\mathcal{E}_{\rm out}\rangle}, \tag{2.20}$$

where we have eliminated the trivial parameter t. We calculate only the correlation function in the numerator, as evaluating it at $\tau = 0$ gives the output flux in the denominator. The numerator expands as

$$\begin{aligned}\langle \mathcal{E}^\dagger_{\rm out}(\tau)\mathcal{E}_{\rm out}\rangle &= \left\langle (\mathcal{E}_{\rm in}^{\dagger ff'} + \mathcal{E}_A^{ff'} + \mathcal{E}_B^{\dagger f})(\tau)(\mathcal{E}_{\rm in}^{ff'} + \mathcal{E}_A^{\dagger ff'} + \mathcal{E}_B^{f})\right\rangle, \\ &= \left\langle \mathcal{E}_{\rm in}^{\dagger ff'}(\tau)\mathcal{E}_{\rm in}^{ff'}\right\rangle + \left\langle (\mathcal{E}_A^{ff'} + \mathcal{E}_B^{\dagger f})(\tau)(\mathcal{E}_A^{\dagger ff'} + \mathcal{E}_B^{f})\right\rangle. \end{aligned} \tag{2.21}$$

We have used the fact that $\mathcal{E}_{\rm in}$ is independent of $\mathcal{E}_A$ and $\mathcal{E}_B$, and the expectation values of the latter are zero. We can calculate the correlation functions for $\mathcal{E}_A^{ff'}$ and $\mathcal{E}_B^f$ from the correlation functions of squeezed fields. They are[9]:

$$\langle X_{\rm sq}^\dagger(\tau)X_{\rm sq}\rangle = \langle Y_{\rm sq}^\dagger(\tau)Y_{\rm sq}\rangle = \frac{\gamma_s}{4}\left[\frac{\lambda}{1-\lambda}e^{-\frac{\gamma_s}{2}(1-\lambda)|\tau|} - \frac{\lambda}{1+\lambda}e^{-\frac{\gamma_s}{2}(1+\lambda)|\tau|}\right], \quad (2.22)$$

and

$$\langle X_{\rm sq}^\dagger(\tau)X_{\rm sq}^\dagger\rangle = -\langle Y_{\rm sq}^\dagger(\tau)Y_{\rm sq}^\dagger\rangle = -\frac{\gamma_s}{4}\left[\frac{\lambda}{1-\lambda}e^{-\frac{\gamma_s}{2}(1-\lambda)|\tau|} + \frac{\lambda}{1+\lambda}e^{-\frac{\gamma_s}{2}(1+\lambda)|\tau|}\right]. \quad (2.23)$$

Other correlation functions can be obtained by taking adjoints of the above. Also note that $X_{\rm sq}$ and $Y_{\rm sq}$ are independent fields, so their cross correlations are always zero. Correlation functions involving $\mathcal{E}_A$ and $\mathcal{E}_B$ can be calculated from their definitions (2.11), giving

$$\langle \mathcal{E}_A^\dagger(\tau)\mathcal{E}_A\rangle = \langle \mathcal{E}_B^\dagger(\tau)\mathcal{E}_B\rangle = \langle X_{\rm sq}^\dagger(\tau)X_{\rm sq}\rangle, \quad (2.24a)$$

$$\langle \mathcal{E}_A(\tau)\mathcal{E}_A^\dagger\rangle = \langle \mathcal{E}_B(\tau)\mathcal{E}_B^\dagger\rangle = \langle X_{\rm sq}^\dagger(\tau)X_{\rm sq}\rangle + \delta(\tau), \quad (2.24b)$$

$$\langle \mathcal{E}_A^\dagger(\tau)\mathcal{E}_A^\dagger\rangle = \langle \mathcal{E}_B^\dagger(\tau)\mathcal{E}_B^\dagger\rangle = 0, \quad (2.24c)$$

$$\langle \mathcal{E}_A^\dagger(\tau)\mathcal{E}_B^\dagger\rangle = \langle \mathcal{E}_B^\dagger(\tau)\mathcal{E}_A^\dagger\rangle = \langle X_{\rm sq}^\dagger(\tau)X_{\rm sq}^\dagger\rangle, \quad (2.24d)$$

$$\langle \mathcal{E}_A^\dagger(\tau)\mathcal{E}_B\rangle = \langle \mathcal{E}_B(\tau)\mathcal{E}_A^\dagger\rangle = 0, \quad (2.24e)$$

where, using symmetry, all the correlation functions for $Y_{\rm sq}$ have been written in terms of the correlation functions involving only $X_{\rm sq}$. The delta function can be thought of as the shot noise term from the quadrature measurements or as a vacuum contribution. The correlation functions for the filtered fields involve integrals over

[9] See Eq. (1) of [36], in which $b = Y_{\rm sq}$, $\lambda = \frac{\gamma_s}{2}(1-\lambda)$, and $\mu = \frac{\gamma_s}{2}(1+\lambda)$. Correlation functions for $X_{\rm sq}$ can be obtained by comparing these with the correlation functions given in Eqs. (10.67-68) of [17].

the above functions. For example

$$\begin{aligned}\left\langle \mathcal{E}_A^{ff'}(\tau)\mathcal{E}_A^{\dagger ff'}\right\rangle &= \lim_{t\to\infty}\gamma_B^2\int_0^{t+\tau}dt_1\int_0^t dt_2 e^{-\gamma_B(t+\tau-t_1)}e^{-\gamma_B(t-t_2)}\gamma_A^2\int_0^{t_1}dt_1' \\ &\int_0^{t_2}dt_2' e^{-\gamma_A(t_1-t_1')}e^{-\gamma_A(t_2-t_2')}\langle\mathcal{E}_A(t_1')\mathcal{E}_A^\dagger(t_2')\rangle, \\ &= \lim_{t\to\infty}\gamma_B^2\int_0^{t+\tau}dt_1\int_0^t dt_2 e^{-\gamma_B(t+\tau-t_1)}e^{-\gamma_B(t-t_2)}\gamma_A^2\int_0^{t_1}dt_1' \\ &\int_0^{t_2}dt_2' e^{-\gamma_A(t_1-t_1')}e^{-\gamma_A(t_2-t_2')}\left[\langle X_{\rm sq}^\dagger(|t_1'-t_2'|)X_{\rm sq}\rangle+\delta(t_1'-t_2')\right].\end{aligned} \tag{2.25}$$

In going to the second line we have assumed that the fields are already in steady state at $t=0$ so that the correlation function only depends on the time difference $|t_1'-t_2'|$. Note that the above equality only holds for $\tau>0$. For $\tau<0$, one can use $\left\langle \mathcal{E}_A^{ff'}(-\tau)\mathcal{E}_A^{\dagger ff'}\right\rangle = \left\langle \mathcal{E}_A^{ff'}\mathcal{E}_A^{\dagger ff'}(\tau)\right\rangle = \left\langle \mathcal{E}_A^{ff'}(\tau)\mathcal{E}_A^{\dagger ff'}\right\rangle^\dagger$, and the fact that the correlation functions are real. The first equality holds because of the stationarity condition. To work out the correlation functions one needs integrals of the form

$$\begin{aligned}I(\gamma_A,\gamma_B,\eta,\tau) =&\lim_{t\to\infty}\gamma_B^2\int_0^{t+\tau}dt_1\int_0^t dt_2 e^{-\gamma_B(t+\tau-t_1)}e^{-\gamma_B(t-t_2)} \\ &\gamma_A^2\int_0^{t_1}dt_1'\int_0^{t_2}dt_2' e^{-\gamma_A(t_1-t_1')}e^{-\gamma_A(t_2-t_2')}e^{-\eta|t_2'-t_1'|}, \\ =&\gamma_A^2\gamma_B^2\left[e^{-\gamma_B\tau}\frac{\eta}{\gamma_B(\gamma_B^2-\gamma_A^2)(\gamma_B^2-\eta^2)}\right. \\ &\left.-e^{-\gamma_A\tau}\frac{\eta}{\gamma_A(\gamma_B^2-\gamma_A^2)(\gamma_A^2-\eta^2)}+e^{-\eta\tau}\frac{1}{(\gamma_A^2-\eta^2)(\gamma_B^2-\eta^2)}\right],\end{aligned} \tag{2.26}$$

and

$$\begin{aligned}I_1(\gamma_A,\gamma_B,\eta,\tau) =&\lim_{t\to\infty}\gamma_B^2\int_0^{t+\tau}dt_1\int_0^t dt_2 e^{-\gamma_B(t+\tau-t_1)}e^{-\gamma_B(t-t_2)} \\ &\gamma_A\int_0^{t_1}dt_1' e^{-\gamma_A(t_1-t_1')}e^{-\eta|t_2-t_1'|}, \\ =&\gamma_A\gamma_B^2\left[e^{-\gamma_B\tau}\frac{\eta}{\gamma_B(\gamma_B-\gamma_A)(\gamma_B^2-\eta^2)}\right. \\ &\left.-e^{-\gamma_A\tau}\frac{2\eta}{(\gamma_B^2-\gamma_A^2)(\gamma_A^2-\eta^2)}+e^{-\eta\tau}\frac{1}{(\gamma_A-\eta)(\gamma_B^2-\eta^2)}\right],\end{aligned} \tag{2.27}$$

and

$$\begin{aligned} I_2(\gamma_A,\gamma_B,\eta,\tau) =& \lim_{t\to\infty}\gamma_B^2\int_0^{t+\tau}dt_1\int_0^t dt_2 e^{-\gamma_B(t+\tau-t_1)}e^{-\gamma_B(t-t_2)} \\ & \gamma_A\int_0^{t_2}dt_2' e^{-\gamma_A(t_2-t_2')}e^{-\eta|t_1-t_2'|}, \\ =& \gamma_A\gamma_B^2\left[-e^{-\gamma_B\tau}\frac{\eta}{\gamma_B(\gamma_B+\gamma_A)(\gamma_B^2-\eta^2)}+e^{-\eta\tau}\frac{1}{(\gamma_A+\eta)(\gamma_B^2-\eta^2)}\right]. \end{aligned} \tag{2.28}$$

Equation (2.26) is needed for $\left\langle \mathcal{E}_A^{ff'}(\tau)\mathcal{E}_A^{\dagger ff'}\right\rangle$, and (2.27) and (2.28) for $\left\langle \mathcal{E}_A^{ff'}(\tau)\mathcal{E}_B^{f}\right\rangle$ and $\left\langle \mathcal{E}_B^{\dagger f}(\tau)\mathcal{E}_A^{\dagger ff'}\right\rangle$ respectively. $\left\langle \mathcal{E}_B^{\dagger f}(\tau)\mathcal{E}_B^{f}\right\rangle$ can be calculated from (2.26) by taking the limit $\gamma_A\to\infty$. The only integral left is the one involving the delta-function, i.e., (2.25). We use $\lim_{\eta\to\infty}\eta e^{-\eta|\tau|}=2\delta(\tau)$ to evaluate it from (2.26), i.e.,

$$\begin{aligned} I_3(\gamma_A,\gamma_B,\tau) &= \lim_{\eta\to\infty}\frac{\eta}{2}I(\gamma_A,\gamma_B,\eta,\tau), \\ &= \frac{\gamma_A^2\gamma_B^2}{2}\left(e^{-\gamma_A\tau}\frac{1}{\gamma_A(\gamma_B^2-\gamma_A^2)}-e^{-\gamma_B\tau}\frac{1}{\gamma_B(\gamma_B^2-\gamma_A^2)}\right). \end{aligned} \tag{2.29}$$

Using the above results, the unnormalized first-order correlation function for the teleported vacuum field can be written as

$$\begin{aligned} \langle\mathcal{E}_{\rm out}^\dagger(\tau)\mathcal{E}_{\rm out}\rangle_{\rm vac} = & \frac{\gamma_s}{4}\frac{\lambda}{1-\lambda}\left[I\left(\gamma_A,\gamma_B,\frac{\gamma_s}{2}(1-\lambda),\tau\right)-I_1\left(\gamma_A,\gamma_B,\frac{\gamma_s}{2}(1-\lambda),\tau\right)\right. \\ & \left.-I_2\left(\gamma_A,\gamma_B,\frac{\gamma_s}{2}(1-\lambda),\tau\right)+I\left(\infty,\gamma_B,\frac{\gamma_s}{2}(1-\lambda),\tau\right)\right] \\ & -\frac{\gamma_s}{4}\frac{\lambda}{1+\lambda}\left[I\left(\gamma_A,\gamma_B,\frac{\gamma_s}{2}(1+\lambda),\tau\right)+I_1\left(\gamma_A,\gamma_B,\frac{\gamma_s}{2}(1+\lambda),\tau\right)\right. \\ & \left.+I_2\left(\gamma_A,\gamma_B,\frac{\gamma_s}{2}(1+\lambda),\tau\right)+I\left(\infty,\gamma_B,\frac{\gamma_s}{2}(1+\lambda),\tau\right)\right] \\ & +I_3\left(\gamma_A,\gamma_B,\tau\right). \end{aligned} \tag{2.30}$$

For input states other than the vacuum

$$g_{\rm out}^{(1)}(\tau)=\frac{\langle\mathcal{E}_{\rm in}^{\dagger ff'}(\tau)\mathcal{E}_{\rm in}^{ff'}\rangle+\langle\mathcal{E}_{\rm out}^\dagger(\tau)\mathcal{E}_{\rm out}\rangle_{\rm vac}}{\langle\mathcal{E}_{\rm out}^\dagger\mathcal{E}_{\rm out}\rangle} \tag{2.31}$$

is the normalized first-order correlation function. Before studying teleportation of the vacuum field we derive a similar expression for the second-order correlation function.

2.4.4 second-order intensity correlation function

The normalized second-order correlation function is defined as

$$g^{(2)}_{\rm out}(\tau) = \frac{\lim_{t\to\infty}\langle \mathcal{E}^\dagger_{\rm out}(t)\mathcal{E}^\dagger_{\rm out}(t+\tau)\mathcal{E}_{\rm out}(t+\tau)\mathcal{E}_{\rm out}(t)\rangle}{\left[\lim_{t\to\infty}\langle \mathcal{E}^\dagger_{\rm out}(t)\mathcal{E}_{\rm out}(t)\rangle\right]^2}. \tag{2.32}$$

The denominator is already known, so only the numerator needs to be calculated. We break it into two parts, the terms containing no input field and the rest:

$$G^{(2)}_{\rm out}(\tau) = G^{(2)}_{\rm out|vac} + G^{(2)}_{\rm out|in},$$

where

$$G^{(2)}_{\rm out|vac} = \left\langle (\mathcal{E}^{\dagger f}_B + \mathcal{E}^{ff'}_A)(\mathcal{E}^{\dagger f}_B + \mathcal{E}^{ff'}_A)(\tau)(\mathcal{E}^{f}_B + \mathcal{E}^{\dagger ff'}_A)(\tau)(\mathcal{E}^{f}_B + \mathcal{E}^{\dagger ff'}_A)\right\rangle, \tag{2.33}$$

are the only terms that contribute for the vacuum input (because the correlation function is normal-ordered), and

$$\begin{aligned} G^{(2)}_{\rm out|in} &= \left\langle \mathcal{E}^{\dagger ff'}_{\rm in}\mathcal{E}^{\dagger ff'}_{\rm in}(\tau)\mathcal{E}^{ff'}_{\rm in}(\tau)\mathcal{E}^{ff'}_{\rm in}\right\rangle \\ &+ \left\langle \mathcal{E}^{\dagger ff'}_{\rm in}\mathcal{E}^{\dagger ff'}_{\rm in}(\tau)\right\rangle \cancel{\left\langle (\mathcal{E}^{f}_B + \mathcal{E}^{\dagger ff'}_A)(\tau)(\mathcal{E}^{f}_B + \mathcal{E}^{\dagger ff'}_A)\right\rangle} + \text{h.c.} \\ &+ \left\langle \mathcal{E}^{\dagger ff'}_{\rm in}\mathcal{E}^{ff'}_{\rm in}(\tau)\right\rangle \left\langle (\mathcal{E}^{\dagger f}_B + \mathcal{E}^{ff'}_A)(\tau)(\mathcal{E}^{f}_B + \mathcal{E}^{\dagger ff'}_A)\right\rangle + \text{h.c.} \\ &+ \left\langle \mathcal{E}^{\dagger ff'}_{\rm in}\mathcal{E}^{ff'}_{\rm in}\right\rangle \left\langle (\mathcal{E}^{\dagger f}_B + \mathcal{E}^{ff'}_A)(\tau)(\mathcal{E}^{f}_B + \mathcal{E}^{\dagger ff'}_A)(\tau)\right\rangle \\ &+ \left\langle \mathcal{E}^{\dagger ff'}_{\rm in}(\tau)\mathcal{E}^{ff'}_{\rm in}(\tau)\right\rangle \left\langle (\mathcal{E}^{\dagger f}_B + \mathcal{E}^{ff'}_A)(\mathcal{E}^{f}_B + \mathcal{E}^{\dagger ff'}_A)\right\rangle, \end{aligned} \tag{2.34}$$

where h.c. denotes Hermitian conjugate. The second line vanish, as marked by the diagonal line; this is because all the correlation functions in them are zero as can be seen in (2.24). The remaining terms can be rewritten as

$$\begin{aligned} G^{(2)}_{\rm out|in} &= \left\langle \mathcal{E}^{\dagger ff'}_{\rm in}\mathcal{E}^{\dagger ff'}_{\rm in}(\tau)\mathcal{E}^{ff'}_{\rm in}(\tau)\mathcal{E}^{ff'}_{\rm in}\right\rangle \\ &+ \left(\left\langle \mathcal{E}^{\dagger ff'}_{\rm in}\mathcal{E}^{ff'}_{\rm in}(\tau)\right\rangle + \left\langle \mathcal{E}^{\dagger ff'}_{\rm in}(\tau)\mathcal{E}^{ff'}_{\rm in}\right\rangle\right)\left\langle \mathcal{E}^{\dagger}_{\rm out}(\tau)\mathcal{E}_{\rm out}\right\rangle_{\rm vac} \\ &+ 2\left\langle \mathcal{E}^{\dagger ff'}_{\rm in}\mathcal{E}^{ff'}_{\rm in}\right\rangle\left\langle \mathcal{E}^{\dagger}_{\rm out}\mathcal{E}_{\rm out}\right\rangle_{\rm vac}, \end{aligned} \tag{2.35}$$

where we have used $\left\langle \mathcal{E}^{\dagger}_{\rm out}(\tau)\mathcal{E}_{\rm out}\right\rangle_{\rm vac} = \left\langle \mathcal{E}^{\dagger}_{\rm out}\mathcal{E}_{\rm out}(\tau)\right\rangle_{\rm vac}$, which holds because the correlation function is real.

Equation (2.33) can also be simplified. Because the squeezed fields and their combinations are Gaussian, the second-order (in intensity) correlation function (2.33) can be broken into first-order correlation functions:

$$\begin{aligned} G^{(2)}_{\text{out}|\text{vac}} &= \cancel{\left\langle (\mathcal{E}_B^{\dagger f} + \mathcal{E}_A^{f f'})(\mathcal{E}_B^{\dagger f} + \mathcal{E}_A^{f f'})(\tau) \right\rangle} \left\langle (\mathcal{E}_B^{f} + \mathcal{E}_A^{\dagger f f'})(\tau)(\mathcal{E}_B^{f} + \mathcal{E}_A^{\dagger f f'}) \right\rangle \\ &+ \left\langle (\mathcal{E}_B^{\dagger f} + \mathcal{E}_A^{f f'})(\mathcal{E}_B^{f} + \mathcal{E}_A^{\dagger f f'})(\tau) \right\rangle \left\langle (\mathcal{E}_B^{\dagger f} + \mathcal{E}_A^{f f'})(\tau)(\mathcal{E}_B^{f} + \mathcal{E}_A^{\dagger f f'}) \right\rangle \\ &+ \left\langle (\mathcal{E}_B^{\dagger f} + \mathcal{E}_A^{f f'})(\mathcal{E}_B^{f} + \mathcal{E}_A^{\dagger f f'}) \right\rangle \left\langle (\mathcal{E}_B^{\dagger f} + \mathcal{E}_A^{f f'})(\tau)(\mathcal{E}_B^{f} + \mathcal{E}_A^{\dagger f f'})(\tau) \right\rangle, \\ &= \langle \mathcal{E}^\dagger_{\text{out}}(\tau)\mathcal{E}_{\text{out}} \rangle^2_{\text{vac}} + \langle \mathcal{E}^\dagger_{\text{out}}\mathcal{E}_{\text{out}} \rangle^2_{\text{vac}}, \end{aligned} \tag{2.36}$$

where the term marked by the diagonal line is zero as explained above. The normalized second-order correlation function is then written as

$$g^{(2)}_{\text{in}}(\tau) = \frac{G^{(2)}_{\text{out}|\text{in}}(\tau) + G^{(2)}_{\text{out}|\text{vac}}(\tau)}{\langle \mathcal{E}^\dagger_{\text{out}}\mathcal{E}_{\text{out}} \rangle^2}. \tag{2.37}$$

2.5 Teleportation of the vacuum field

When the input field is in the vacuum state, (2.31) becomes

$$g^{(1)}_{\text{out}}(\tau) = \frac{\langle \mathcal{E}^\dagger_{\text{out}}(\tau)\mathcal{E}_{\text{out}} \rangle_{\text{vac}}}{\langle \mathcal{E}^\dagger_{\text{out}}\mathcal{E}_{\text{out}} \rangle_{\text{vac}}}. \tag{2.38}$$

In this section we explore the optical spectrum—the Fourier transform of the correlation function $G^{(1)}_{\text{out}}(\tau) = g^{(1)}_{\text{out}}(\tau)\langle \mathcal{E}^\dagger_{\text{out}}\mathcal{E}_{\text{out}} \rangle$—as a function of $\gamma_A, \gamma_B, \gamma_s$, and λ to investigate the dependence of the teleportation 'fidelity' on these parameters. The second-order correlation function of the teleported vacuum can be written in terms of the first-order correlation function as shown in (2.36), so we will not trouble with this in this section. Normalization is chosen with the spectrum written as

$$S(\omega) = \frac{1}{2\pi}\int_{-\infty}^{\infty} d\tau e^{i\omega\tau}\langle \mathcal{E}^\dagger_{\text{out}}(\tau)\mathcal{E}_{\text{out}} \rangle. \tag{2.39}$$

Since the input field is in the vacuum state, the easiest way to teleport the state, i.e., to produce nothing at the output port, is to choose Bob's filter bandwidth to be zero. Obviously this case is not very interesting, so for now we fix Bob's bandwidth; it is chosen to be larger than all the other bandwidths so there is effectively no filtering on Bob's part. To start with we fix Alice's bandwidth to be ten times the squeezing

bandwidth and plot the output spectra as we vary the degree of squeezing. The results are plotted in Fig. 2.7. The top-most curve is for $\lambda = 0.0$ and the bottom curve is for $\lambda = 0.9$. As the amount of squeezing increases the central part of the spectrum approaches the input spectrum, which of course is zero. Note, however, that this happens only within the squeezing bandwidth. The sidebands arise from the shot noise of Alice's measurements and imperfect cancellation between the two-mode entangled fields (the latter only contributes a tiny fraction just outside the squeezing bandwidth).

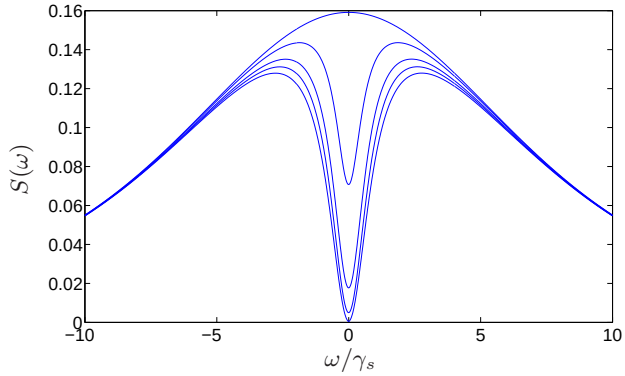

Figure 2.7: Spectra of the teleported vacuum field for $\gamma_A/\gamma_s = 10$, $\gamma_B/\gamma_s = 15$, and $\lambda = 0, 0.2, 0.5, 0.7, 0.9$ (from top to bottom).

We now look into the effect of Alice's bandwidth. Figure 2.8 shows the spectra for $\lambda = 0.9$ and $\gamma_A/\gamma_s = 5, 2, 1, 0.5$. As Alice's bandwidth is decreased the side bands shrink, but the central part of the spectrum gets narrower also. For $\gamma_A < \gamma_s$ the sidebands rise again, although the width of the whole spectrum is now comparable to the squeezing bandwidth (which means less high frequency noise). As Alice's bandwidth is turned down one sees less shot noise, which accounts for the reduction of the noise outside the squeezing bandwidth. Within the squeezing bandwidth, there are two contributions: one that passed through Alice and the other that came to Bob directly. What allows for teleportation is the cancellation of these two contributions, as clearly shown in the SED picture. However, once Alice's bandwidth gets comparable to the squeezing bandwidth, some of the fields are filtered out by Alice, resulting in incomplete cancellation; this accounts for the narrowing of the dip as Alice's bandwidth is decreased.

The moral is that one needs to make Alice's bandwidth big enough so that she does not filter out the useful part of the entangled field correlations; but, of

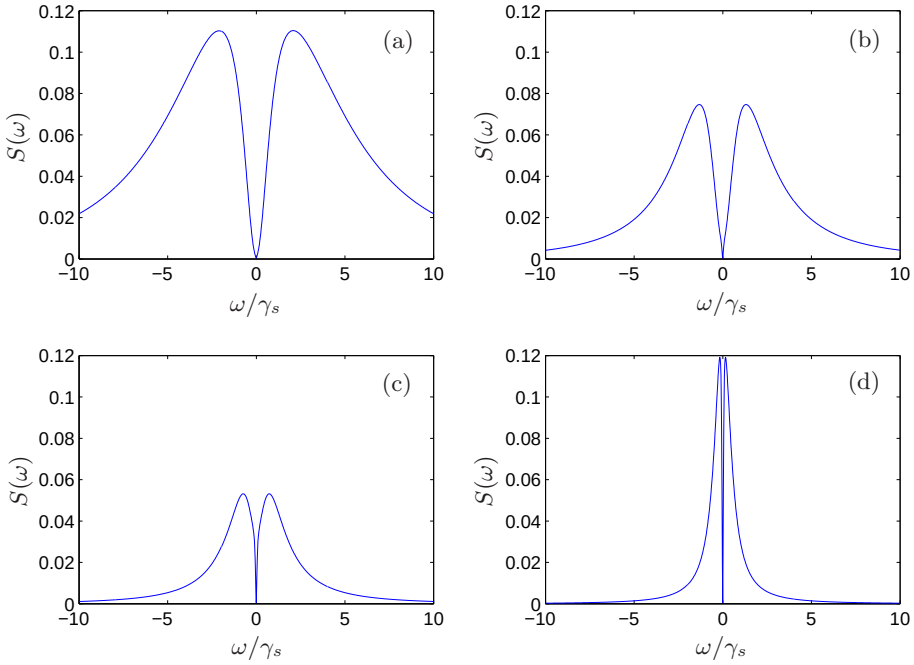

Figure 2.8: Spectra of the teleported vacuum field for $\gamma_B/\gamma_s = 15$, $\lambda = 0.9$, and $\gamma_A/\gamma_s = 5, 2, 1, 0.5$ for (a),(b),(c),(d) respectively.

course, she then sees the appearance of a broad shot noise component outside the squeezing bandwidth. This shot noise component outside the squeezing bandwidth can be filtered out using Bob's filter bandwidth appropriately. The aim would be to achieve zero light across the entire spectrum, leaving a small frequency hole within which a non-vacuum field can be teleported. This issue will be addressed in the following section.

2.6 Resonance fluorescence

Admittedly, teleportation of the vacuum field is not very interesting. One needs to look at a more interesting input field to determine what sort of bandwidths and squeezing are needed for a good teleportation. For this purpose we choose the scattered field of resonance fluorescence: the field scattered from a qubit driven by a laser. It is chosen because it is a non-classical field, i.e., does not allow an SED description, and also because it has well defined properties, namely the Mollow

triplet spectrum and photon antibunching [10], which we can use as signatures of a successful teleportation.

2.6.1 Spectra

Figure 2.9 shows the incoherent spectrum of the input field.[10] The triple peaks are called the Mollow triplet. They are going to be used as a signature for a successful teleportation of the spectrum. γ_{in} is the natural linewidth of the qubit and Y is a dimensionless parameter setting the driving field strength, defined as $Y = \frac{\sqrt{2}\Omega}{\gamma_{\text{in}}}$, where Ω is the Rabi frequency and γ is the Einstein A coefficient. The resonance frequency of the qubit has been set to 0 for convenience.

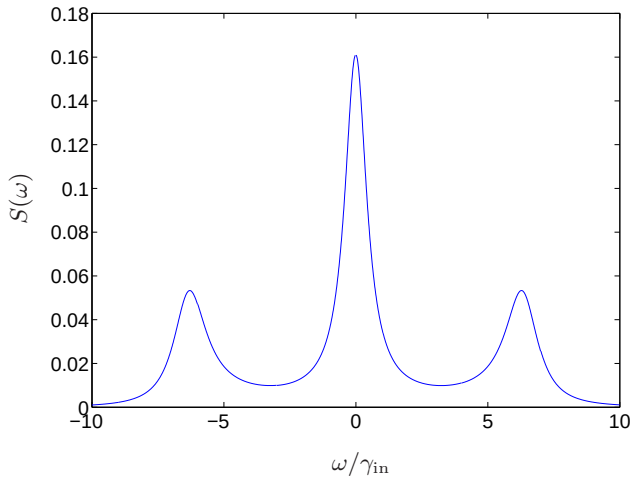

Figure 2.9: Incoherent spectrum of resonance fluorescence for $Y = 9$.

We first calculate $\left\langle \mathcal{E}_{\text{in}}^{\dagger ff'}(\tau)\mathcal{E}_{\text{in}}^{ff'} \right\rangle$. The input correlation function in steady state is (see Sect 2.3 of [10])

$$\begin{aligned}\left\langle \mathcal{E}_{\text{in}}^{\dagger}(\tau)\mathcal{E}_{\text{in}} \right\rangle = &\frac{\gamma_{\text{in}}}{2}\frac{Y^2}{(1+Y^2)^2} + \frac{\gamma_{\text{in}}}{4}\frac{Y^2}{1+Y^2}e^{-(\gamma_{\text{in}}/2)\tau} \\ &- \frac{\gamma_{\text{in}}}{8}\frac{Y^2}{(1+Y^2)^2}\left[1 - Y^2 + (1-5Y^2)\frac{\gamma_{\text{in}}}{4\delta}\right]e^{-(3\gamma_{\text{in}}/4-\delta)\tau} \\ &- \frac{\gamma_{\text{in}}}{8}\frac{Y^2}{(1+Y^2)^2}\left[1 - Y^2 - (1-5Y^2)\frac{\gamma_{\text{in}}}{4\delta}\right]e^{-(3\gamma_{\text{in}}/4+\delta)\tau}, \end{aligned} \tag{2.40}$$

[10] The coherent part is a delta function which we cannot plot. See Sect. 2 of [10] for a detailed analysis of resonance fluorescence. We adopt the definitions of that book.

where $\delta = (\gamma_{\rm in}/4)\sqrt{1-8Y^2}$. Thus, the input contribution to the output spectrum can be written in terms of (2.26) as

$$\begin{aligned}\left\langle \mathcal{E}_{\rm in}^{\dagger ff'}(\tau)\mathcal{E}_{\rm in}^{ff'}\right\rangle &= \frac{\gamma_{\rm in}}{2}\frac{Y^2}{(1+Y^2)^2} + \frac{\gamma_{\rm in}}{4}\frac{Y^2}{1+Y^2}I(\gamma_A,\gamma_B,\gamma_{\rm in}/2,\tau) \\ &- \frac{\gamma_{\rm in}}{8}\frac{Y^2}{(1+Y^2)^2}\left[1-Y^2+(1-5Y^2)\frac{\gamma_{\rm in}}{4\delta}\right]I(\gamma_A,\gamma_B,3\gamma_{\rm in}/4-\delta,\tau) \\ &- \frac{\gamma_{\rm in}}{8}\frac{Y^2}{(1+Y^2)^2}\left[1-Y^2-(1-5Y^2)\frac{\gamma_{\rm in}}{4\delta}\right]I(\gamma_A,\gamma_B,3\gamma_{\rm in}/4+\delta,\tau).\end{aligned} \tag{2.41}$$

The incoherent part of the spectrum is calculated by taking the Fourier transform of the above equation omitting the constant term. The effect of squeezing on the vacuum spectrum has already been shown in the previous section—the higher the squeezing the bigger the 'dip'. Equation (2.21) says that the input contribution to the spectrum will merely sit on top of the vacuum part. Therefore we choose the bandwidth of the input field to be orders of magnitude smaller than the squeezing bandwidth, i.e., $\gamma_{\rm in} << \gamma_s$. Figure 2.10 shows the effect of Bob's bandwidth on teleported spectra. As γ_B is decreased one sees a reduction of the unwanted sidebands, but past a certain point the input field starts to be filtered also. For a given input bandwidth, then, Bob's filter bandwidth has to be chosen to be bigger than that bandwidth. In general, the smaller the input bandwidth relative to the squeezing bandwidth the better: the input signal has to sit well inside the dip so that Bob's filter cavity can safely filter out the unwanted shot noise without affecting it.

Figure 2.11 plots total output spectra for various values of Y, comparing them with the results from quantum trajectory simulations as promised earlier. Good agreement with the quantum trajectory results verifies that the Heisenberg picture calculation works. The small discrepancies at $\omega = 0$ are due to the fact that the Heisenberg picture calculations ignore the coherent part of the spectra, whereas in quantum trajectory theory they are naturally included. The coherent part is not a delta function in trajectory simulations because a realistic measurement scheme is taken. For example, the spectrum can be measured via heterodyne detection with an intrinsic filter, which gives a finite width (hence height) to the delta function. As Y is increased the contribution from the coherent part gets smaller.

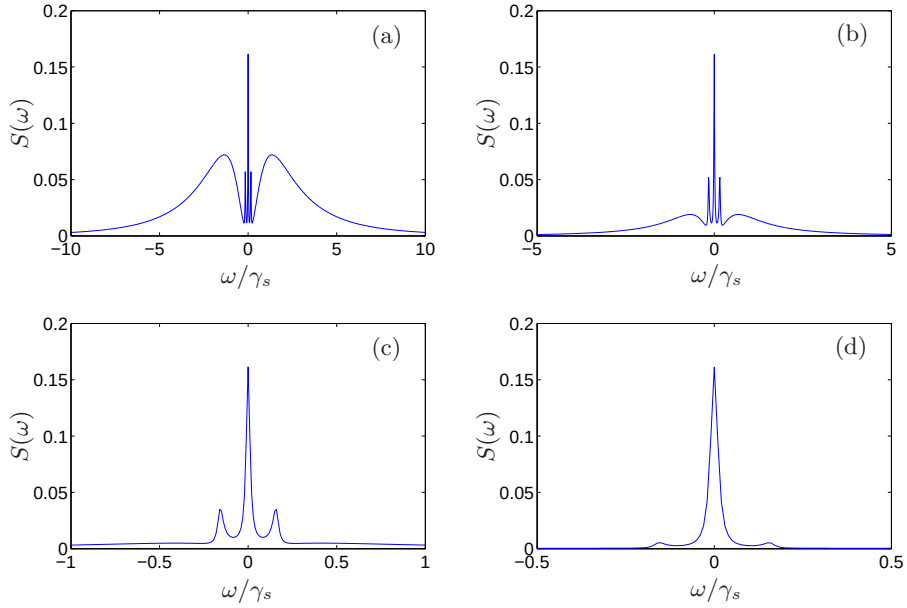

Figure 2.10: Spectra of teleported resonance fluorescence field for $Y = 9$, $\gamma_A/\gamma_s = 10$, $\gamma_{\text{in}/\gamma_s} = 0.025$, $\lambda = 0.9$, and $\gamma_B/\gamma_s = 2, 0.5, 0.2, 0.05$ for (a), (b), (c), (d) respectively.

2.6.2 Intensity correlation functions

The intensity correlation function of the teleported field is a lot harder to calculate than the spectrum because of the first term on the r.h.s of (2.35). The Gaussian moment theorem does not apply because the scattered field of resonance fluorescence is not a Gaussian field. Two- and four-time correlation functions (or rather one- and three-time correlation functions in the steady state) need to be calculated for the input. This is done in Appendix B. The next step is to evaluate the filtering integral

$$\begin{aligned}\left\langle \mathcal{E}_{\text{in}}^{\dagger ff'}\mathcal{E}_{\text{in}}^{\dagger ff'}(\tau)\mathcal{E}_{\text{in}}^{ff'}(\tau)\mathcal{E}_{\text{in}}^{ff'}\right\rangle &= \lim_{t\to\infty}\gamma_{\text{in}}^2\gamma_B^4\gamma_A^4 \\ &\int_0^t dt_1\int_0^{t+\tau}dt_2\int_0^{t+\tau}dt_3\int_0^t dt_4 e^{-\gamma_B(t-t_1)}e^{-\gamma_B(t+\tau-t_2)}e^{-\gamma_B(t+\tau-t_3)}e^{-\gamma_B(t-t_4)} \\ &\int_0^{t_1}dt_1'\int_0^{t_2}dt_2'\int_0^{t_3}dt_3'\int_0^{t_4}dt_4' e^{-\gamma_A(t_1-t_1')}e^{-\gamma_A(t_2-t_2')}e^{-\gamma_A(t_3-t_3')}e^{-\gamma_A(t_4-t_4')} \\ &T\left\{\langle\sigma_+(t_1')\sigma_+(t_2')\sigma_-(t_3')\sigma_-(t_4')\rangle\right\},\end{aligned} \tag{2.42}$$

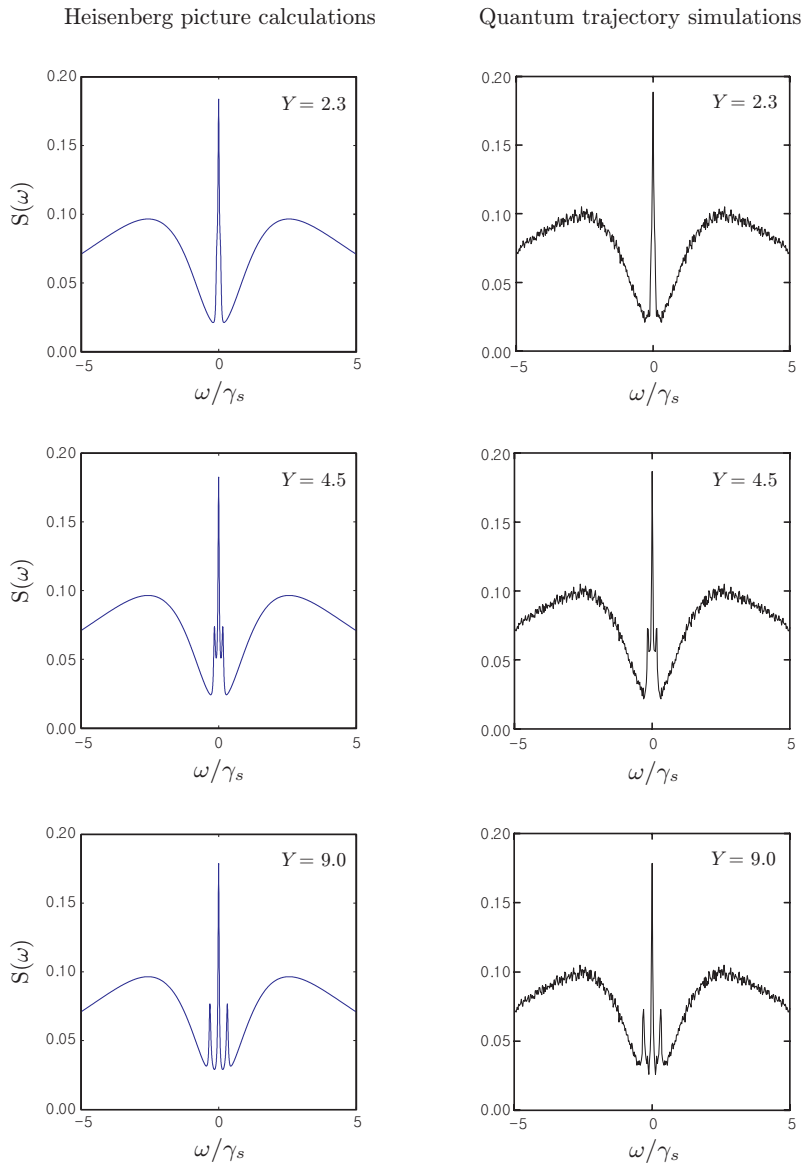

Figure 2.11: Comparison between spectra calculated in the Heisenberg picture and from quantum trajectory simulations, for $\gamma_A/\gamma_s = 12.5$, $\gamma_B/\gamma_s = 2.5$, $\lambda = 0.5$, and $\gamma_{\rm in}/\gamma_s = 0.05$.

with the four-time correlation functions computed in Appendix B. T denotes time ordering, such that $\sigma_+(t_1')$ and $\sigma_+(t_2')$ are swapped if $t_2' < t_1'$, and $\sigma_-(t_3')$ and $\sigma_-(t_4')$ are swapped if $t_3' < t_4'$. This particular ordering is chosen (the total field operator (B.2) commutes with its adjoint and itself at different times) since it allows us to

drop the free field contributions to the 4-time correlation function. Evaluation of this integral requires splitting it up into time-ordered integrals. To save writing, we define $S_i(0,\tau,\tau,0)$ as the time-ordered integrals where i denotes the 3 different regions defined in table 2.1:

i	Integration region
1	$t'_2 > t'_3 > t'_1 > t'_4$
2	$t'_2 > t'_3 > t'_4 > t'_1$
3	$t'_2 > t'_3 > t'_4 > t'_1$

Table 2.1: Regions of integration for $S_i(0,\tau,\tau,0)$.

For example

$$S_1(0,\tau,\tau,0) = \lim_{t\to\infty}\gamma_{\rm in}^2\gamma_B^4\gamma_A^4 \int_0^t dt_1\int_0^{t+\tau} dt_2\int_0^{t+\tau} dt_3\int_0^t dt_4 e^{-\gamma_B(t-t_1)}e^{-\gamma_B(t+\tau-t_2)}e^{-\gamma_B(t+\tau-t_3)}e^{-\gamma_B(t-t_4)} \int_0^{m_{1234}} dt'_4\int_{t'_4}^{m_{123}} dt'_1\int_{t'_1}^{m_{23}} dt'_3\int_{t'_3}^{t_2} dt'_2 e^{-\gamma_A(t_1-t'_1)}e^{-\gamma_A(t_2-t'_2)}e^{-\gamma_A(t_3-t'_3)}e^{-\gamma_A(t_4-t'_4)} \langle\sigma_+(t'_1)\sigma_+(t'_2)\sigma_-(t'_3)\sigma_-(t'_4)\rangle, \tag{2.43}$$

where m_{1234} denotes the smallest value among t_1, t_2, t_3, t_4, etc. This, then, is the contribution to (2.42) from the region 1, i.e., for $t'_2 > t'_3 > t'_1 > t'_4$. Other regions can be calculated from this definition: e.g. the contribution from the integration region $t'_1 > t'_3 > t'_2 > t'_4$ is $S_1(\tau,0,\tau,0)$, because for this region $T\{\langle\sigma_+(t'_1)\sigma_+(t'_2)\sigma_-(t'_3)\sigma_-(t'_4)\rangle\} = \langle\sigma_+(t'_2)\sigma_+(t'_1)\sigma_-(t'_3)\sigma_-(t'_4)\rangle$, and upon changes of dummy variables one sees that the roles of t_1 and t_2 are changed. The cases where $t'_3 > t'_2$ are obtained by taking the complex conjugate of the four-time correlation function, which is equivalent to taking the complex conjugate of the whole integral. Thus for $t'_3 > t'_2 > t'_4 > t'_1$ the integral is equal to $S_1^*(0,\tau,\tau,0)$. Using similar arguments for other regions one can write (2.42) as

$$\left\langle \mathcal{E}_{\rm in}^{\dagger ff'}\mathcal{E}_{\rm in}^{\dagger ff'}(\tau)\mathcal{E}_{\rm in}^{ff'}(\tau)\mathcal{E}_{\rm in}^{ff'}\right\rangle = \sum_{i=1}^{3}\left[S_i(0,\tau,\tau,0) + S_i(\tau,0,\tau,0) + S_i(0,\tau,0,\tau) + S_i(\tau,0,0,\tau)\right] + \text{c.c}, \tag{2.44}$$

where c.c denotes the complex conjugate. The second term is for $t'_1 > t'_2$, the third for $t'_4 > t'_3$, the fourth for $t'_1 > t'_2$ *and* $t'_4 > t'_3$, and finally the c.c terms are for $t'_3 > t'_2$.

Calculation of $S_i(0, \tau, \tau, 0)$ gives a myriad of terms that would take a few pages to write down. We therefore adopt an algorithmic approach which works in the same way as that used to calculate the spectra: the most general integral (equivalent to $I(\gamma_A, \gamma_B, \eta, \tau)$) is solved and used repeatedly in different combinations. This calculation is explained in Appendix B and a fortran code for its evaluation is given in Appendix C. The latter plots the total intensity correlation function of the teleported scattered field of resonance fluorescence. Using this code we plot several figures to determine the kind of parameters required for a high fidelity teleportation.

For reference, Fig. 2.12 shows the intensity correlation function of the input field for $Y = 9$. Figures 2.13 and 2.14 show the intensity correlation functions of the teleported field using the same parameters as for the spectra plotted in (b) and (c) in Fig. 2.10. Clearly, in both cases, the intensity correlation function at the output is very different from that of the input. In particular, both figures show sharp central peaks at zero delay going above $g^{(2)}_{\rm out}(0) = 1$, which means there is photon bunching rather than antibunching—the non-classicality of the input field has not been teleported.[11] Notice how well the spectra are teleported for the same parameters. Because the intensity correlation function is a function of time, all the high frequency noise contributes near $\tau = 0$, resulting in the sharp peak. In order to produce a better result Bob has to choose a smaller filter bandwidth; but as shown in Fig. 2.10 this deteriorates the signal. The input bandwidth must be decreased relative to the squeezing bandwidth first. In Fig. 2.15 we plot teleported $g^{(2)}_{\rm out}(\tau)$'s for $\gamma_B/\gamma_s = 0.05, 0.025, 0.01, 0.005$ and $\gamma_{\rm in}/\gamma_s = 0.0025$. $\gamma_B/\gamma_s = 0.025$ seems to be the best choice of the four. Bigger than that and the sideband noise is not filtered effectively; smaller than that and the signal starts to get affected. For (b) and (c), $g^{(2)}_{\rm out}(0) < 1$, so there is antibunching in that sense. According to the definitions of Mandel and co-workers [37, 38], however, these examples do not show antibunching as the functions are not initially increasing.[12] It is interesting that this feature is unavoidable for a successful teleportation; no matter how small one chooses Bob's bandwidth, as long as it is bigger than the input bandwidth there will always be a little bit of unfiltered noise that will show itself at the center as a little peak.

[11] To the best of author's knowledge the antibunching is *the* non-classicality in the sense that all other non-classical aspects of resonance fluorescence (e.g., squeezing) are related to it.

[12] For a discussion of this point see Sect 2.3.6 in [10].

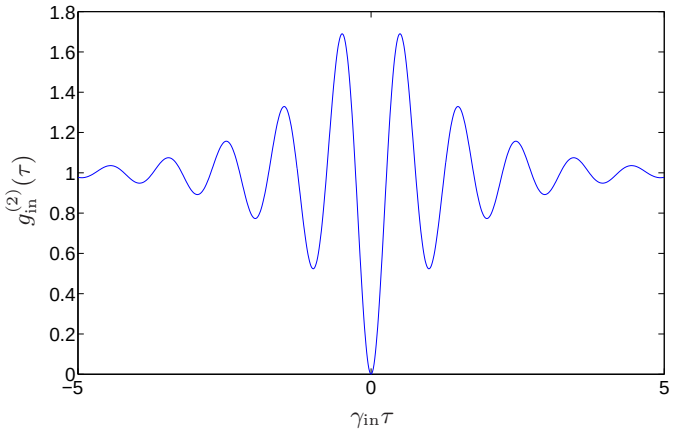

Figure 2.12: Intensity correlation function of resonance fluorescence for $Y = 9$.

When teleporting an unknown field the input bandwidth is not known exactly. Then the best one can do is to choose Bob's bandwidth to be orders of magnitude bigger than what might be anticipated for the input bandwidth. In Fig. 2.16 we plot intensity correlation functions for $\gamma_B = 100\gamma_{\rm in}$ with varying $\gamma_{\rm in}$. We have chosen $\lambda = 0.99$ (46dB line-center squeezing) to show how good the teleportation can get. In (a) we have chosen $\gamma_{\rm in} = 0.0001\gamma_s$ so that γ_B is a hundred times smaller than γ_s and $\gamma_{\rm in}$ a hundred times smaller still. As one can see, even this is not good enough. Bob's filter is still letting through too much unwanted noise at this value. Choosing it an order of magnitude smaller does a better job, as shown in (b), but the whole figure is a bit squashed. Finally, choosing $\gamma_B/\gamma_s = 0.0001$ and $\gamma_{\rm in} = 0.000001$ gives a very good teleportation. We have plotted the input $g^{(2)}(\tau)$ in (c) for comparison. Notice how small the input bandwidth has to be compared to the squeezing bandwidth. There is six orders of magnitude difference! This is obtained from looking at the second-order correlation only. One might expect that teleportation of higher order correlation functions could require more stringent bandwidth and squeezing requirements; nevertheless, it seems plausible that, in principle, all orders of correlations can be teleported with enough squeezing and carefully chosen bandwidths obeying the hierarchy described in this chapter and summarized near the end of this section.

Teleportation works very well for the last set of parameters, but what is going to happen if we increase γ_B further? From the consideration of the spectrum you might expect this to have only a small effect on the teleported field, but Fig. 2.17

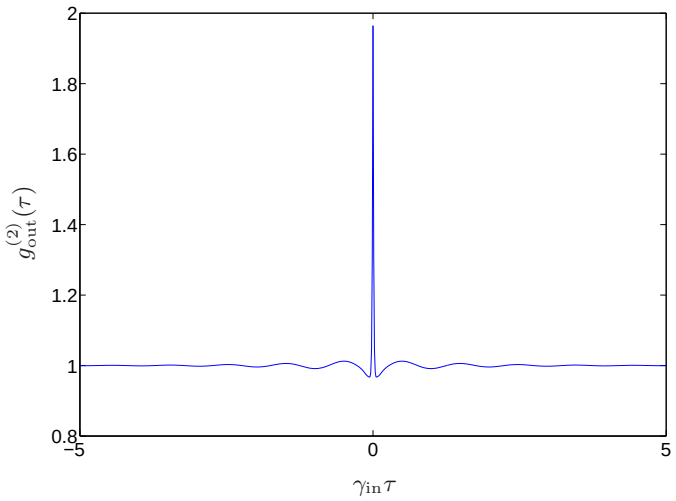

Figure 2.13: Intensity correlation function of teleported resonance fluorescence for $Y = 9$, $\gamma_A/\gamma_s = 10$, $\gamma_B/\gamma_s = 0.5$, $\lambda = 0.9$, and $\gamma_{\rm in}/\gamma_s = 0.025$.

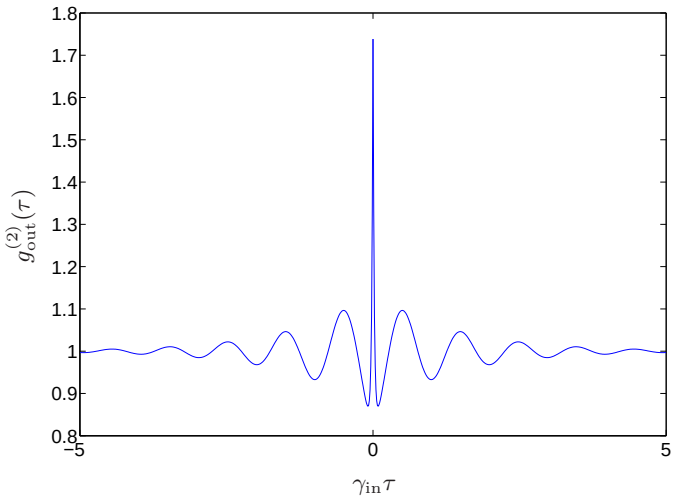

Figure 2.14: Intensity correlation function of teleported resonance fluorescence for $Y = 9$, $\gamma_A/\gamma_s = 10$, $\gamma_B/\gamma_s = 0.2$, $\lambda = 0.9$, and $\gamma_{\rm in}/\gamma_s = 0.025$.

says otherwise. Bob's bandwidth has only been increased by tenfold compared to (c) in Fig. 2.16, but the result is detrimental. This tells us that γ_B has to be chosen carefully. It has to be bigger than $\gamma_{\rm in}$ but not too big—otherwise the unwanted noise dominates once again. This point is discussed a little more with the help of an analytical formula given in the next section.

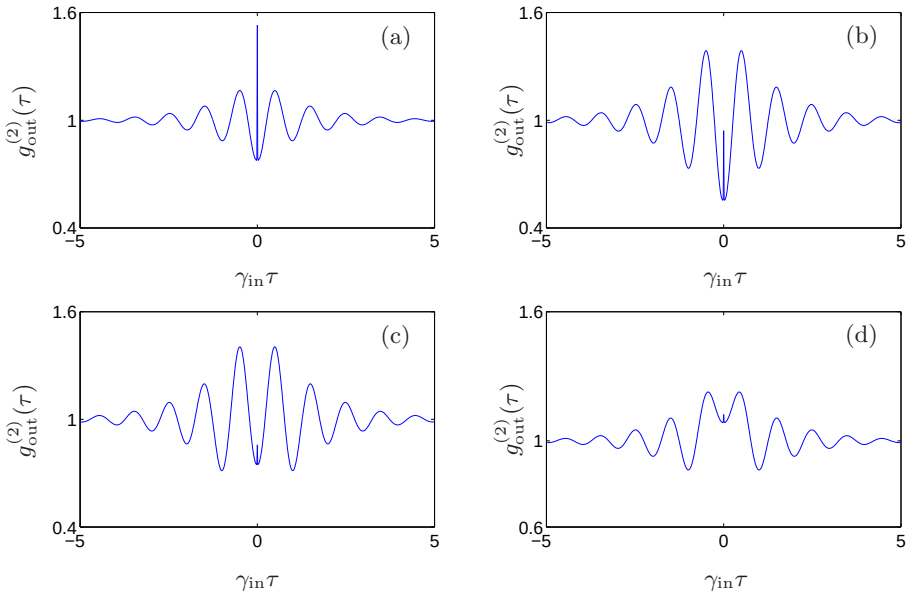

Figure 2.15: Intensity correlation functions of teleported resonance fluorescence for $Y = 9$, $\gamma_A/\gamma_s = 10$, $\gamma_{\rm in}/\gamma_s = 0.0025$, $\lambda = 0.9$, and $\gamma_B/\gamma_s = 0.05, 0.025, 0.01, 0.005$ for (a),(b),(c),(d) respectively.

The limitations on bandwidths can be summarized in the inequality

$$\gamma_A >> \gamma_s >> \gamma_B >> \gamma_{\rm in}.$$

Alice's bandwidth γ_A has to be greater than γ_s and $\gamma_{\rm in}$ to let all the useful correlations and input signal go through. The squeezing bandwidth γ_s has to be greater than $\gamma_{\rm in}$ so the input field sits well within the 'dip'. In other words, the input field has to be embedded within the squeezing bandwidth where correlations between the entangled fields are maximal. γ_s also has to be bigger than γ_B so that Bob can filter out the unwanted noise (consisting mainly of Alice's shot noise) that has not been cancelled. Finally Bob's bandwidth γ_B has to be greater than $\gamma_{\rm in}$, but not too much greater, so that all of the input field goes through unaffected.

2.7 Analytical formulae

In the limit $\gamma_A >> \gamma_s, \gamma_B, \gamma_{\rm in}$ and $\gamma_B >> \gamma_{\rm in}$ it is possible to write down concise formulae for the correlation functions of the teleported field. We do not use $\gamma_s >> \gamma_B$

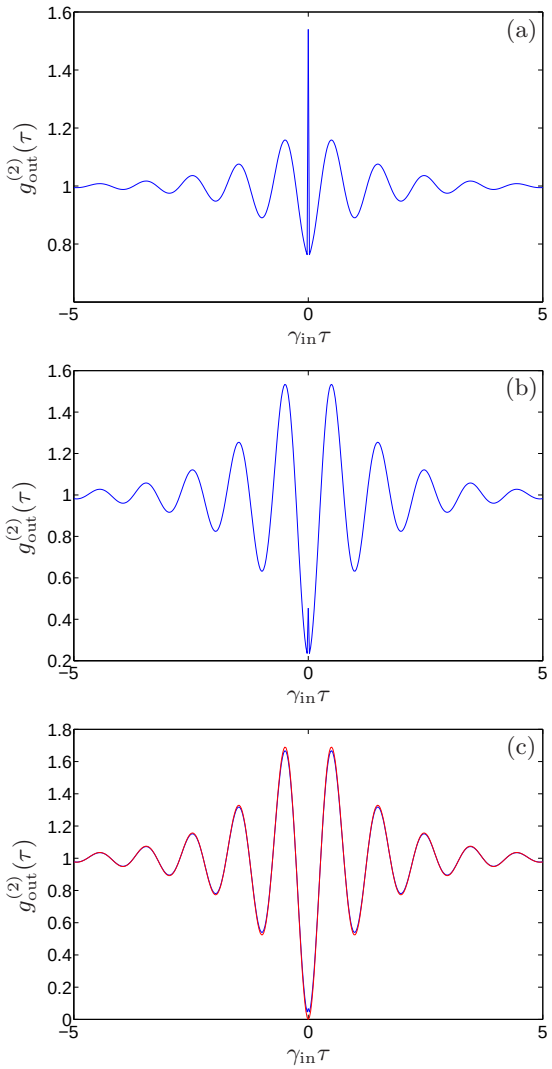

Figure 2.16: Intensity correlation function of teleported resonance fluorescence for $Y = 9$, $\gamma_A/\gamma_s = 10$, $\lambda = 0.99$, $\gamma_B = 100\gamma_{\rm in}$, and (a) $\gamma_{\rm in}/\gamma_s = 0.0001$, (b) $\gamma_{\rm in}/\gamma_s = 0.00001$, (c) $\gamma_{\rm in}/\gamma_s = 0.000001$.

as an additional limit, because it cannot be done consistently, as will be shown shortly.

2.7.1 First-order correlation function

We start from (2.21). Because $\gamma_A, \gamma_B >> \gamma_{\rm in}$ no part of the input field gets filtered and we can remove the superscripts f, f' from the input field operators. Also, in the

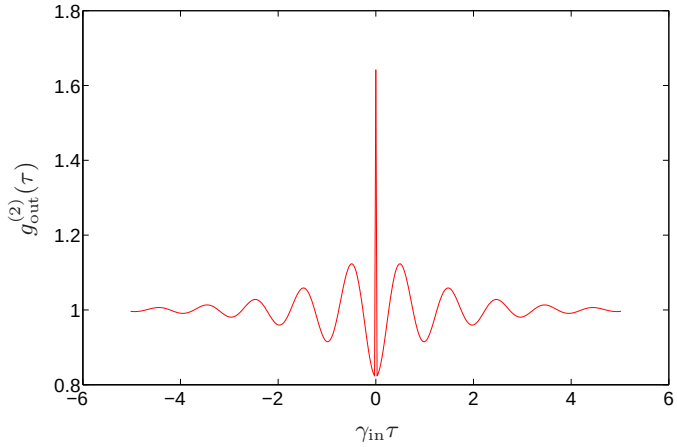

Figure 2.17: Intensity correlation function of teleported resonance fluorescence for $Y = 9$, $\gamma_A/\gamma_s = 10$, $\lambda = 0.99$, $\gamma_B/\gamma_s = 0.001$, and $\gamma_{\rm in}/\gamma_s = 0.000001$.

limit $\gamma_A >> \gamma_s, \gamma_B$, (2.30) reduces to

$$\gamma_B\chi(\tau) \equiv \langle \mathcal{E}^\dagger_{\rm out}(\tau)\mathcal{E}_{\rm out}\rangle_{\rm vac} = \frac{\gamma_B}{2}\left(1 + \frac{\lambda\gamma_s^2}{\gamma_B^2 - (\gamma_s/2)^2(1+\lambda)^2}\right)e^{-\gamma_B\tau} - \frac{\lambda\gamma_s}{1+\lambda}\frac{\gamma_B^2}{\gamma_B^2 - (\gamma_s/2)^2(1+\lambda)^2}e^{-\frac{\gamma_s}{2}(1+\lambda)\tau}. \tag{2.45}$$

$\chi(0)$ is then the number of photons inside the filter cavity for a vacuum input. At this point one might want to take the limit $\gamma_s >> \gamma_B$. One has to be careful in doing so, however, because after taking the limit and ignoring the γ_B^2 terms in the denominators, one obtains

$$\chi(\tau) \to \frac{1}{2}\left(1 - \frac{4\lambda}{(1+\lambda)^2}\right)e^{-\gamma_B\tau} - \frac{4\lambda}{(1+\lambda)^3}\frac{\gamma_B}{\gamma_s}e^{-\frac{\gamma_s}{2}(1+\lambda)\tau}, \tag{2.46}$$

where the second term on the right cannot be ignored for small τ, because as $\lambda \to 1$ the first term tends to zero and could be of the same order of magnitude as the second term. This is the reason why we can not assume $\gamma_s >> \gamma_B$ consistently in our formula.

Using the definition of $\chi(\tau)$, the normalized first-order correlation function for the teleported field is given by

$$g^{(1)}_{\rm out}(\tau) = \frac{1}{f_{\rm out}}\left[f_{\rm in}g^{(1)}_{\rm in}(\tau) + \gamma_B\chi(\tau)\right], \tag{2.47}$$

where f_{in} is the flux of input photons and

$$f_{\text{out}} = f_{\text{in}} + \gamma_B \chi(0) \tag{2.48}$$

is the total flux at the output. Clearly $g^{(1)}_{\text{out}}(\tau) \to g^{(1)}_{\text{in}}(\tau)$ as $\lambda \to 1$ and $\gamma_B/\gamma_s \to 0$.

2.7.2 second-order correlation function

From equations (2.35) and (2.36) one obtains

$$g^{(2)}_{\text{out}}(\tau) = 1 + \left(\frac{f_{\text{in}}}{f_{\text{out}}}\right)^2 \left(g^{(2)}_{\text{in}}(\tau) - 1\right) + \frac{\gamma_B \chi(\tau)}{f^2_{\text{out}}} \left(2 f_{\text{in}} g^{(1)}_{\text{in}}(\tau) + \gamma_B \chi(\tau)\right). \tag{2.49}$$

Again, $\chi(\tau) \to 0$ as $\lambda \to 1$ and $\gamma_B/\gamma_s \to 0$, and thus $g^{(2)}_{\text{out}}(\tau) \to g^{(2)}_{\text{in}}(\tau)$.

Now consider $g^{(2)}_{\text{out}}(0)$ while fixing the value of γ_B/γ_s. For $\lambda \approx 1$, $\gamma_B \chi(0) \approx 0$; but it is not exactly zero, and as a consequence $g^{(2)}_{\text{out}}(0)$ is not exactly zero (as is $g^{(2)}_{\text{in}}(0)$). The discrepancy arises from $\gamma_B \chi(0)$; but $\chi(0)$ only depends on λ and γ_B/γ_s (see (2.46)). Thus upon increasing γ_B—while keeping γ_B/γ_s constant—$\gamma_B \chi(0)$ increases, and hence $g^{(2)}_{\text{out}}(0)$ deviates further from zero. In essence, the output flux increases when γ_B is increased, which accounts for the need for a careful choice of $\gamma_B/\gamma_{\text{in}}$ as was noted in the paragraph below Fig. 2.16.

Part II

Quantum entanglement in cascaded open systems

Chapter 3

Laser-qubit interaction

The general theme of Part II, consisting of this chapter and the next, is quantum entanglement. In this chapter we consider the issue of entanglement between a laser source and a qubit, together comprising a resonance fluorescence system—i.e. a qubit driven by a laser. It is one of the simplest systems in quantum optics and is of interest in the field of quantum computing as a prototype of qubit manipulation. This chapter is not concerned with the properties of the scattered field of resonance fluorescence, which are already well known; rather, we investigate topics such as: the decoherence induced by the quantum nature of the laser field, entanglement between the laser source and the atom, and the quantum state of a laser. The work in this chapter raises the question of entanglement between the driven qubit and the field scattered from it, which we will try to quantify in the next chapter with the help of a measure of entanglement called 'contextual entanglement' [23].

3.1 History

3.1.1 Decoherence

To explain the motivation of this work, it is best to start with a little history. In 2002, Gea-Banacloche (GB) [39] and van Enk and Kimble (vEK) [40] studied the decoherence induced by the quantum nature of a laser field, i.e., entanglement between a driven qubit and the driving laser beam. They concluded that entanglement (albeit very small) indeed exists between the qubit and the beam. Their work raised the question of whether this entanglement is additional to or a part of the decoherence due to spontaneous emission of the qubit. Itano soon clarified that the total

decoherence rate is determined by the spontaneous emission rate only [41], and the decoherence due to laser beam-qubit entanglement is included in it [42, 43]. Later on, Silberfarb and Deutsch have reached the same conclusion from a more thorough modelling of the system [44]. More recently, Nha and Carmichael [45] used the cascaded open systems approach [46, 47] to arrive at the same conclusions; they divide the total decoherence into two parts—one due to photon scattering into the laser mode and the other to scattering out of it—and conclude that the first part accounts for what GB and vEK attributed to the quantum nature of a laser field. Our work takes off from this point. The work of Nha and Carmichael assumed the laser to be in a coherent state; we relax the assumption by introducing a more realistic laser model. We reach the same conclusion, i.e., that the total decoherence rate is accounted for by the spontaneous emission rate alone.

3.1.2 The quantum state of a laser

A second topic of interest in this chapter is the quantum state of a laser. It has been a topic of ongoing debate following the appearance of Mølmer's provocative paper 'Optical coherence: A convenient fiction' [48]. Mølmer argues that "mean optical amplitudes are not created and not detected in experiments" and thus "optical coherences may be regarded as a convenient fiction". In the context of laser fields the argument is essentially the following. Because the phase of a laser is not known, the density operator for the laser should be written as

$$\rho = \int \frac{d\phi}{2\pi} ||\alpha|e^{i\phi}\rangle\langle|\alpha|e^{i\phi}| = e^{-|\alpha|^2} \sum_n \frac{|\alpha|^{2n}}{n!} |n\rangle\langle n|; \tag{3.1}$$

but this means that one can think of a laser as being in a mixture of number states, which have no coherence.[1] Mølmer's argument led Rudolph and Sanders to claim that continuous variable teleportation has not been achieved in experiments yet, due to the absence of intrinsic coherence in conventional lasers [52]. van Enk and Fuchs immediately replied in favour of coherent states [53]. Wiseman also gave an argument in favour of coherent states, arguing that a laser acts as a clock [54]. There is also a neutral argument by Bartlett *et al.* which they call the 'reference frames' approach [55]. For those not familiar with the debate, the last contains a good introduction to the subject.

[1] Accordingly, there are two kinds of laser theories. The Scully-Lamb master equation describes a birth-death evolution between number states [49], whereas the Lax and Haken schools describe the laser field by a stochastically evolving coherent state [50, 51].

We give a different argument for why one should assign a privileged role to coherent states [56]. Mathematically, we do not hope to find a difference between the two sides; on the whole the two sides differ in where they place the quantum-classical boundary or cut [55]. Instead we propose an objective criterion, noting that the primary purpose of a laser is to drive a target. The quantum state of a laser is then proposed to be the state which allows the laser and target dynamics to be separately described (disentangled) at all times and the behaviour of the target to follow from that of the laser. At the end of this chapter, we show that a coherent state is the unique state that satisfies this criterion.[2] Our argument receives strength in the light of the decoherent histories formulation of quantum mechanics (see [59] and references therein), which looks for an observer independent formulation of quantum mechanics by placing (consistent) histories at the heart of the matter. According to this formulation, the density operator does not give the whole story, but rather a family of 'consistent' histories (which are somewhat like different quantum trajectories) does, supporting the use of trajectories (histories). Note, however, that consistent histories are not exactly equivalent to quantum trajectories, in that no measurements are actually necessary in the consistent histories approach.

3.2 Laser model

For the more realistic laser model alluded to earlier, we use the birth-death model developed by Rice and Carmichael [60]. In this model there are two modes: a laser mode and a carrier mode. Carriers (as in a semiconductor) are injected into the system with energy to drive the laser mode; this pumping is assumed incoherent, so one is allowed to count, or track, every quantum of energy injected. It is also assumed that one tracks the quanta of energy coming out of the system, so the whole system is described by an equation for the probability density for finding n atoms and N carriers.

The birth-death model can be implemented straightforwardly within quantum trajectory theory as follows. Each process involving energy transfer is associated with a jump operator: laser pumping is described by the jump operator $J_P = \sqrt{P}\frac{1}{\sqrt{c^\dagger c}}c^\dagger$, emission into the laser mode by $J_{\rm las} = \sqrt{\beta}a^\dagger c$, emission into other modes by $J_{\rm em} = \sqrt{1-\beta}c$, and emission out of the laser mode by $J_{\rm cav} = \sqrt{\gamma_S}a$; P deter-

[2] A similar line of reasoning—to give a criterion for laser state assignment—has been articulated by Gea-Banacloche. He proposes that the longest lived state, while interacting with environment, be assigned to the laser [57, 58].

mines the pumping rate, c is the annihilation operator of the carrier mode, a the annihilation operator of the laser mode, β the rate of spontaneous emission into the laser mode, and γ_S is the full-width of the laser cavity. The form of J_P is adopted so that the pumping rate is constant, independent of the number of carriers (no stimulated emission into the carrier mode). The master equation is then written as

$$\dot{\rho}(t) = (\mathcal{L}_S + \mathcal{D}[J_{\rm cav}])\,\rho \equiv (\mathcal{D}[J_P] + \mathcal{D}[J_{\rm las}] + \mathcal{D}[J_{\rm em}] + \mathcal{D}[J_{\rm cav}])\,\rho. \tag{3.2}$$

where $\mathcal{D}[J]\rho = J\rho J^\dagger - \frac{1}{2}J^\dagger J\rho - \frac{1}{2}\rho J^\dagger J$ is the usual Lindblad term [27]. Note that if the initial state is a Fock state, $|n,N\rangle\langle n,N|$, the system stays in a Fock state, generally with different numbers, under the evolution. By expanding the density operator as $\rho = \sum p_{n,N}|n,N\rangle\langle n,N|$ one obtains

$$\begin{aligned}\dot{p}_{n,N} =& -\gamma_S[np_{n,N} - (n+1)p_{n+1,N}] - \beta[(n+1)Np_{n,N} - n(N+1)p_{n-1,N+1}] \\ &+ P[p_{n,N-1} - p_{n,N}] - (1-\beta)[Np_{n,N} - (N+1)p_{n,N+1}].\end{aligned} \tag{3.3}$$

which is the birth-death master equation given by Rice and Carmichael [60].

We now reproduce the average photon numbers and photon number distributions obtained from this model, to convince the reader that it behaves as a laser should. Conventional lasers are known to exhibit a threshold behaviour: if the pump power is smaller than the threshold power there is no output, while when it becomes bigger, a very small increase in pumping power results in a big change in laser intensity. This threshold behaviour is captured in the above model for $\beta << 1$. The threshold pump power is equal to $P_{\rm thr} = \gamma_S/\beta$ in the model. Figure 3.1 shows the photon number distributions for $\beta = 0.0001$ obtained from numerical simulations. Other parameters used in the simulations are $P_{\rm thr} = 500$ and $P/P_{\rm thr} = 0.1, 1, 10, 50$. The analytical curves in the figure are obtained from [10] (see 273ff) with $C = P/2$,[3] or equivalently $n_{spon} = P$, at and below threshold (i.e. $P \leq 1$). Above threshold, the analytical curves are simply normal distributions with mean $n_{\rm sat}(P/P_{\rm thr} - 1)$ and variance $n_{\rm sat}P/P_{\rm thr}$, where $n_{\rm sat} = 1/\beta$ is called the saturation photon number (the photon number that characterises when the nonlinearity of the gain medium kicks in). The agreement between the theory and simulations is good, indicating that the model works. Note that the distribution is not Poisson in the above-threshold cases. This discrepancy is negligible for $P/P_{\rm thr} >> 1$, however. The exact values of mean and variance depends on the laser model, especially on the pumping mechanism.

[3] This amounts to assuming that the lower level is unpopulated for all times. See the second paragraph below (7.75) in [10].

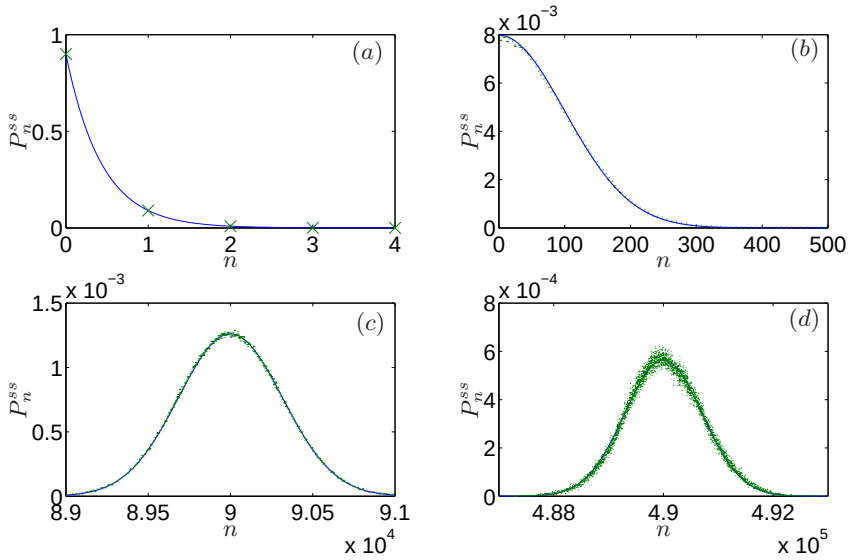

Figure 3.1: Photon number distributions for various pump parameters with $\beta = 0.0001$. Solid (blue) curves are analytical values, crosses (green) and dotted curves are results from numerical simulations. The values of P/P_{thr} are (a) 0.1, (b) 1.0, (c) 10.0, (d) 50.0.

3.3 Laser-qubit interaction

We now include a qubit in the picture, which is driven by a laser field described within the model developed in the previous section. The cascaded open systems approach [46] provides a natural description of this system, as it explicitly takes into account the one-way coupling between the laser source and the qubit. Figure 3.2 depicts the system schematically. The forward channel is defined by the laser mode, which focuses at the target and subsequently spreads. The amount it spreads is determined by the amount of focusing: the more the laser field is focused the more it spreads. The remaining modes are collectively called the side channel; these modes only obtain light through spontaneous emission from the qubit. This is a very simplified model but agrees with the more complete three-dimensional model studied by van Enk [61], where, in essence, it is the electric dipole mode of the laser beam that couples most strongly to the atom (which emits in the dipole mode), and the one-dimensional cascaded model follows if one assumes that the laser is focused onto the atom in one half of the dipole mode (that impinging from the left hand

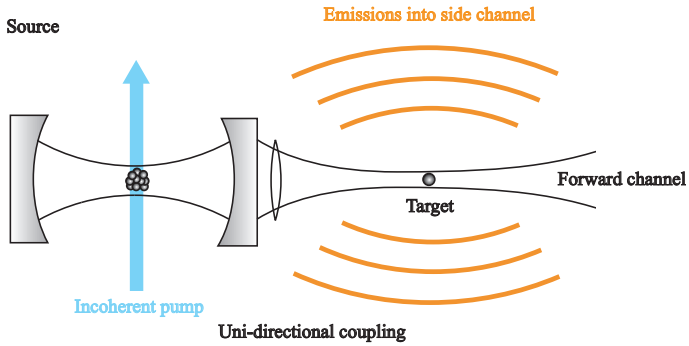

Figure 3.2: Schematic illustration of laser-qubit interaction.

side).[4] Of course, no laser actually emits in the dipole mode, but our simple model is sufficient for our purpose.

The master equation for this system (in the interaction picture) is

$$\dot{\rho} = (\mathcal{L}_S + \mathcal{L}_T + \mathcal{L}_{ST})\rho, \tag{3.4}$$

where

$$\mathcal{L}_T = \mathcal{D}[J_s], \qquad \mathcal{L}_{ST} = -i[H_{ST}, \cdot\,] + \mathcal{D}[J_f],$$

with

$$J_s = \sqrt{\gamma_T^s}\, b, \qquad J_f = \sqrt{\gamma_S}\, a + \sqrt{\gamma_T^f}\, b,$$

where b is the lowering operator for the target and

$$H_{ST} = i\frac{1}{2}\sqrt{\gamma_S \gamma_T^f}(a^\dagger b - a b^\dagger);$$

$\gamma_T = \gamma_T^f + \gamma_T^s$ is the total spontaneous emission rate of the target qubit, where γ_T^s and γ_T^f are the spontaneous emission rates into the side channel and the forward channel respectively. We have assumed the central cavity frequency to be equal to the atomic frequency. $\mathcal{L}_S$ is the superoperator for the source, defined in (3.2). The

[4] As noted in [61], only $\gamma_s/\gamma_t \leq 1/2$ ($|\eta| \geq 2$ in the notation of that reference) is allowed in our model, because laser beams travel in a specific direction. See below (3.4) for the definitions of the symbols.

one-way coupling nature can be seen easily by writing down $\mathcal{L}_{ST}$ explicitly:

$$\begin{aligned}\mathcal{L}_{ST} =& \frac{1}{2}\sqrt{\gamma_S\gamma_T^f}\left[\left(a^\dagger b - ab^\dagger - a^\dagger b - ab^\dagger\right)\cdot - \cdot\left(a^\dagger b - ab^\dagger + a^\dagger b + ab^\dagger\right)\right] \\ &+ \sqrt{\gamma_S\gamma_T^f}\left(b\cdot a^\dagger + a\cdot b^\dagger\right) + \mathcal{D}\left[\sqrt{\gamma_s}a\right] + \mathcal{D}\left[\sqrt{\gamma_T^f}b\right], \\ =& \sqrt{\gamma_S\gamma_T^f}\left(a\cdot b^\dagger - ab^\dagger\cdot + b\cdot a^\dagger - \cdot a^\dagger b\right) + \mathcal{D}\left[\sqrt{\gamma_S}a\right] + \mathcal{D}\left[\sqrt{\gamma_T^f}b\right]. \end{aligned} \tag{3.5}$$

At this point it is convenient to redefine the superoperators so that

$$\dot{\rho} = (\mathcal{L}_S^{'} + \mathcal{L}_T^{'} + \mathcal{L}_{ST}^{'})\rho, \tag{3.6}$$

where

$$\mathcal{L}_S^{'} = \mathcal{L}_S + \mathcal{D}\left[\sqrt{\gamma_S}a\right], \tag{3.7}$$

$$\mathcal{L}_T^{'} = \mathcal{D}\left[\sqrt{\gamma_T}b\right], \tag{3.8}$$

$$\mathcal{L}_{ST}^{'} = \sqrt{\gamma_S\gamma_T^f}\left(a\cdot b^\dagger - ab^\dagger\cdot + b\cdot a^\dagger - \cdot a^\dagger b\right). \tag{3.9}$$

In this form one can see that the a's appear only to the left of density operators and the $a^\dagger$s only to the right, apart from the $a^\dagger a$'s in the Lindblad term. That means photons are only *taken* from the first cavity and are not put back into it by the interaction, i.e., the interaction is one-way (the Lindblad term only describes the decay of the field). This fact suggests that the coherent states, as eigenstates of a, should play an important role, which indeed they do, as we will show later when we discuss state separability between source and target.

3.4 Quantum trajectories for resonance fluorescence

To prove the validity of the laser model even when it drives a qubit, we reproduce the familiar results of resonance fluorescence. We show that the mean polarization and inversion, the spectrum, and the intensity correlation function all agree with the usual results derived with a c-number description of the laser field (see for e.g. Ch. 2 of [10]).

The reader has met all the jump operators earlier. They are summarized in Table 3.1. M is the total number of quanta, $\mathrm{M} = a^\dagger a + b^\dagger b + c^\dagger c$, where c is the annihilation operator for carriers. The last column of the table shows the change in M for each jump process. By keeping track of M one can get rid of mode c in the

description, because $\mathrm{M} = n_a + n_b + n_c$. This helps by reducing the dimensionality of the Hilbert space. Lastly we would like to point out that when all the detectors are ideal (so that no information is lost), initially pure states remain pure throughout the evolution of a trajectory.

Jump operators	Description	Operator expression	Δ M
$\mathcal{J}_P$	laser pumping	$\sqrt{P}\frac{1}{\sqrt{c^\dagger c}}c^\dagger$	+1
$\mathcal{J}_{\mathrm{las}}$	emission into the laser mode	$\sqrt{\beta}a^\dagger c$	0
$\mathcal{J}_{\mathrm{em}}$	emission into modes other than the laser mode	$\sqrt{1-\beta}c$	-1
$\mathcal{J}_f$	scattering into the forward channel	$\sqrt{\gamma_S}a + \sqrt{\gamma_T^f}b$	-1
$\mathcal{J}_s$	scattering into the side channel	$\sqrt{\gamma_T^s}b$	-1

Table 3.1: Jump operators for quantum trajectories of the laser-qubit system.

The between-jump evolution is described by the non-Hermitian Hamiltonian

$$\begin{aligned} H_{\mathrm{n.H.}} &= -i\hbar\frac{1}{2}\left(\mathcal{J}_P^\dagger\mathcal{J}_P + \mathcal{J}_{\mathrm{las}}^\dagger\mathcal{J}_{\mathrm{las}} + \mathcal{J}_{\mathrm{em}}^\dagger\mathcal{J}_{\mathrm{em}} + \mathcal{J}_f^\dagger\mathcal{J}_f + \mathcal{J}_s^\dagger\mathcal{J}_s - \sqrt{\gamma_S\gamma_T}a^\dagger b\right), \\ &= -i\hbar\frac{1}{2}\left(\gamma_S a^\dagger a + \gamma_T b^\dagger b + P + \beta a a^\dagger c^\dagger c + (1-\beta)c^\dagger c + 2\sqrt{\gamma_S\gamma_T}ab^\dagger\right). \quad (3.10) \end{aligned}$$

One can generate quantum trajectories with these operators and calculate the known quantities from previous resonance fluorescence calculations. The usual description of resonance fluorescence assumes that the laser field can be described by a c-number, so only the qubit is described quantum mechanically. In contrast the trajectory model produces conditioned states of the form $(c_g(t)|n\rangle|g\rangle + c_e(t)|n-1\rangle|e\rangle)\otimes|M-n\rangle$ at a given time (assuming that the initial state was in a pure state with fixed number of photons and carriers and a fixed atomic state). Thus in the trajectory model the phase relationship between the atomic states, $|g\rangle$ and $|e\rangle$, is preserved in the form of entanglement. The entanglement means that the reduced density matrix for the atom is diagonal in the atomic states, i.e., there is no atomic coherence. One therefore has to be careful when calculating the atomic polarization, since $\mathrm{tr}[\rho_{REC}b] = 0$, where ρ_{REC} is the conditioned density matrix; one needs to calculate

a mutual property between the source and the atom. One formula that works is $\sum_{REC} P(REC) \left(\mathrm{tr}[\rho_{REC} a^\dagger b] / \sqrt{\mathrm{tr}[\rho_{REC} a^\dagger a]} \right)$. One can think of the $a^\dagger$ part as providing a phase reference, which, operationally, is always provided by the exciting laser in an experiment.

Figure 3.3 shows the results from the simulations and known analytical formulae (see p 57 of [10]) for the atomic polarization and inversion in the steady state. To characterize the laser field amplitude we introduce the parameter $Y = \sqrt{2}\Omega/\gamma_T$, where Ω is the Rabi frequency, which in our model is equal to $2\sqrt{\gamma_S \gamma_T^f \bar{n}}$, with average photon number $\bar{n}$. As one can see, the quantum trajectory simulations with the explicit laser model produce the same results as the analytical results derived using the c-number description of the laser field.[5] We now plot spectra and intensity correlation functions to check further the validity of the model.

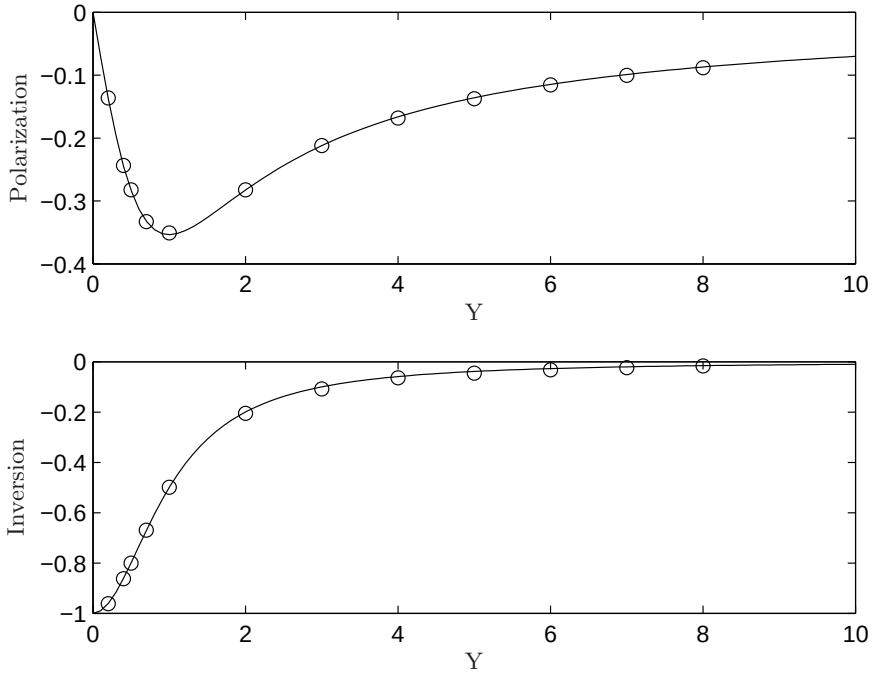

Figure 3.3: Numerical (circles) and analytical (solid line) results for polarization (above) and inversion (below) of resonance fluorescence. The parameters $\beta = 0.001$, $\gamma_T = 1.0$, and $\gamma_T^f = 0.0002$ have been used, with varying values of γ_S to ensure $\bar{n} >> 1$.

[5]The two models agree with each other as long as $\bar{n} >> 1$.

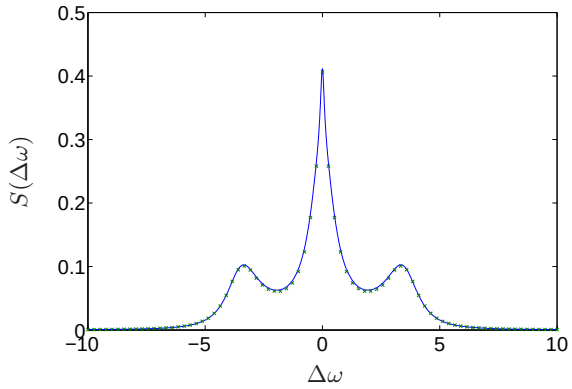

Figure 3.4: Numerical (crosses) and analytical results for the resonance fluorescence spectrum (side channel). The parameters $Y = 5$, $\beta = 0.001$, $\gamma_S = 0.002$, $\gamma_T = 1.0$, $\gamma_T^s = 0.9$, and $\Gamma = 0.1$ have been used.

The optical spectrum is plotted in Fig. 3.4, where the crosses are calculated numerically, using quantum trajectories, and the solid line is the analytical result. The scanning interferometer method described in Sect. 19.3 of [17] has been used to calculate the spectrum numerically. In this method a small portion of light in the side channel is deflected using a beam splitter, and a scanning interferometer with half-width Γ is placed in the deflected field. Then the number of photons inside the cavity is proportional to the optical spectrum, with Γ added to the half-width. The analytical parts have been calculated also by adding the half-width Γ to the coherent and incoherent parts of the spectrum derived using the coherent state assumption.[6]

Now to the steady state intensity correlation function $g_{ss}^{(2)}$. We start with $g_{ss}^{(2)}$ at the side channel because its analytical expression is well known. The top figure in Fig. 3.5 shows both the numerical and analytical results. The agreement is excellent. The figure below shows $g_{ss}^{(2)}$ measured in the forward channel. The analytical curve has been calculated from the definition

$$g_{ss}^{(2)}(\tau) = \left\langle J_f^\dagger(0) J_f^\dagger(\tau) J_f(\tau) J_f(0) \right\rangle_{ss} / \left\langle J_f^\dagger J_f \right\rangle_{ss}^2, \tag{3.11}$$

together with $J_f = \sqrt{J_S}\alpha + \sqrt{\gamma_T^f} b$. Hopefully the reader is by now convinced that our laser model works just like the one assuming a coherent state for the laser. In the

[6] If one uses a c-number to describe the laser, one obtains a delta function (zero laser linewidth) for the coherent part of the spectrum. Our laser model produces a non-zero linewidth, but this value is expected to be very small when the laser cavity linewidth is very small and the mean photon number very big (for e.g. see p 346 of [10]).

next section we prove that the decoherence rate of the qubit is fully determined by the spontaneous emission rate for the birth-death model, even though entanglement exists between the source and the qubit during a single trajectory, the same result as was obtained for the coherent state model of the laser.

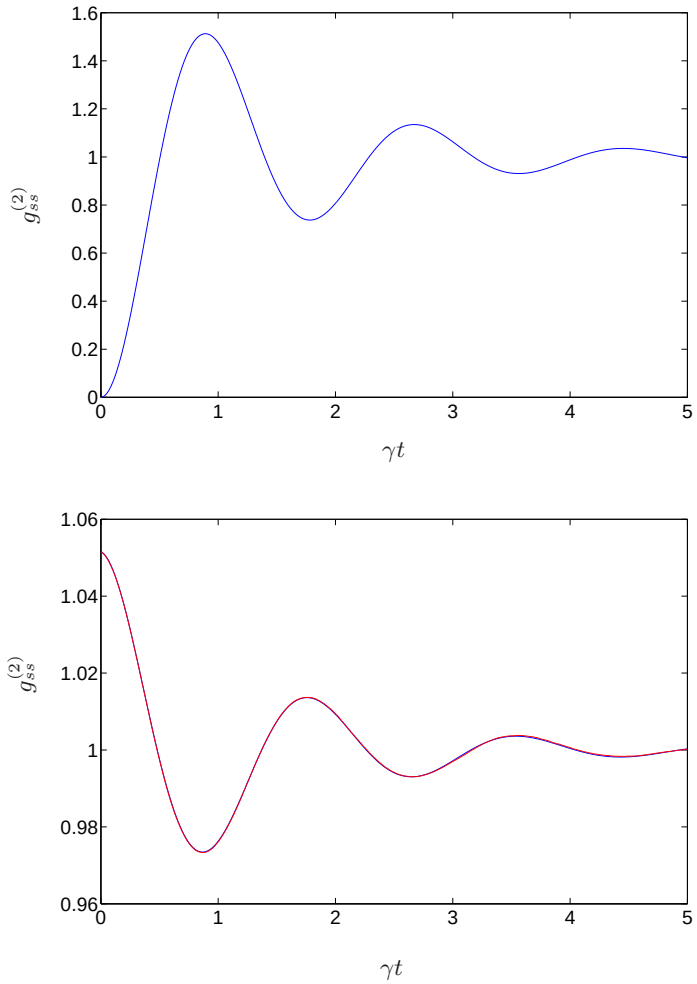

Figure 3.5: Numerical and analytical results for the steady state intensity correlation function in the side (top) and forward (bottom) channels. The parameters $Y = 5$, $\beta = 0.001$, $\gamma_S = 0.002$, $\gamma_T = 1.0$, and $\gamma_T^s = 0.6$ have been used.

3.5 Decoherence

Now to the main topics mentioned at the start of this chapter. Decoherence due to the quantum nature of a laser and the closely related issue of entanglement between the source and target are addressed in this section. In the next section we briefly discuss the quantum state of the laser.

Let us assume that the system starts from the ground state, i.e., with zero photons in the laser mode and zero carriers, and the qubit in the ground state. Then the state at any time t during the evolution of a single trajectory takes the form $c_g(t)|n\rangle|g\rangle|M-n\rangle + c_e(t)|n-1\rangle|e\rangle|M-n\rangle$ as we have mentioned above. The source is entangled with the qubit, and this could result in additional decoherence on top of the qubit spontaneous emission. At this level, there seems to be additional decoherence, because if one traces out the source there is no coherence whatsoever between the ground and excited states of the qubit (as we have already noted when we talked about atomic polarization). However, it will be shown in a short while that the total decoherence rate is still accounted for by the spontaneous emission rate.

We first show, following the work of Nha and Carmichael [45], that when a coherent state is used for the laser, all decoherence of the qubit is accounted for through spontaneous emission. We adopt a model Hamiltonian for generating a coherent state:

$$H_L = i\hbar\frac{\gamma_S}{2}(\lambda(t)a^\dagger - \lambda^*(t)a), \tag{3.12}$$

where $\lambda(t)$ is the complex amplitude of a time-dependent classical current driving the laser mode. Then $\mathcal{L}_S^{'}$ in (3.7) becomes

$$\mathcal{L}_S^{'} = \frac{1}{i\hbar}[H_L, \cdot] + \mathcal{D}\left[\sqrt{\gamma_S}a\right]. \tag{3.13}$$

It follows that the density operator factorizes into source and target parts:

$$\rho = |\alpha(t)\rangle\langle\alpha(t)| \otimes \rho_T(t), \tag{3.14}$$

with $\alpha(t)$ satisfying the equation

$$\dot{\alpha}(t) = \frac{\gamma_S}{2}(\lambda(t) - \alpha(t)). \tag{3.15}$$

The master equation for the source part can be written as[7]

$$\frac{d|\alpha(t)\rangle}{dt} = \left(\dot{\alpha}(t)a^\dagger - \frac{1}{2}\frac{d}{dt}|\alpha(t)|^2\right)|\alpha(t)\rangle, \tag{3.16}$$

and the target part as (see (3.6), (3.8), and (3.9))

$$\dot{\rho}_T = \frac{1}{i\hbar}[H_{eff}, \rho_T] + \mathcal{D}[\sqrt{\gamma_T}b]\rho_T, \tag{3.17}$$

where $H_{eff} = i\hbar\sqrt{\gamma_S\gamma_T^f}\left[\alpha^*(t)b - \alpha(t)b^\dagger\right]$. Now one sees that the target qubit decoheres only through the spontaneous emission described by the term $\mathcal{D}[\sqrt{\gamma_T}b]$, because the first term on the r.h.s is unitary and acts only on the qubit state. One can extend this analysis to a broader range of laser models; the result holds as long as the source is classical (in the sense of having a positive-definite Glauber-Sudarshan P function) and the description is coarse-grained (pumping details discarded), as we will show presently, following the work in [62].

3.5.1 Source-target separability

We propose that one can write the density operator in a separable form (after tracing over the carrier degree of freedom—i.e. coarse graining)

$$\rho(t) = \int dz P(z)|\alpha_z\rangle\langle\alpha_z| \otimes \rho_{T|\alpha_z}(t) \equiv \left\langle |\alpha_z\rangle\langle\alpha_z| \otimes \rho_{T|\alpha_z}(t)\right\rangle. \tag{3.18}$$

The target density operator is now conditioned upon a particular stochastic path followed by the laser amplitude, α_z, where z is a parameter labelling a stochastic path and $P(z)$ is the probability density for a particular trajectory α_z. Note that a stochastic description is necessary to separate the dynamics of the source and target, because the target dynamics is not Markovian. The integral (angled brackets) in the above equation then denotes the ensemble average over all stochastic paths. We will show that this *ansatz* does, indeed, solve the master equation. From (3.6), the

[7] This equation can readily be obtained by considering the displacement operator that generates the coherent state from the vacuum.

master equation can now be written as

$$\left\langle \frac{d|\alpha_z\rangle\langle\alpha_z|}{dt} \otimes \rho_{T|\alpha_z}(t) + |\alpha_z\rangle\langle\alpha_z| \otimes \frac{d}{dt}\rho_{T|\alpha_z}(t) \right\rangle$$
$$= \left\langle \mathcal{L}_S^{'}\left(|\alpha_z\rangle\langle\alpha_z|\right) \otimes \rho_{T|\alpha_z}(t) + |\alpha_z\rangle\langle\alpha_z| \otimes \mathcal{L}_T^{'}\rho_{T|\alpha_z}(t) + \mathcal{L}_{ST}^{'}\left(|\alpha_z\rangle\langle\alpha_z| \otimes \rho_{T|\alpha_z}(t)\right) \right\rangle \tag{3.19}$$

Here, the one-way nature of the interaction and the special status of coherent states (as eigenstates of an annihilation operator) play an important role, namely

$$\mathcal{L}_{ST}^{'}|\alpha_z\rangle\langle\alpha_z| \otimes \rho_{T|\alpha_z}(t) = |\alpha_z\rangle\langle\alpha_z| \otimes \sqrt{\gamma_S\gamma_T^f}[\alpha_z^* b - \alpha_z b^\dagger, \rho_{T|\alpha_z}(t)]. \tag{3.20}$$

Thus, one can rewrite (3.19) as

$$\left\langle \frac{d|\alpha_z\rangle\langle\alpha_z|}{dt} \otimes \rho_{T|\alpha_z}(t) + |\alpha_z\rangle\langle\alpha_z| \otimes \frac{d\rho_{T|\alpha_z}(t)}{dt} \right\rangle = \left\langle \mathcal{L}_S^{'}\left(|\alpha_z\rangle\langle\alpha_z|\right) \otimes \rho_{T|\alpha_z}(t) \right\rangle$$
$$+ \left\langle |\alpha_z\rangle\langle\alpha_z| \otimes \left(\mathcal{L}_T^{'}\rho_{T|\alpha_z}(t) + \sqrt{\gamma_S\gamma_T^f}[\alpha_z^* b - \alpha_z b^\dagger, \rho_{T|\alpha_z}(t)] \right) \right\rangle. \tag{3.21}$$

It is now easy to see that the master equation is separable. For a particular choice of α_z, the source dynamics must obey

$$\left\langle \frac{d|\alpha_z\rangle\langle\alpha_z|}{dt} \otimes \rho_{T|\alpha_z}(t) - \mathcal{L}_S^{'}|\alpha_z\rangle\langle\alpha_z| \otimes \rho_{T|\alpha_z}(t) \right\rangle = 0, \tag{3.22}$$

and the target dynamics follows through the equation

$$\frac{d\rho_{T|\alpha_z}(t)}{dt} = \mathcal{L}_T^{'}\rho_{T|\alpha_z}(t) + \sqrt{\gamma_S\gamma_T^f}[\alpha_z^* b - \alpha_z b^\dagger, \rho_{T|\alpha_z}(t)]., \tag{3.23}$$

which is the standard master equation of resonance fluorescence in a classical field of amplitude α_z. Equation (3.22) dictates the form taken by $\mathcal{L}_S^{'}$; it follows from coarse graining and assumed classicality of the source, which suggests that the laser dynamics can be described by a Fokker-Planck equation. Then one can derive an explicit expression of $\mathcal{L}_S^{'}$ for a given laser model, as following work shows.

An explicit expression for $\mathcal{L}_S^{'}$

The fact that one can describe a laser source with a positive-definite P distribution means that the source dynamics follows a Fokker-Planck equation. To do this one needs an explicit model as a starting point. We begin from a birth-death model related to Scully-Lamb theory of laser which yields the following Fokker-Planck equation [10].[8]

$$\begin{aligned}\frac{\partial P(\alpha,\alpha^*,t)}{\partial t} =& \frac{\gamma_S}{2}\left[\left(\frac{\partial}{\partial\alpha}\alpha+\frac{\partial}{\partial\alpha^*}\alpha^*\right)\left(1-\frac{P}{P_{\rm thr}}+\frac{P}{P_{\rm thr}}\frac{|\alpha|^2}{n_{\rm sat}}\right)\right.\\ &\left.+2n_{\rm spon}\frac{\partial^2}{\partial\alpha\partial\alpha^*}\right]P(\alpha,\alpha^*,t),\end{aligned} \tag{3.24}$$

where $n_{\rm spon}$ is the number of photons in the laser mode due to spontaneous emission well below threshold, responsible for fluctuations. One can write down the Ito stochastic differential equation equivalent to it as (see [33])

$$d\alpha_z = -\frac{\gamma_S}{2}\alpha_z\left(1-\frac{P}{P_{\rm thr}}+\frac{P}{P_{\rm thr}}\frac{|\alpha|^2}{n_{\rm sat}}\right)dt+\sqrt{\gamma_S n_{\rm spon}}dZ. \tag{3.25}$$

This equation must be consistent with (3.22) if the $\mathcal{L}_S^{'}$ is to describe the classical source correctly. To find the $\mathcal{L}_S^{'}$ that is consistent with (3.22), we write

$$|\alpha_z\rangle\langle\alpha_z| = e^{\alpha_z a^\dagger-\alpha_t^* a}|0\rangle\langle 0|e^{-\alpha_z a^\dagger+\alpha_t^* a}, \tag{3.26}$$

and then

$$d\left(|\alpha_z\rangle\langle\alpha_z|\right) = e^{d\alpha_z a^\dagger-d\alpha_t^* a}|\alpha_z\rangle\langle\alpha_z|e^{-d\alpha_z a^\dagger+d\alpha_t^* a}. \tag{3.27}$$

Because (3.22) appears inside the stochastic integral, one can expand the exponentials in (3.27) and invoke the Ito rule—$\overline{dZ^*dZ}=dt$, $\overline{dZdZ}=\overline{dZ^*dZ^*}=0$.[9]—and

[8] The birth-death model used in this thesis, being a birth-death model, will give an equivalent Fokker-Planck equation in thermodynamic limit, i.e., large photon and carrier numbers.

[9] See [33]. The overbars denote averaging inside the integral.

ignore the higher order terms to write

$$\left\langle d\left(|\alpha_z\rangle\langle\alpha_z|\right)\otimes\rho_{T|\alpha_z}(t)\right\rangle = \left\langle \left\{-i[H_{\alpha_z},|\alpha_z\rangle\langle\alpha_z|] + \left(\mathcal{L}_{\text{noise}}+\mathcal{D}\left[\sqrt{\gamma_S}a\right]\right)|\alpha_z\rangle\langle\alpha_z|\right\}\otimes\rho_{T|\alpha_z}(t)\right\rangle, \quad (3.28)$$

where

$$H_{\alpha_z} = i\frac{\gamma_S}{2}\frac{P}{P_{\text{thr}}}\left(1-\frac{|\alpha_z|^2}{n_{\text{sat}}}\right)\left(\alpha_z a^\dagger - \alpha_z^* a\right), \quad (3.29)$$

and

$$\mathcal{L}_{\text{noise}} = \gamma_S n_{\text{spon}}\left(a\cdot a^\dagger + a^\dagger\cdot a - \tfrac{1}{2}[a^\dagger a + aa^\dagger,\cdot]_+\right). \quad (3.30)$$

$[\cdot,\cdot]_+$ denotes an anticommutator. We have thus derived an explicit form of $\mathcal{L}_S^{'}$, namely

$$\mathcal{L}_S^{'}\cdot = -i[H_{\alpha_z},\cdot] + \mathcal{L}_{\text{noise}}\cdot + \mathcal{D}\left[\sqrt{\gamma_S}a\right]\cdot, \quad (3.31)$$

which must hold if the source is classical and obeys (3.24) after the coarse graining. Comparing with (3.7), one sees that $\mathcal{L}_S\cdot = -i[H_{\alpha_z},\cdot] + \mathcal{L}_{\text{noise}}\cdot$ for our model.

3.5.2 Section summary

Let us recap what has been said in this section. We have proved that as long as the source driving a target is classical and the internal degrees of the freedom are ignored, the master equation separates into source and target dynamics. To achieve this separation the description had to be in terms of individual trajectories followed by the source variable with the target states being conditioned on them. Physically, the dependence on the full trajectory arises because the target has some memory; to describe its dynamics one needs to know the history of the trajectory followed by the source field. Another crucial ingredient which allowed the separation is the cancellation of photon creation terms in the interaction part of the master equation. From the physics of cascaded systems this is obvious since photons are always *taken* from the source to be put into the target. Finally, note that (3.23) says that the total decoherence rate is governed by the spontaneous emission rate alone: the decoherence rate is governed by γ_T for all α_z. There is, in fact, another source of

decoherence not included in our description, namely the phase diffusion of the laser field. If one has no knowledge of how this phase is diffusing then the coherence of the qubit state will be lost in the laser phase-diffusion time. One does, however, have knowledge of the phase diffusion since one can use the laser itself as a phase reference. This part of the decoherence is describable in terms of the straightforward concept of classical correlation.[10] It need not be spoken about using the idea of entanglement.

3.6 Quantum state of a laser

The argument of the previous section can be inverted to give a privileged role to the coherent states when assigning the laser quantum state. The bottom line is that if a pair of systems are entangled, they cannot be thought of as being separate entities, each therefore having a state. Thus, we propose that the criterion for assignment of any state to a laser is for the laser to have a well-defined state at all times, separable from the state of its illuminated target. We have already proved that the coherent state does just this. That it is the only state, i.e., the *unique* state, that allows the separability at all times can be seen easily by considering quantum trajectories; certainly any state other than the coherent state would change its identity when the photodetector in the forward channel clicks. The coherent state is thus the only state that satisfies the proposed criterion, and we propose that it be assigned as the laser quantum state [56].

[10] A quantitative account of phase diffusion was first given in [63]. Also see [10] Ch. 8.

Chapter 4

Entanglement measures

In the previous chapter we have shown that a laser source and its target are entangled in the QTT (quantum trajectory theory) description. In this chapter, we investigate further the question of entanglement between a driven qubit and the field scattered from it. In fact, as was mentioned earlier, this question was raised in the work of Nha and Carmichael [45], where they argued that the field scattered into the forward channel and the qubit are entangled. This entanglement is inferred from the quantum trajectory description. Quantum trajectories work by disentanglement—entanglement between a system and its environment (the qubit and the scattered field) is turned into correlations, via detections, between the measurement results and the conditioned state. Then, certainly, the scattered field is entangled with the qubit, since the scattered record is correlated with the (conditioned) state of the qubit. Initial steps towards understanding this entanglement are taken in this chapter. We start by giving an introduction to conventional measures of quantum entanglement, then a measure defined through QTT [23]; we take the attitude that since the entanglement is inferred through QTT, we should use a measure defined within it. We then briefly talk about entanglement between a laser and its target, before we study entanglement between a spontaneously emitting qubit and its emitted field. After a little excursion on qubit state transfer, we finally tackle the question of entanglement between a laser-driven qubit and its radiated field.

4.1 Basics

Since the discovery of Einstein, Podolsky, and Rosen (EPR) [18], quantum entanglement has led to two revolutionary ideas, both mentioned in Ch. 1. The first,

discovered by John Bell, is that entangled states can have correlations stronger than those allowed by any local realistic theory (often called a local hidden variable theory).[1] This work is important in that it ruled out a whole class of local realistic theories, which Einstein hoped would replace quantum mechanics one day. The second revolutionary idea came from Charles Bennett and co-workers who realized that quantum entanglement provides a resource for quantum information processing and quantum computing.[2]

The second revolution has led physicists to search for a quantitative measure of entanglement. The main interest of people working in the field of quantum information is how useful a given entangled system is for quantum information processing. For bipartite systems (which we will stick to in this chapter) the standard is provided by the singlet state (any one of the four Bell-states will do, but the singlet state is the usual choice), called the ebit. The purpose of this chapter is to investigate an alternative point of view on quantum entanglement based on QTT for bipartite systems. This approach, explained below, was first introduced by Nha and Carmichael [23]. We begin by going over a few basic information-theoretic measures of entanglement, followed by explicit evaluations of the 'Entanglement of Formation' (defined in the following subsection) and a QTT measure of entanglement called 'Contextual Entanglement' (defined in Sect. 4.1.2) for two simple bipartite systems.

4.1.1 Conventional entanglement measures

For pure bipartite states the measure of entanglement is given by the entropy of entanglement (EE) [66]. It is defined as the von Neumann entropy of the (either) reduced density operator:

$$S(\rho) = -\mathrm{Tr}\rho_A \log_2 \rho_A = -\mathrm{Tr}\rho_B \log_2 \rho_B, \tag{4.1}$$

where ρ_A and ρ_B are the reduced density operators obtained by tracing over the system B and A respectively. EE measures the degree of randomness of the constituent systems. If the whole system is in a maximally entangled state, the constituents are described by completely random density operators, whereas if it is in a product state, the constituents are described by pure states, which have zero entropy. Furthermore, EE is actually the number of singlets needed to create a given state with

[1] For original papers of Bell see [2]. There have been many experimental verifications in favour of quantum mechanics (of course); one of the most famous was carried out by Aspect *et al.* [3].

[2] Familiar examples include quantum teleportation [5] and superdense coding [20]. See [64, 65] and references therein for more examples.

local operations and classical communications (LOCC) only, and also the number of singlets that can be concentrated out of the state [66], again with LOCC only.[3]

For mixed states there are many measures of entanglement. The problem with quantifying entanglement for a mixed state is that there are many equivalent decompositions of the density operator, and these have different average EEs. For example, a completely mixed state with $\rho = \frac{1}{4}I_4$ can be written either as a mixture of Bell states (with maximum entanglement), or as a mixture of product states (with no entanglement). For this reason conventional measures of entanglement are usually variational in nature, i.e., they involve finding the maximum or minimum over all possible states.

Three important measures of mixed-state entanglement are explained here; for a comprehensive survey the reader may consult [67]. The first is called the entanglement of formation (EF). It is defined as the minimal possible average EE over all pure state decompositions [68]. If EF satisfies additivity,[4] it gives, in the asymptotic sense defined in footnote 3, the number of pure singlets required to create a given state via LOCC only, c.f. the entanglement cost explained in [67]. The second measure is called the distillable entanglement (DE). It is the converse of EF: DE is the number of pure singlets that can be produced from a given state by LOCC (in the asymptotic sense). Interestingly, EF and DE are different in general but are both equal to EE for pure states. The third measure is called the relative entropy of entanglement (REE). It is defined in terms of the quantum relative entropy [69]

$$S(\rho||\sigma) = \mathrm{tr}\{\rho\log_2\rho - \rho\log_2\sigma\}, \tag{4.2}$$

which is a measure of distinguishability between the two states ρ and σ. REE is defined as the minimum relative entropy between a given state ρ and the set of all separable states. To see the meaning of REE it is useful to define the quantum mutual information

$$I(\rho_{AB}) = S(\rho_A) + S(\rho_B) - S(\rho_{AB}), \tag{4.3}$$

which measures the total (i.e. quantum + classical) correlations in ρ_{AB} by comparing

[3] These sentences are to be taken in the following asymptotic sense: if there are n copies of the state, EE gives the number of singlets per copy that are needed to create the state as $n \to \infty$ (similarly for the number of singlets concentrated).

[4] A function of a density operator ρ, $f(\rho)$, is said to be additive if $f(\rho_1 \otimes \rho_2) = f(\rho_1) + f(\rho_2)$.

ρ_{AB} with $\rho_A \otimes \rho_B$. Quantum mutual information can be written as

$$I(\rho_{AB}) = S(\rho_{AB}||\rho_A \otimes \rho_B). \tag{4.4}$$

In this light REE can be seen as trying to measure the quantum part of the correlations by comparing a given state with the closest classically correlated state.

These measures are very hard to calculate because of their variational nature, i.e., one needs to calculate over all possible sets of some sort. For a pair of qubits however, there exists a formula for evaluating EF [70, 71]. For this reason we only calculate EF in this chapter.[5]

4.1.2 Contextual entanglement based on quantum trajectories

Generally, a given mixed state has a combination of classical and quantum correlations. The classical part is completely useless for quantum information protocols such as quantum teleportation, which is why these measures try to quantify the quantum part of the correlations only. Here we take a different point of view following the work of Nha and Carmichael [23], which is summarized nicely in this excerpt from their paper:

> We observe that entangled states are pervasive in the quantum mechanics of composite systems, often arising in situations that have no immediate quantum information connection. With the aim of understanding entanglement in this broader sense, we propose to explore, rather than discard, the multiplicity of mixed state decompositions. The ambiguity arising in the multiplicity is viewed as a signature of complementarity, i.e., an expected feature that reflects the very essence of a quantum-mechanical description.

Thus we look at entanglement not as a resource, but some kind of information given to us by experiments. Entanglement is not really an observable since it depends on how the density operator is decomposed. In QTT, different unravelings correspond to different experimental situations and give different information. Assuming ideal detections the state is pure at all times (given a pure state initially), so the trajectory average of EE can be used to quantify entanglement as proposed in [23]. We call this measure of entanglement contextual entanglement (CE). CE gives an upper limit on EF although it is not an efficient way for the purpose of evaluating EF, nor is it

[5] Very recently a closed formula for the REE for two qubits has also been found [72].

clear that the decomposition giving EF can be obtained by an (idealized) physical experiment (i.e., giving a particular family of quantum trajectories). CE can be used for other purposes. For example, reversing the argument, it can determine how good a particular measurement scheme is in making a distinction between the constituent systems. The higher its value, the less the distinguishability. In this view, the measurement scheme that gives EF is the scheme that gives maximal distinction. CE has been applied to a cascaded qubit system to deduce that in some operating regime the system undergoes a cycle between maximally entangled states, the phenomenon which has been dubbed 'entangled-state cycle' [73]. See also [74] for 'entangled-state cycles' of atomic collective-spin states. The introduction and conclusions of [73] contain good discussions on the limitations of quantum information-theoretic approaches to entanglement quantification, in line with and supporting the point of view we take in this chapter. Finally, note that CE reduces to EE for closed systems, as do all the other measures introduced earlier.

4.2 Entanglement between the laser and qubit

We want to use EF and CE to understand the entanglement between the scattered field and the qubit for the resonance fluorescence system in Ch. 3. Before we jump into the topic, however, it will be interesting to calculate both measures for some simple systems. The first system is actually the resonance fluorescence system, but we calculate the entanglement between the laser source and qubit. Consider the laser to be described by the birth-death model of Sect. 3.2. Then the conditioned state of the laser and qubit at an arbitrary time has the form $|\psi_{\rm REC}\rangle = (c_g|n\rangle|g\rangle + c_e|n-1\rangle|e\rangle) \otimes |M-n\rangle$ which has nonzero EE between the laser source and target. On the other hand, it is clear from the work in Ch. 3 that the EF for this system is zero (EF is zero for separable states).

Figure 4.1 shows the CE for various values of Y. The CE is calculated by tracing out the carrier degree of freedom first—which leaves a pure state of the form $|\psi_{\rm REC}\rangle = c_g|n\rangle|g\rangle + c_e|n-1\rangle|e\rangle$—and calculating the EE of the resulting state. As long as the average number of photons in the laser cavity is large, i.e., $\bar{n} >> 1$, the CE remains the same within sampling fluctuations for a fixed value of Y. That is, varying other parameters such as the degree of focusing or laser cavity linewidth while fixing Y does not change the CE. As Y is increased, the fraction of time spent in the excited state increases, which means that the c_e is bigger on average. However, it also means that the rate of spontaneous emission is larger. Since every

spontaneous emission destroys entanglement, there is a tradeoff between the two effects and the maximum value of the CE is situated around $Y = 1$. For a large value of Y, the qubit spends about half the time in the excited state and the CE is more or less constant. This value of CE can be found by assuming that c_g and c_e execute the Rabi oscillation, i.e., neglecting spontaneous emission, and calculating the EE. For $Y = 8$ the number thus calculated gives 0.5571, which is quite close to the simulated value 0.5617.

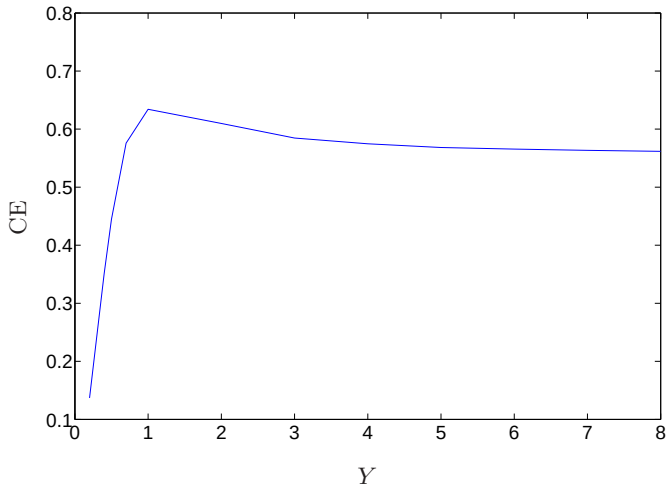

Figure 4.1: Contextual entanglement (for a photon counting setup) versus Y for $\bar{n} >> 1$.

Note that for this system the state of the qubit is taken at a later time to that of the laser, where the time difference arises from retardation, i.e., the finite transit time of light traveling from the laser to the qubit; the entanglement is not between states at a given time.

The stark difference between EF and CE stems from differences in their approaches. EF takes the density operator and its evolution to be the complete story, i.e., it ignores the data made available in the environment, whereas CE uses this extra information to single out a particular unravelling of the density operator. In this case, the entanglement is generally not going to be useful in practice, but speaks about a level of fine quantum mechanical detail that is present in principle. It recovers detail that is discarded by simply tracing over the reservoir in an open system evolution.

One can also envisage different trajectories with different measurement schemes,

comprised of homodyne-, heterodyne-, and photo-detectors; different combinations would generally yield different values of CE. Unfortunately homodyne or heterodyne measurements do not conserve the total number of quanta in the system, and as a consequence the Hilbert space of the laser mode increases proportional to the mean photon number. For a reasonable mean photon number, then, calculation of the CE takes a very long time. For this reason we do not compute the CE for homodyne or heterodyne detection here.

4.3 Entanglement in spontaneous emission

How can we quantify entanglement between a source and its radiated field? One way to do this is to place a filtering cavity in the scattered-field region and measure the entanglement between the source and the cavity mode. The scattered field is usually broadband, in which case one will vary the central frequency of the cavity and look at the entanglement along a range of frequencies. We call this measure the 'Entanglement Spectrum' (ES). In this light, the CE in the last section can be seen as measuring entanglement between a laser source and its field by placing a probe qubit (rather than a cavity) in the field region. Before we jump into the investigation of ES for a driven qubit, we study ES for a spontaneously emitting qubit first. The system comprises a two-level atom and a cavity, where the field radiated from the atom drives the cavity. The atom starts in the excited state and eventually goes through spontaneous emission; the emitted photon is made to impinge on the cavity, initially in the ground state. The cavity does not affect the atom directly—i.e., the coupling is one way. Clearly, this system is a limiting case of the driven qubit we are interested in and should provide some insight into that problem.

4.3.1 At resonance

The system described above is depicted in Fig. 4.2. The atom is replaced by a cavity. The two cavities have decay rates γ_a and γ_b, where the former corresponds to the natural linewidth of the atom. The beam splitter in the middle—with a reflection coefficient η—controls the amount of light coupled to the cavity; a and b are the cavity mode annihilation operators, and J_1 and J_2 are field operators whose explicit definitions are given in (4.6). The master equation for this system, in the interaction

picture, is

$$\dot{\tilde{\rho}} = \tfrac{1}{2}\sqrt{(1-\eta)\gamma_a\gamma_b}\left[(a^\dagger b - a b^\dagger), \tilde{\rho}\right] + \mathcal{D}\left[J_1\right]\tilde{\rho} + \mathcal{D}\left[J_2\right]\tilde{\rho}, \tag{4.5}$$

where $\mathcal{D}[J]$ is the Lindblad term given below (3.2), and

$$J_1 = \sqrt{\eta\gamma_a}a, \qquad J_2 = \sqrt{(1-\eta)\gamma_a}a + \sqrt{\gamma_b}b. \tag{4.6}$$

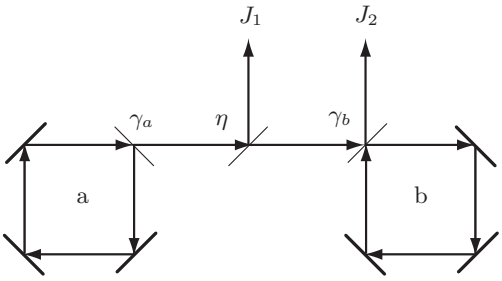

Figure 4.2: Schematic diagram of the spontaneously emitting qubit coupled into a cavity. Cavity a (the qubit) starts with 1 photon and cavity b with 0 photons.

For $\tilde{\rho}(0) = |10\rangle\langle 10|$ the solution to this master equation is readily found to be

$$\tilde{\rho}(t) = \begin{pmatrix} \delta(t) & 0 & 0 & 0 \\ 0 & \alpha(t) & \beta(t) & 0 \\ 0 & \beta(t) & \chi(t) & 0 \\ 0 & 0 & 0 & 0 \end{pmatrix}, \tag{4.7}$$

where

$$\alpha(t) = \frac{4(1-\eta)\gamma_a\gamma_b}{(\gamma_a-\gamma_b)^2}e^{-\gamma_b t}\left(1 + e^{(\gamma_b-\gamma_a)t} - 2e^{\frac{1}{2}(\gamma_b-\gamma_a)t}\right), \tag{4.8a}$$

$$\beta(t) = \frac{2\sqrt{(1-\eta)\gamma_a\gamma_b}}{(\gamma_b-\gamma_a)}e^{-\frac{1}{2}(\gamma_a+\gamma_b)t}\left(1 - e^{\frac{1}{2}(\gamma_b-\gamma_a)t}\right), \tag{4.8b}$$

$$\chi(t) = e^{-\gamma_a t}, \tag{4.8c}$$

$$\delta(t) = 1 - \alpha(t) - \chi(t). \tag{4.8d}$$

The matrix elements are $\delta(t) = \langle 00|\tilde{\rho}(t)|00\rangle$, $\alpha(t) = \langle 01|\tilde{\rho}(t)|01\rangle$, and $\chi(t) = \langle 10|\tilde{\rho}(t)|10\rangle$. Since this is a bipartite qubit system, the EF can be calculated analyt-

ically [70, 71]—it is plotted for various values of η in Fig. 4.3. As η is increased, less and less of the emitted field is coupled into the second cavity, so the EF decreases, until at $\eta = 1.0$ it is zero because there is no field coupled into the second cavity. As for the shape of each curve, the state begins and ends as $|10\rangle\langle 10|$ and $|00\rangle\langle 00|$, respectively, hence the EF is zero initially and tends to zero for long times (this happens after about $\gamma_a t = 5.0$ as can be seen from Fig. 4.3). The EF grows initially as the field enters the second cavity, but then decreases as the field leaks out of it. The maximum would occur at $\gamma_a t = \ln(2)$ (when half of the field has leaked out of the first cavity) were all the field captured in the second cavity, but because of the leakage it occurs somewhat later. The case where all the field is captured will be considered in the next section. Figure 4.4 shows the EF for various values of γ_b/γ_a and $\eta = 0$. It clearly shows that there is an optimal ratio γ_b/γ_a of between 3 and 5 ((d) – (f)), giving the maximum EF. This is because γ_b has two effects: it determines how short a time the field stays in the second cavity, and it also determines how much field enters the cavity in the first place. The two effects compete against each other, resulting in the optimal ratio. Also note that as γ_b increases, the maximum occurs earlier because the field leaks out of the second cavity faster.

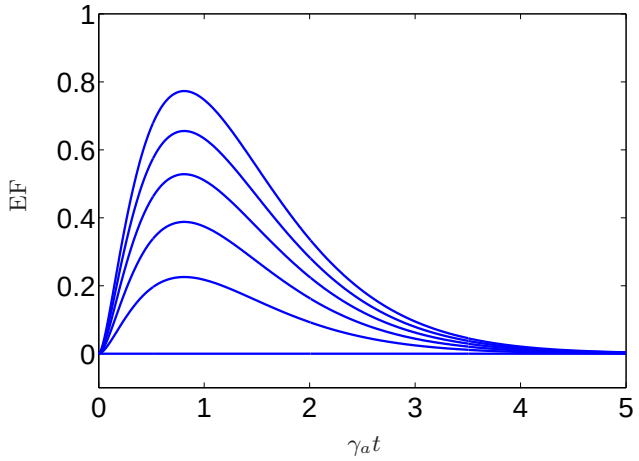

Figure 4.3: Entanglement of formation for the two-qubit spontaneous emission system, for $\gamma_b/\gamma_a = 2$ and $\eta = 0.0$, 0.2, 0.4, 0.6, 0.8, 1.0, from top to bottom.

CE can be calculated readily for the photon counting case, i.e., photodetectors placed at J_1 and J_2. In this case the non-Hermitian Hamiltonian for the quantum

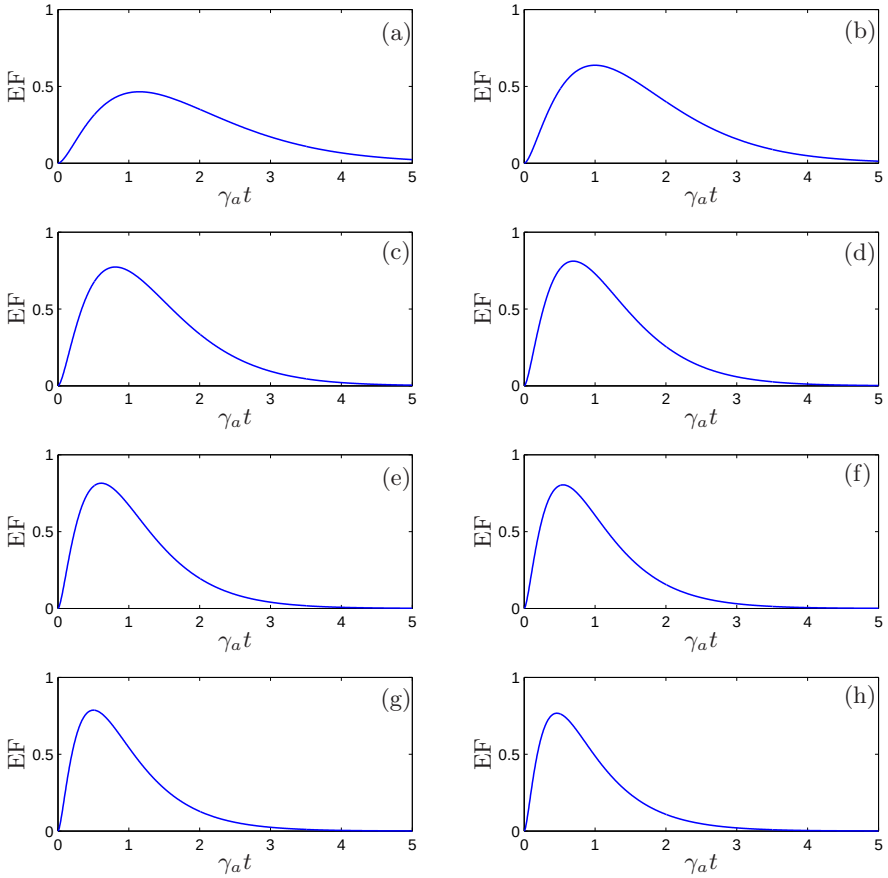

Figure 4.4: Entanglement of formation for the two-qubit spontaneous emission system, for $\eta = 0$ and $\gamma_b/\gamma_a = 0.5,\ 1, 2,\ 3,\ 4,\ 5,\ 6,\ 7$, from (a) to (h).

trajectories is

$$H_{\text{n.H.}} = i\hbar\left(-\frac{\gamma_a}{2}a^\dagger a - \frac{\gamma_b}{2}b^\dagger b - \sqrt{(1-\eta)\gamma_a\gamma_b}ab^\dagger\right), \tag{4.9}$$

which leads to the solution

$$|\psi_{\text{no}}(t)\rangle = \frac{1}{\sqrt{\alpha(t)+\chi(t)}}\left(\sqrt{\alpha(t)}|01\rangle + \sqrt{\chi(t)}|10\rangle\right) \tag{4.10}$$

for the initial state $|\psi_{\text{no}}(0)\rangle = |10\rangle$; $\alpha(t)$ and $\chi(t)$ are as defined in (4.8a) and (4.8c)

respectively. Whenever one of the detectors clicks there is no longer a photon in the system and the state is $|00\rangle$, which is the steady-state. CE for this case is simply the EE for $|\psi_{\rm no}(t)\rangle$ multiplied by the probability of having no clicks up to time t. The results are plotted in Fig. 4.5 for the same set of parameters as in Fig. 4.3. The CE is larger than the EF, as expected from the definition of EF; photon counting does not give the decomposition of the density operator that results in the minimum average EE. Also note that the tails in the plot of the CE are considerably longer than those of the EF. This can be explained from the following difference between the quantum trajectory and the master equation descriptions. In the quantum trajectory description, the conditioned state has a significant EE until the detector clicks, no matter how large the t, whereas in the master equation description the decay is uniform. Of course, the probability for having no click up to $\gamma_a t \approx 5$, say, is very small, which means we will not have too many trajectories that have non-zero EE at this time; nevertheless, the contribution from these trajectories is significant.

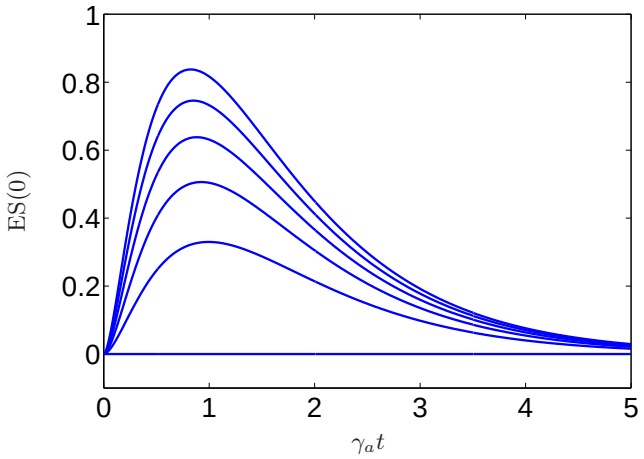

Figure 4.5: Contextual entanglement for the photon counting cases, for $\gamma_b/\gamma_a = 2$ and $\eta = 0.0$, 0.2 , 0.4, 0.6, 0.8, 1.0, from top to bottom.

Other measurement schemes

We now investigate what happens for other experimental setups. For simplicity we look at the $\eta = 0$ case only, thus removing J_1 from consideration. Photodetection, homodyne, and heterodyne measurements are the three most common measurements employed in quantum optics, so the natural candidates are homodyne and hetero-

dyne measurements. Figure 4.6 shows the CE for the three measurement schemes, together with the EF. The top three curves are the CE for photon counting, homodyne, and heterodyne measurements, reading from top to bottom, and the lowest one is of course the EF. Quantum trajectories for homodyne detection are generated

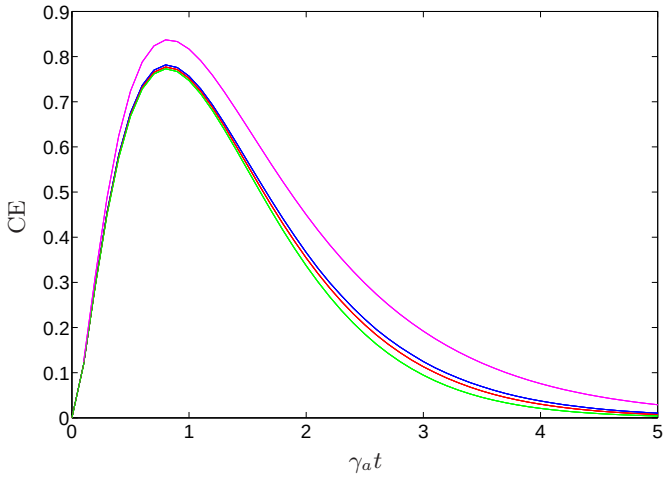

Figure 4.6: Contextual entanglement for the photon counting, homodyne, and heterodyne trajectories, and the entanglement of formation, from top to bottom. The parameters used are $\gamma_b/\gamma_a = 2$ and $\eta = 0.0$.

by the stochastic Schrödinger equation [17]

$$d|\psi_{\rm REC}\rangle = \left[\left(-\frac{\gamma_a}{2}a^\dagger a - \frac{\gamma_b}{2}b^\dagger b - \sqrt{\gamma_a\gamma_b}ab^\dagger\right)dt + \left(\left\langle e^{i\theta}J_2^\dagger + e^{-i\theta}J_2\right\rangle_{\rm REC}dt + dW\right)e^{-i\theta}J_2\right]|\psi_{\rm REC}\rangle, \tag{4.11}$$

where $|\psi_{\rm REC}\rangle$ is the unnormalized conditioned state, as in Ch. 18 of [17], dW is a Wiener increment, and θ is the angle that determines the quadrature to be measured by the homodyne detector. There is no preferred phase, so the CE is independent of θ and we choose $\theta = 0$. Similarly, the heterodyne trajectories are generated by [17]

$$d|\psi_{\rm REC}\rangle = \left[\left(-\frac{\gamma_a}{2}a^\dagger a - \frac{\gamma_b}{2}b^\dagger b - \sqrt{\gamma_a\gamma_b}ab^\dagger\right)dt + \left(\left\langle J_2^\dagger\right\rangle_{\rm REC}dt + dZ\right)J_2\right]|\psi_{\rm REC}\rangle, \tag{4.12}$$

where dZ is now a complex Wiener increment. The CE for the homodyne and heterodyne cases is much closer to the EF than in the photon counting case, which

means that the measurements distinguish the states of the individual cavity modes better than a photon counting measurement. Somehow the added local oscillator in homodyne (or heterodyne) detection has increased the distinguishability. Considering that a measurement tries to project the state into an eigenstate of the variable it is measuring, e.g., homodyne detection tries to project the state into a quadrature eigenstate, heterodyne into a coherent state, and of course photodetection into a Fock state, we have an intuitive idea as to why the heterodyne case gives the minimum and photodetection the maximum CE among the three. Heterodyne and homodyne schemes give the CE very close to the EF, meaning they are nearly the maximally distinguishing measurement schemes. It would be interesting to see if this is the case for other systems. Note that the tails of the CE are much shorter for homodyne and heterodyne detection than for the photon counting case, supporting the explanation given earlier about the long tails in the photon counting case.

4.3.2 On- and off-resonance

Now we allow the second cavity to be off-resonant with the first cavity (or spontaneously emitting qubit). This introduces an additional term $-i\Delta\omega[b^\dagger b, \tilde{\rho}]$ to the master equation (4.5). With this addition, (4.8a) and (4.8b) become

$$\alpha(t) = \left| \frac{\sqrt{4(1-\eta)\gamma_a\gamma_b}}{(\gamma_b + 2i\Delta\omega - \gamma_a)} e^{-\frac{1}{2}(\gamma_b+2i\Delta\omega)t} \left(1 - e^{\frac{1}{2}(\gamma_b+2i\Delta\omega-\gamma_a)t}\right)\right|^2 \tag{4.13}$$

and

$$\beta(t) = -\frac{\sqrt{4(1-\eta)\gamma_a\gamma_b}}{(\gamma_b + 2i\Delta\omega - \gamma_a)} e^{-\frac{1}{2}(\gamma_b+2i\Delta\omega+\gamma_a)t} \left(1 - e^{\frac{1}{2}(\gamma_b+2i\Delta\omega-\gamma_a)t}\right) \tag{4.14}$$

respectively. It is now an easy matter to calculate the ES for a given time t. Consider the solution $|\psi_{\rm no}(t)\rangle$ to the non-Hermitian Hamiltonian. From this solution one can calculate the EE—we will call this $E_{\rm no}(t)$. Now, because the system collapses to the ground state after a jump, and remains there, the entanglement is zero after the jump. Thus the ES is given by

$$\{\text{Probability to jump at time } t\} \times E_{\rm no}(t) = \langle\overline{\psi_{\rm no}}(t)|\overline{\psi_{\rm no}}(t)\rangle E_{\rm no}(t). \tag{4.15}$$

This is plotted in Fig. 4.7 as a function of $\Delta\omega$. Generally, over all frequencies, the ES increases for some time before decreasing again. On top of that there is

an oscillation (oscillation exists in the time domain also) whose frequency increases with time. Also, as expected, the maximum always occurs when $\Delta\omega = 0$. Figure 4.8 shows the ES and EF as a function of $\Delta\omega$ at $t = 1.0$. It shows the expected behaviour, i.e., the ES is smaller than the EF at all frequencies. Of course, this feature holds at all times.

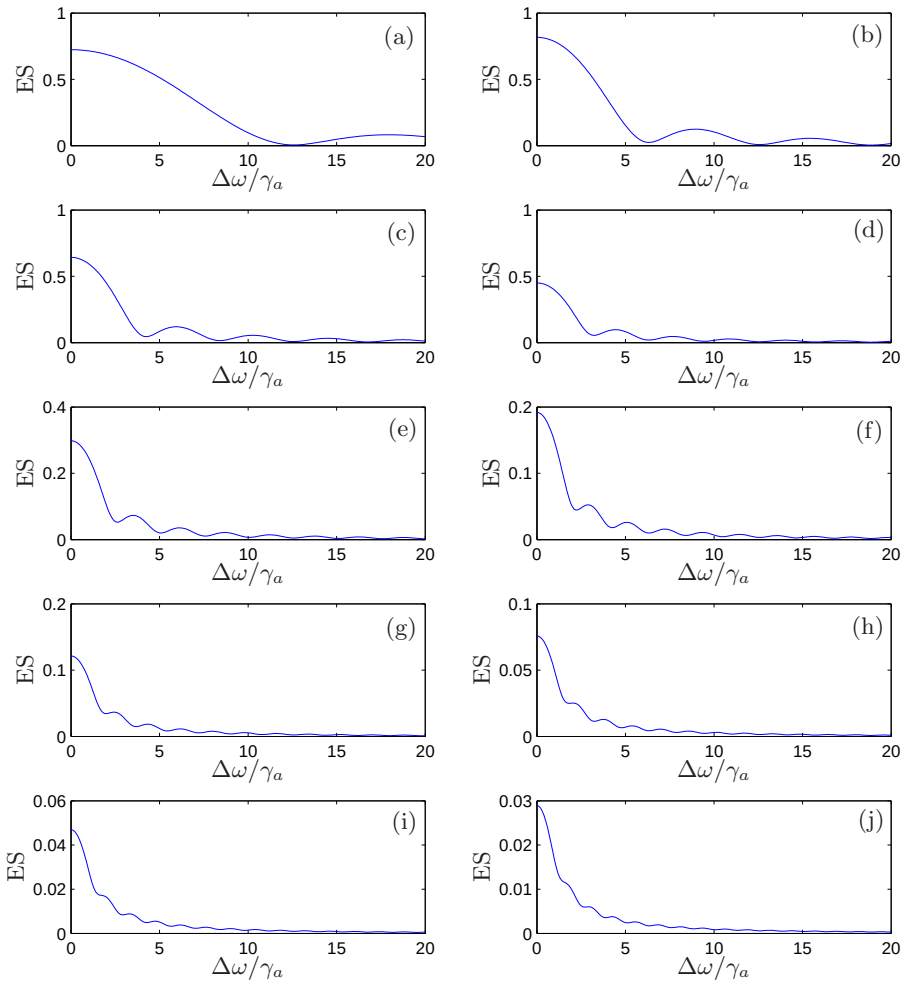

Figure 4.7: Entanglement spectrum as a function of $\Delta\omega$ at $t = 0.5, 1.0, \cdots, 5.0$ in that order from (a)-(i); $\gamma_b/\gamma_a = 2$.

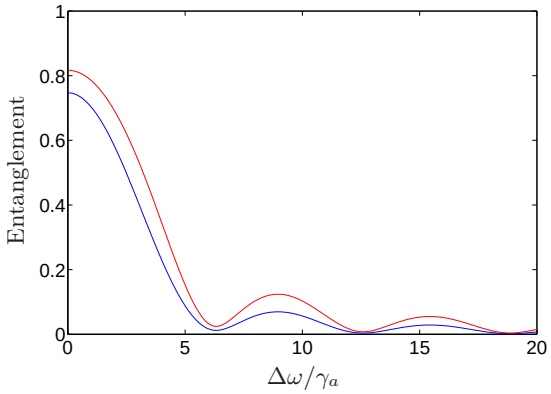

Figure 4.8: Entanglement spectrum (top) and entanglement of formation (bottom) as a function of $\Delta\omega$ at $t = 1.0$ for $\gamma_b/\gamma_a = 2$.

4.3.3 Photon capture

Mathematically, the EF does not reach the maximum value 1 because $\delta(t)$ is non-zero, i.e., there is a finite probability that the photon is in neither cavity. One can change this situation by capturing the spontaneously emitted photon completely in the second cavity. Remember, we are interested in measuring entanglement between a spontaneously emitting qubit and its field, so we fix γ_a; then γ_b has to be time dependent[6] to make the capture possible. The idea is essentially that of quantum state transfer [75], and our result is a special limiting case of a result in [76]. To capture the photon completely in this way is probably not experimentally feasible for typical optical cavities, but it provides a nice example of when the EF is equal to the CE as we show below.

The equality between the EF and the CE can be inferred easily from the work above. Their difference arises from the finite probability of the photon leaking out, i.e., there is a finite probability of a click in one of the photodetectors. In the photon capture regime, however, $\delta(t) = 0$, because there is no leakage. The system is a closed one, so the state is pure, and therefore must coincide with the conditioned state of QTT. We show now how the qubit-state transfer works and plot the EF and the CE.

The idea is to set $\eta = 0$, $\Delta\omega = 0$ and choose the time dependence of $\gamma_b(t)$ so that the output field from the second cavity is zero by destructive interference. The time dependence can be determined within QTT as follows. With the initial condition

[6]The system is assumed to remain Markovian.

$|\psi_{\rm REC}(0)\rangle = \alpha(0)|10\rangle + \beta(0)|01\rangle$, the conditioned state given that there is no click up to time t is

$$|\psi_{\rm REC}(t)\rangle = \alpha(t)|10\rangle + \beta(t)|01\rangle, \tag{4.16}$$

where

$$\alpha(t) = \alpha(0)e^{-\frac{\gamma_a}{2}t}, \qquad \dot{\beta}(t) = -\frac{\gamma_b(t)}{2}\beta(t) - \sqrt{\gamma_a\gamma_b(t)}\alpha(t). \tag{4.17}$$

The condition for no jumps is therefore

$$\begin{aligned}\langle\psi_{\rm REC}(t)|J_2^\dagger J_2|\psi_{\rm REC}(t)\rangle &= \gamma_a\alpha(0)^2e^{-\gamma_a t} + 2\sqrt{\gamma_a\gamma_b(t)}\alpha(0)e^{-\frac{\gamma_a}{2}t}\beta(t) + \gamma_b(t)\beta^2(t)\\ &= 0,\end{aligned} \tag{4.18}$$

where $\alpha(0)$ and $\beta(0)$ are assumed real for simplicity. Equations (4.17) and (4.18) can be solved to obtain the function $\gamma_b(t)$ that gives zero total output field from the second cavity. It is easier, however, to use the normalization condition $\alpha(t)^2+\beta(t)^2 = 1$. This gives $\beta(t) = -\sqrt{1-\alpha(t)^2}$, where the minus sign must be chosen to obtain destructive interference. Substituting this into (4.18) gives

$$\gamma_b(t) = \gamma_b(0)\frac{e^{-\gamma_a t}}{1 + [\gamma_b(0)/\gamma_a](1 - e^{-\gamma_a t})}. \tag{4.19}$$

$\gamma_b(0)$ is obtained from the initial flux condition $\gamma_b(0)(1-\alpha(0)^2) = \gamma_a\alpha(0)^2$; thus in the limit $\alpha(0) \to 1$, $\gamma_b(0) \to \infty$. One may choose $\alpha(0) = 1$ and $\gamma_b(0) >> 1$ in practice, with negligible chance that the photodetector clicks. Figure 4.9 shows plots of the EF and the CE for $\gamma_b(0)/\gamma_a = 100$. Both are identical to the EE because the state is pure. The maximum entanglement now occurs at $\gamma_a t = \ln(2)$, i.e., when the photon has a 50% probability to be in either cavity.

4.3.4 Photon transfer in a linear cascaded cavity array

As a little aside we consider a generalization of the above work to produce a maximally entangled state of the form

$$|\psi\rangle = \frac{1}{\sqrt{N}}\left(|1,0,\cdots,0\rangle + |0,1,\cdots,0\rangle + \cdots + |0,0,\cdots,1\rangle\right) \tag{4.20}$$

in a linear cascaded N-cavity array; for example, for three cavities one can insert one more cavity in the middle in Fig. 4.2, with a time dependent damping rate on its

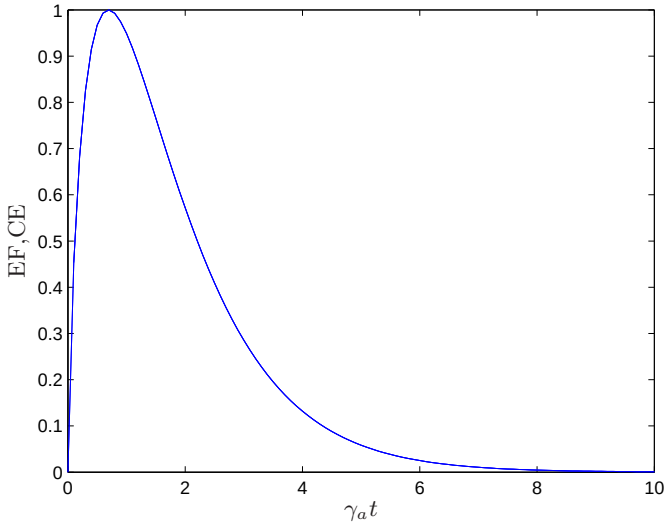

Figure 4.9: Contextual entanglement and entanglement of formation for the qubit transfer case, for $\gamma_b(0)/\gamma_a = 100$.

left mirror and a constant one on its right mirror. The equations for the decay rates can then be found in a similar way to the 2-cavity case. For more than 3 cavities, however, it turns out that one needs time dependent decay rates on the right hand mirror of the intermediate cavities too.[7] The situation is depicted in Fig. 4.10: a_k is the annihilation operator for the kth cavity mode, and we have labeled the decay rates for the left mirrors as γ_k and the right ones as $\widetilde{\gamma}_k$; thus $\gamma_1 = 0$ and $\widetilde{\gamma}_N = 0$ by default. There are infinitely many choices of $\widetilde{\gamma}_k$ available, corresponding to infinitely

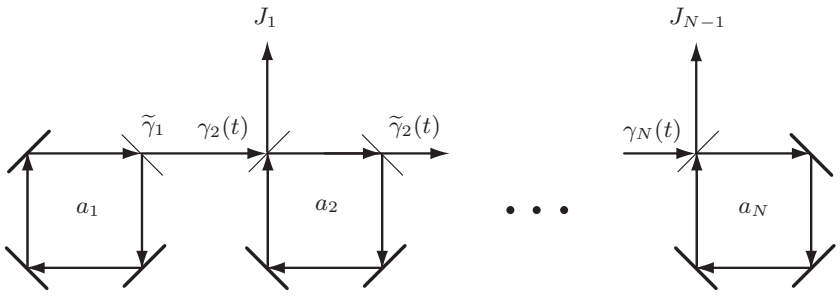

Figure 4.10: A linear cascaded cavity qubit transfer system with N cavities.

[7] This was found by a direct calculation. For constant decay rates for the right hand mirrors the maximally entangled state can not be created.

many functions that may be tried. Among these we choose a decreasing function with a single parameter. In order to let all of the field go to the Nth cavity, the $\widetilde{\gamma}_k$'s must tend to a non-zero constant value in the long time limit. Thus we try the form

$$\widetilde{\gamma}_k(t) = \frac{\widetilde{\gamma}_k(0)}{2}\left(e^{-\widetilde{\gamma}_1 t}+1\right), \tag{4.21}$$

for $k = 2, 3\cdots, N$. The aim is to choose the $\widetilde{\gamma}_k(0)$'s appropriately so that at some time t_0 all the cavities have equal probability to contain the photon.

Let us write the state at time t as

$$|\psi(t)\rangle = C_1(t)|1,0,\cdots,0\rangle + C_2(t)|0,1,\cdots,0\rangle + \cdots + C_N(t)|0,0,\cdots,1\rangle. \tag{4.22}$$

Because $C_1(t) = C_1(0)e^{-\widetilde{\gamma}_1 t/2}$

$$\widetilde{\gamma}_1 t_0 = 2\ln[\sqrt{N}C_1(0)], \tag{4.23}$$

assuming $C_1(0) > 0$. The other coefficients obey the equations

$$\dot{C}_k(t) = -\frac{1}{2}\left(\gamma_k(t)+\widetilde{\gamma}_k(t)\right)C_k(t) - \sqrt{\widetilde{\gamma}_{k-1}(t)\gamma_k(t)}C_{k-1}(t), \tag{4.24}$$

which with the no-firing conditions,

$$\sqrt{\gamma_k(t)}C_k(t) = -\sqrt{\widetilde{\gamma}_{k-1}(t)}C_{k-1}(t), \tag{4.25}$$

become

$$\dot{C}_k(t) = \frac{1}{2}\left(\gamma_k(t)-\widetilde{\gamma}_k(t)\right)C_k(t). \tag{4.26}$$

These equations are converted into equations for the γ_k's by taking the time derivative of (4.25) and comparing the result with (4.26). Thus one obtains

$$\begin{aligned}\dot{\gamma}_k(t) &= -\gamma_k(t)\left(\gamma_k(t)-\gamma_{k-1}(t)+\widetilde{\gamma}_{k-1}(t)-\widetilde{\gamma}_k(t)-\frac{\dot{\widetilde{\gamma}}_{k-1}(t)}{\gamma_{k-1}(t)}\right),\\ &= \begin{cases} -\gamma_2(t)\left(\gamma_2(t)-\widetilde{\gamma}_2(t)+\widetilde{\gamma}_1\right) & k=2\\ -\gamma_k(t)\left(\gamma_k(t)-\gamma_{k-1}(t)+\widetilde{\gamma}_{k-1}(t)-\widetilde{\gamma}_k(t)+\frac{e^{-\widetilde{\gamma}_1 t}}{1+e^{-\widetilde{\gamma}_1 t}}\right) & k\geq 3\end{cases}.\end{aligned} \tag{4.27}$$

The initial conditions are again determined by the no-firing conditions, (4.25), plus the initial conditions for the C_k's. We define $X << 1$ such that $(C_1(0))^2 = 1 - X$

and $(C_k(0))^2 = X/(N-1)$. Then

$$\gamma_k(0) = \begin{cases} \frac{(1-X)(N-1)}{X}\widetilde{\gamma}_1 & k = 2 \\ \widetilde{\gamma}_{k-1}(0) & k \geq 3 \end{cases}. \tag{4.28}$$

The solutions to the system of equations (4.27) cannot be found in analytical form, so we resort to a numerical method. We want $C_k(t_0) = 1/\sqrt{N}$, which implies $\gamma_k(t_0) = \widetilde{\gamma}_{k-1}(t_0)$. The following, then, are the steps one can follow to obtain the $\gamma_k(t)$'s that give the state (4.20).

1. Guess an initial value of $\widetilde{\gamma}_2(0)$.
2. Solve for $\gamma_2(t_0)$ using (4.27).
3. Compare it with $\widetilde{\gamma}_1$. If they are not equal (within some precision) choose another value of $\widetilde{\gamma}_2(0)$ and go to 2. If they are equal move on.
4. Repeat 1-3 for $\widetilde{\gamma}_3(0)$ and $\gamma_3(t_0)$.
5. Repeat 1-3 for $\widetilde{\gamma}_4(0)$ and $\gamma_4(t_0)$ ...

It is a straightforward, though laborious, task to find all the $\widetilde{\gamma}_k(0)$'s and hence all $\gamma_k(t)$'s in this way. Rather, one can write a computer code that does the searching automatically. $\widetilde{\gamma}_k(0) \geq \widetilde{\gamma}_1$, because if this inequality does not hold for any k the corresponding cavity will act as a bottleneck and the cavities after it cannot get a large enough field in time (remember we are trying to have an equal probability amplitude for every cavity.). It is found that $\widetilde{\gamma}_{k+1}(0) > \widetilde{\gamma}_k(0)$ for small k, but the initial values decrease after $k \approx N/2$. These decay rates have to increase with k initially, because the later cavities have to fill up sufficiently fast before too much field leaks out of the earlier cavities. This reasoning does not work for k close to N because the last cavity holds on to the field, so the $(N-1)$th cavity cannot release its field too fast, which in turn means it does not want the field to come in too fast.

Figure 4.11 shows the result for a 7-cavity array, where we plot the $|C_k(t)|^2$'s versus time. The curves peak at progressively later times as k increases. The maximally entangled state occurs around $t = 2/\widetilde{\gamma}_1$ where all the curves meet. Figures 4.12 and 4.13 show the $\gamma_k(t)$'s and the $\widetilde{\gamma}_k(t)$'s. The maximum values of the $\gamma_k(t)$'s occur at progressively later times so that the required destructive interferences can take place. The $\widetilde{\gamma}_k(t)$'s are completely defined by their initial values given in the caption of Fig. 4.11.

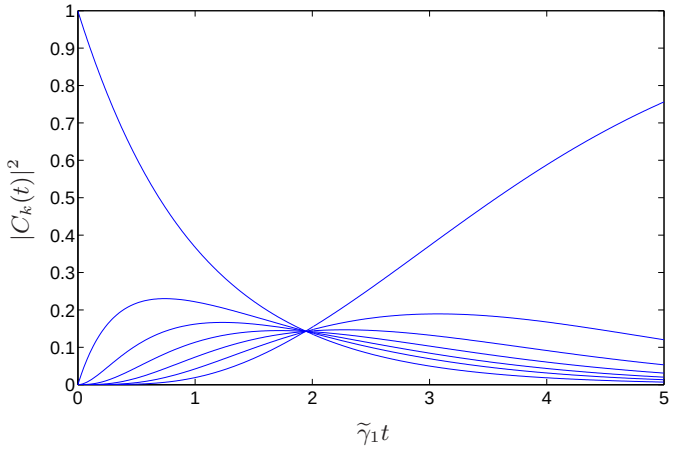

Figure 4.11: $|C_k(t)|^2$ versus $\widetilde{\gamma}_1 t$ for $N = 7$, with the initial condition $\{\widetilde{\gamma}_k(0)\} = \{1, 2.8, 3.45, 3.67, 3.35, 2.3, 0\}$. The curves peak at progressively later times as k increases.

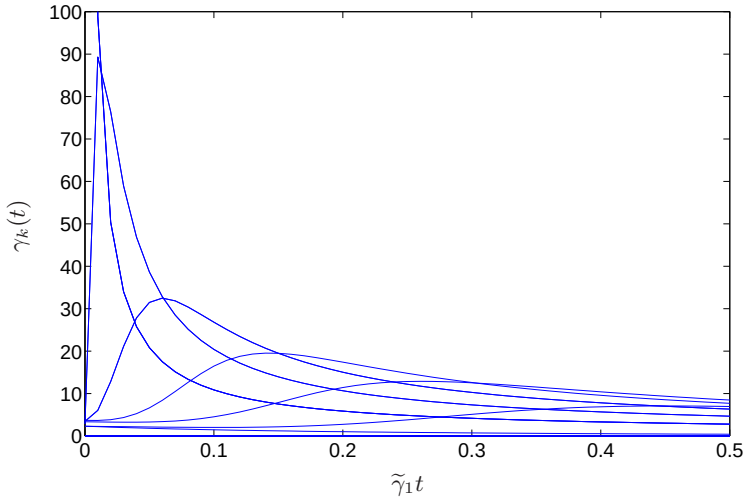

Figure 4.12: $\gamma_k(t)$ versus $\widetilde{\gamma}_1 t$ used to generate the curves plotted in Fig. 4.11.

One can also choose arbitrary conditions for the $|C_k(t_0)|^2$'s. Again, t_0 is determined from the known form of $C_1(t)$, but now $\gamma_k(t_0) = \widetilde{\gamma}_{k-1}(t_0)C_{k-1}(t_0)/C_k(t_0)$. The procedure to be followed is exactly the same as before. As an example, Fig. 4.14 shows the $|C_k(t)|^2$'s that yield $\{C_k(t_o)\} = \{\frac{1}{\sqrt{6}}, \frac{1}{\sqrt{3}}, \frac{1}{\sqrt{3}}, \frac{1}{\sqrt{6}}\}$. A vertical line has been placed at t_0 for the convenience of the reader. Because the second and third cavities have a larger field at t_0, one needs $\widetilde{\gamma}_3(0) < 1$, which is another aspect that is different

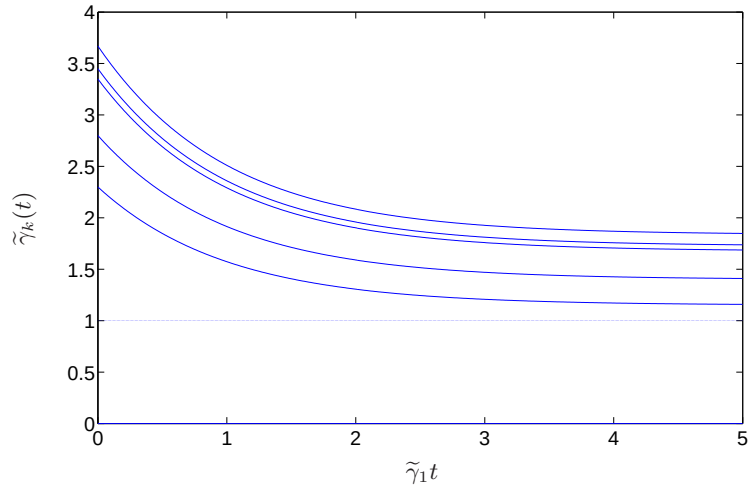

Figure 4.13: $\widetilde{\gamma}_k(t)$ versus $\widetilde{\gamma}_1 t$ used to generate the curves plotted in Fig. 4.11.

from the maximal entanglement case.

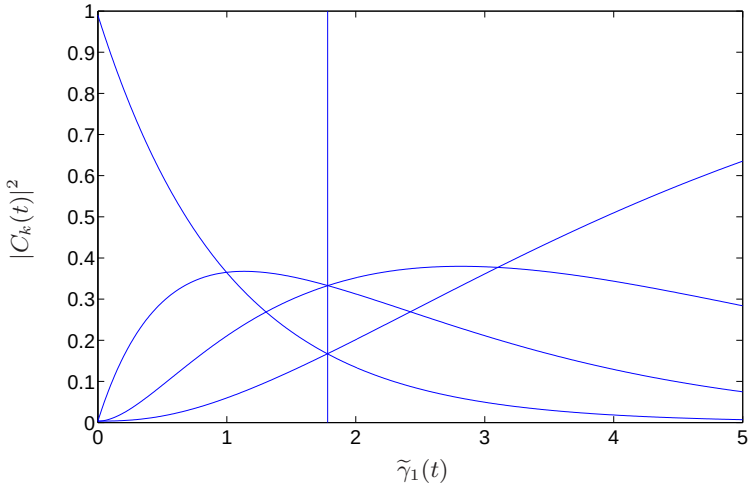

Figure 4.14: $|C_k(t)|^2$ versus $\widetilde{\gamma}_1 t$ for $N = 4$. $\{C_k(t_o)\} = \{\frac{1}{\sqrt{6}}, \frac{1}{\sqrt{3}}, \frac{1}{\sqrt{3}}, \frac{1}{\sqrt{6}}\}$ and $\{\widetilde{\gamma}_k(0)\} = \{1, 1.31, 0.79, 0\}$. The vertical line is at t_0.

4.4 Entanglement of a driven qubit

Finally, this section studies entanglement between a source and its radiated field. As before, we do this by using a cavity to collect the radiated field and calculate CE between the source and the cavity mode. We are not interested in entanglement between the laser source and the rest of the system, so we adopt the c-number representation of the laser. If one uses the birth-death model, the system becomes a tripartite one (after tracing over the carrier degree of freedom), and it is not clear how the entanglement for a subsystem should be defined.

4.4.1 Entanglement spectrum

Let us begin by showing how one calculates the entanglement spectrum (ES). Figure 4.15 illustrates a scheme for measuring the ES in the side channel. The introduced travelling wave cavity has two partially reflecting mirrors,[8] each with a decay rate Γ, so the full-width of the cavity is 2Γ. A beam splitter with transmittivity η controls the amount of scattered field collected and sent to the cavity. To measure the ES in the forward channel, one simply has to move the beam splitter and cavity to the forward channel. We choose $\eta << 1$ as we did when modelling a measurement of the optical spectrum. This has the advantage that only the first few number states need to be considered; we truncate at 1 photon. Clearly, the entanglement will be smaller for smaller η and go to zero as η goes to zero. Nevertheless, it is not so much the absolute value we are interested in as the variation with frequency, i.e., the spectrum.

The master equation (in the interaction picture) for this system is

$$\dot{\tilde{\rho}} = \frac{1}{i\hbar}[H_s, \tilde{\rho}] + \mathcal{D}[J_f]\tilde{\rho} + \mathcal{D}[J_s]\tilde{\rho}, \tag{4.29}$$

where

$$H_s = \frac{i\hbar}{2}\left[\sqrt{\gamma_S\gamma_T^f}\alpha(\sigma_- - \sigma_+) + \sqrt{\gamma_T^s\Gamma}(\sigma_+ c - \sigma_- c^\dagger)\right], \tag{4.30}$$

with all variables as defined in Sect. 3.3, except for α, Γ, and c: α is the amplitude of the laser (replacing a), taken real for convenience, and c is the cavity mode annihilation operator; $\mathcal{D}[J_f]$ and $\mathcal{D}[J_s]$ are as introduced in Sect. 3.3 with the replacement

[8] The second mirror allows the intracavity field to be measured. For the purpose of this chapter, it is not really needed and can be ignored.

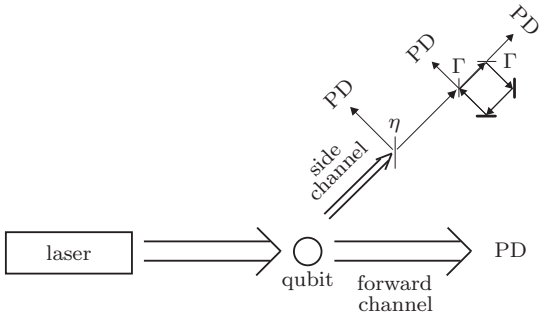

Figure 4.15: Setup for measuring the entanglement spectrum in the side channel. η is the fraction of light transmitted at the beam splitter, 2Γ is the full-width of the cavity, and PD denotes a photodetector.

$a \to \alpha$ in J_f.

Quantum trajectories for the side channel case are generated by the continuous evolution Hamiltonian (see Ch. 19 of [17])

$$H_{\text{cont}} = -\frac{i\hbar}{2}\left[\gamma_s\alpha^2 + \gamma_T\sigma_+\sigma_- + 2(\Gamma + i\Delta\omega)c^\dagger c + 2\sqrt{\gamma_S\gamma_T^f}\alpha\sigma_+ + 2\sqrt{\eta\gamma_T^s\Gamma}\sigma_- c^\dagger\right], \tag{4.31}$$

and the jump operators

$$J_f = \sqrt{\gamma_S}\alpha + \sqrt{\gamma_T^f}\sigma_-, \qquad J_s = \sqrt{(1-\eta)\gamma_T^s}\sigma_-,$$
$$J_{c1} = \sqrt{\eta\gamma_T^s}\sigma_- + \sqrt{\Gamma}c, \qquad J_{c2} = \sqrt{\Gamma}c.$$

$\Delta\omega$ is the difference between the transition frequency of the qubit and the resonance frequency of the cavity. For the forward channel the quantum trajectories are produced by the continuous evolution Hamiltonian (see Ch. 19 of [17])

$$H_{\text{cont}} = -\frac{i\hbar}{2}\left[\gamma_s\alpha^2 + \gamma_T\sigma_+\sigma_- + 2(\Gamma + i\Delta\omega)c^\dagger c + 2\sqrt{\gamma_S\gamma_T^f}\alpha\sigma_+ + 2\sqrt{\eta\Gamma}J_f c^\dagger\right], \tag{4.32}$$

and the jump operators

$$\tilde{J}_f = \sqrt{1-\eta}J_f, \qquad J_s = \sqrt{\gamma_T^s}\sigma_-,$$
$$J_{c1} = \sqrt{\eta}J_f + \sqrt{\Gamma}c, \qquad J_{c2} = \sqrt{\Gamma}c.$$

Figure 4.16 shows the ES for various values of γ_T^f with $\eta = 0.0001$ and the other parameters as defined in the caption; α is chosen so that $Y = 2\sqrt{2\gamma_S\gamma_T^f}\alpha/\gamma_T = 5$. The frequency spacing we use in this section is 0.25, as can be seen from the sharp changes in the figures, especially in Fig. 4.16. The general shape of the ES in the side channel follows that of the spectrum (c.f. Fig. 3.4), although the central peaks are smaller. The ES decreases as γ_T^f is increased, which is just as expected because the higher the γ_T^f, the less the light scattered into the side channel. An interesting feature is that as γ_T^f is increased, i.e. γ_T^s decreased, the sideband shrinks in size relative to the central peak. On the other hand, the spectra for small values of γ_T^s still retain the sideband showing that the ES can be different to the spectrum.

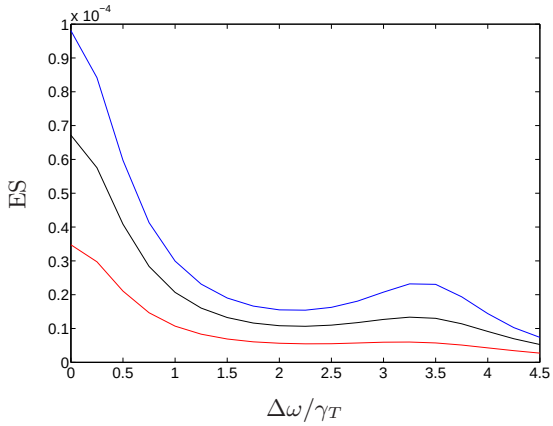

Figure 4.16: Entanglement spectrum for the side channel, for $\eta = 0.0001$, $Y = 5$, $\gamma_S/\gamma_T = 0.01$, $\Gamma/\gamma_T = 0.05$, and $\gamma_T^f/\gamma_T = 0.25$ (top, blue), 0.5 (middle, black), and 0.75 (bottom, red).

Figure 4.17 shows the ES for the field in the forward channel. The ES at the central frequency seems to be dominated by the laser field, which is supported by the fact that the smaller the γ_T^f, i.e., the larger the laser amplitude, the bigger the ES(0). For other frequencies, the ES increases as γ_T^f is increased, which is just what one would expect, as bigger γ_T^f means higher photon flux into the cavity.

There is a kind of symmetry between the forward and the side channel cases apart from the presence of the laser field. Figures 4.18–4.19 compare the ES in the forward (red curves) and the side (blue curves) channels to show this symmetry. The first of the three is for the case $\gamma_T^f = \gamma_T^s$. For this case the ES seems to be the same except at the central frequency (within the resolution). This is just what one would expect, as the only difference between the two cases is the presence of the laser field,

which should make a difference only at $\Delta\omega = 0$. The expectation (symmetry) is broken, however, when $\gamma_T^f \neq \gamma_T^s$ as shown in the next two figures. If only a quarter of the field is made to impinge on the beam splitter, the ES in the forward channel has the bigger sideband, whereas if three quarters of the field is made to impinge on the beam splitter, the ES in the side channel has the bigger sideband. Actually, the difference could be attributed to the laser field. The laser field—having no linewidth by itself in our model—acquires linewidth as it enters the cavity, and although this linewidth is small ($\Gamma/\gamma_T = 0.05$), the field can be of the same order of magnitude to the scattered field from the atom at higher frequencies, because of the big difference between the strengths of the two fields. When $\gamma_T^s = \gamma_T^f$, the laser field amplitude α is the same for the two cases, hence the coinciding curves in off-resonant frequencies. For other values of γ_T^f, however, the values of α differ—the bigger the γ_T^f, the smaller the α. One can see that this explains why the side band of the ES is bigger in the forward channel in Fig. (4.19) and in the side channel in Fig. (4.20). The sideband is bigger when the laser amplitude is larger. Since the laser field causes the central peak and the sideband, it makes sense that the photon number in the cavity (hence the ES) depends on the amplitude of the laser.

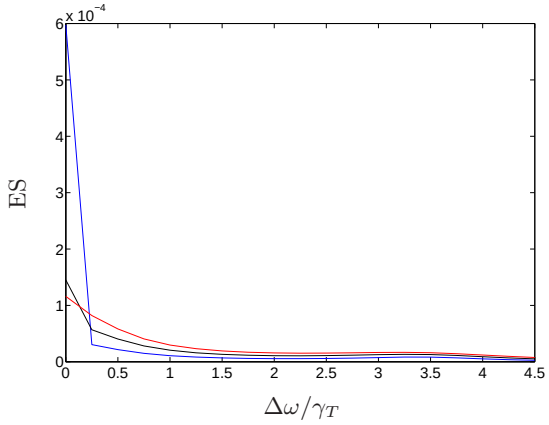

Figure 4.17: Entanglement spectrum for the forward channel, for $\eta = 0.0001$, $Y = 5$, $\gamma_S/\gamma_T = 0.01$, $\Gamma/\gamma_T = 0.05$, and $\gamma_T^f/\gamma_T = 0.25, 0.5, 0.75$, blue, black, and red curve respectively.

Free-field limit

In the limit $\gamma_T^f \to 0$ and $\eta \to 0$ (which we will call the free-field limit), one can ignore all the jumps except for the side jump, and in this limit an analytical calculation is

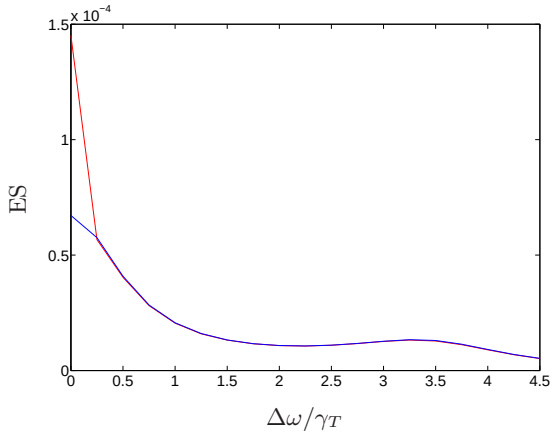

Figure 4.18: Entanglement spectrum for the forward (red) and side (blue) channel, for $\eta = 0.0001$, $Y = 5$, $\gamma_S/\gamma_T = 0.01$, $\Gamma/\gamma_T = 0.05$, and$\gamma_T^f/\gamma_T = 0.5$.

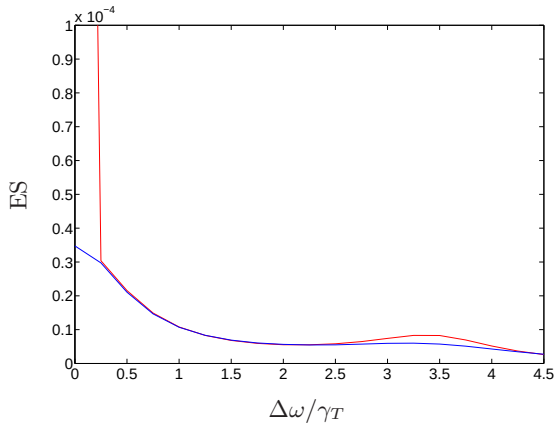

Figure 4.19: Entanglement spectrum for the forward (with $\gamma_T^f/\gamma_T = 0.25$, red) and side (with $\gamma_T^f/\gamma_T = 0.75$, blue) channel, for $\eta = 0.0001$, $Y = 5$, $\gamma_S/\gamma_T = 0.01$, and $\Gamma/\gamma_T = 0.05$.

possible as we show presently. The conditioned state would evolve under the non-Hermitian Hamiltonian until the moment the jump happens. The atom then jumps to the ground state and goes through the continuous evolution again until it jumps once more etc.. Consider calculating the average value of an operator $\hat{A}$ as a time average, and let the averaging time be T. Imagine a trajectory starting from the ground state and evolving until time τ, at which point it jumps to the ground state.

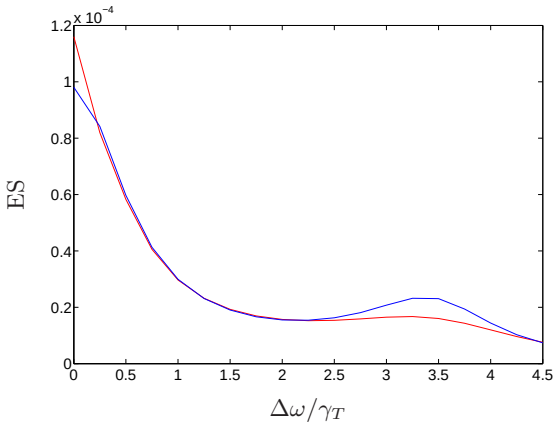

Figure 4.20: Entanglement spectrum for the forward (with $\gamma_T^f/\gamma_T = 0.75$, red) and side (with $\gamma_T^f/\gamma_T = 0.25$, blue) channel, for $\eta = 0.0001$, $Y = 5$, $\gamma_S/\gamma_T = 0.01$, and $\Gamma/\gamma_T = 0.05$.

The average value computed from this particular trajectory is

$$\frac{1}{\tau}\int_0^\tau dt\langle\psi_{\rm no}(t)|\hat{A}|\psi_{\rm no}(t)\rangle, \tag{4.33}$$

where no denotes 'no jump until time τ'. Real trajectories contain many of this type of trajectory, each making a jump at different times. To compute the average one has to integrate over a long time, say T, where all the trajectories of the above type occur with correct probabilities. Then the average is computed by

$$\frac{1}{T}\int_0^\infty d\tau\gamma_T P_{\rm e} T\langle\overline{\psi_{\rm no}}(\tau)|\overline{\psi_{\rm no}}(\tau)\rangle\int_0^\tau dt\langle\psi_{\rm no}(t)|\hat{A}|\psi_{\rm no}(t)\rangle. \tag{4.34}$$

Let us now illustrate where this formula came from. The integral over t gives the total contribution of a particular trajectory described above. $\langle\overline{\psi_{\rm no}}(\tau)|\overline{\psi_{\rm no}}(\tau)\rangle d\tau$, where the overline means that the state is unnormalized, is the waiting-time distribution, which is the probability that there is no jump until time τ followed by a jump in time interval $[\tau, \tau + d\tau]$; so this gives the probability that the given no-jump interval from $t = 0$ to $t = \tau$ occurs. $\gamma_T P_{\rm e} T$, where $P_{\rm e}$ is the steady state probability for the qubit to be in the excited state, gives the total number of jumps. Thus $\gamma_T P_{\rm e} T\langle\overline{\psi_{\rm no}}(\tau)|\overline{\psi_{\rm no}}(\tau)\rangle d\tau$ gives the total number of no-jump intervals where the jump occurs after time τ. Finally, integrating over τ and dividing by T gives us the average value of $\hat{A}$.

The above equation can be simplified by changing the order and limits of the integrations to give

$$\begin{aligned}\gamma_T P_{\rm e} \int_0^\infty dt \langle\psi_{\rm no}(t)|\hat{A}|\psi_{\rm no}(t)\rangle \int_t^\infty d\tau \langle\overline{\psi_{\rm no}}(\tau)|\overline{\psi_{\rm no}}(\tau)\rangle \\ = \gamma_T P_{\rm e} \int_0^\infty dt \langle\psi_{\rm no}(t)|\hat{A}|\psi_{\rm no}(t)\rangle\langle\overline{\psi_{\rm no}}(t)|\overline{\psi_{\rm no}}(t)\rangle \\ = \gamma_T P_{\rm e} \int_0^\infty dt \langle\overline{\psi_{\rm no}}(t)|\hat{A}|\overline{\psi_{\rm no}}(t)\rangle. \qquad (4.35)\end{aligned}$$

The second line follows because the probability that a jump occurs sometime after t is simply the probability that no jump occurs until time t; the third follows from the definition of the normalized conditioned state. The final piece of information we need is $P_{\rm e}$, which can be read off from any textbook that treats resonance fluorescence. In the notation used in this thesis, $P_{\rm e} = \frac{1}{2}\frac{Y^2}{1+Y^2}$, to a good approximation for $\eta << 1$. The figure below shows the result for $Y = 5, \gamma_T = 2$, and $\eta = 0.0001$, along with the plots obtained from the numerical simulations for $\gamma_T^f = 0.1, 0.01$. The numerical results converge to the analytical result as γ_T^f is decreased.

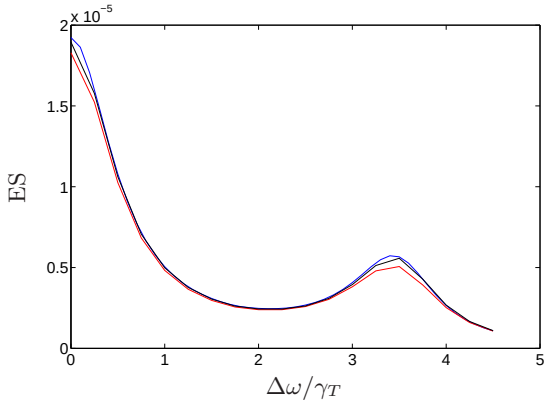

Figure 4.21: Entanglement spectrum in the free field limit (top, blue), and in the side channel (middle, black, and bottom, red), for $Y = 5$, $\gamma_S/\gamma_T = 0.01$, and $\Gamma/\gamma_T = 0.05$. Entanglement spectra in the side channel are for $\eta = 0.0001$ and $\gamma_T^f = 0.1$(bottom, red), 0.01(middle, balck).

One piece of information we have not shown yet is the dependence of the entanglement spectrum on η. It is expected to vary linearly to first order, because smaller coupling means less entanglement. Table 4.1 shows the dependence of the entanglement spectrum at resonance when $\eta << 1$. Indeed, the ES(0) scales (roughly)

linearly with η, as can be seen from the decreasing exponent; it is not exactly linear, which is to be expected because the entropy of entanglement is a nonlinear function.

η	0.01	0.001	0.0001	0.00001	0.000001
ES(0)	1.27×10^{-3}	1.60×10^{-4}	1.92×10^{-5}	2.25×10^{-6}	2.57×10^{-7}

Table 4.1: ES(0) as a function of η for $Y = 5$ and $\Gamma/\gamma_T = 0.005$.

4.4.2 Entanglement of formation

One can calculate the EF readily for the same setup used to calculate the ES, because the system essentially comprises of two qubits [71]. The EF in the steady state turns out to be zero for both the side and the forward channel cases. To calculate the steady state one can first write down the equation for the steady state

$$\dot{\rho}_{ss} = \mathcal{L}\rho_{ss} = 0 \tag{4.36}$$

in a matrix notation; ρ_{ss} is then a column vector and $\mathcal{L}$ a square matrix. One can solve for the steady state density matrix by calculating the eigenvectors of eigenvalue 0 for the square matrix, and then using the initial condition to work out how much a given eigenvector contributes to the total solution. It turns out that for the case at hand there is only one eigenvector with eigenvalue 0. Once the steady state density matrix is obtained, the EF can be readily calculated using the formula in [71].

The fact that the EF (in the steady state) is zero is a little surprising since the EF for the spontaneous emission case was non-zero; one would think that since the qubit is continuously driven it should go through spontaneous emission frequently, giving some kind of 'averaged out' value of the EF for the spontaneous emission case. Perhaps the fact that the driving field is classical has played a role here, which makes it interesting to think about a non-classical driving field. However, it would not be easy to calculate EF for that case, because the system then has three degrees of freedom for which there is no known analytical expression (to the best of the author's knowledge). We emphasize that the EF is zero in the *steady state*; it is probably not zero in the transient regime just like in the spontaneous emission case.

Chapter 5

Summary, conclusion, and future directions

This chapter provides a summary of each chapter and states the main results in the conclusion section. Possible avenues of further research are suggested in the last section.

5.1 Summary

Chapter 2 gave a brief introduction to quantum teleportation, from qubit teleportation to continuous variable teleportation. We proposed teleporting a beam of light (quantum field), and then introduced three ways of analyzing broadband quantum teleportation of optical fields: quantum trajectory theory, stochastic electrodynamics, and the Heisenberg operator method. The advantages and disadvantages of each method were explained. The Heisenberg operator method was subsequently applied to teleportation of the vacuum field and the scattered field of resonance fluorescence. The roles of the various bandwidths involved were deduced as well as an inequality that they must satisfy for high fidelity teleportation. Analytical formulae for the first- and second-order correlation functions of the teleported light were provided.

Chapter 3 developed a birth-death model of the laser which was subsequently applied to (resonantly) drive a qubit. Various well-known features of resonance fluorescence were reproduced from a cascaded open systems analysis to show the validity of the model. Decoherence of a driven qubit due to entanglement between the laser source and the qubit was studied in detail, assuming a classical source. Lastly the issue of laser quantum state was discussed in the light of the results in

the chapter.

Chapter 4 introduced contextual entanglement, a measure of entanglement defined through quantum trajectories. Explicit calculations were given for a couple of simple cases where we compared contextual entanglement to the entanglement of formation. The systems investigated were: a cascaded system of two qubits coupled via spontaneous emission and the resonance fluorescence system. We introduced a way of quantifying entanglement between a source and its radiated field, which we called the entanglement spectrum. The entanglement spectrum has been evaluated for a qubit undergoing spontaneous emission and a driven qubit. An analytical expression for the entanglement spectrum was derived for a qubit going through spontaneous emission and compared with the entanglement of formation, showing their dependence on time. At this point a little excursion was taken to investigate qubit state transfer in a linear cascaded cavity array. After this, we returned to studying the entanglement spectrum for a driven qubit. An analytical computation for the driven qubit case was also carried out (in a limiting case) to give credence to numerical results. It was subsequently used to show the dependence of ES(0) on η (coupling strength of the qubit to the collecting cavity).

5.2 Conclusion

Part I

Part I investigated the interplay of bandwidths in broadband quantum teleportation where we have shown that a teleporter must include a filtering cavity at the output port of the conventional teleporter [1] in order to teleport a beam of light. We have found that the bandwidths should obey the inequality $\gamma_A >> \gamma_s >> \gamma_B >> \gamma_{\text{in}}$ for the teleportation to be successful (see (2.45)). Analytical formulae for the first and second order correlation functions were given for $\gamma_A >> \gamma_s, \gamma_B >> \gamma_{\text{in}}$. A more general expression was also provided (in the form of a fortran code), which although less compact is suitable for direct numerical evaluation.

Part II, Chapter 3

The main theme of Part II is quantum entanglement. Quantum trajectory theory has been used to study entanglement in qubit systems, namely in the system of resonance fluorescence and a cascaded two-qubit system coupled via spontaneous emission. We have proved that when there is a classical source of light—i.e., a

source that can be described by a positive definite Glauber-Sudarshan P function—driving a qubit, the master equation is separable as long as the source dynamics is coarse grained, i.e., detailed accounting of the laser pumping is ignored. Then, considering a conventional laser source, for example, there is no additional qubit decoherence due to the quantum nature of the laser that drives it. Conversely, we propose that this separability can be thought of as a criterion for assigning a (phase diffusing) coherent state to the laser source.

Part II, Chapter 4

The second half of Part II presented explicit calculations of contextual entanglement and compared it with the entanglement of formation. The two measures generally differ, except in closed systems where they are the same (as the entropy of entanglement) by their definitions. By evaluating the CE and EF between a laser and a qubit driven by it, we have shown explicitly that CE (for the photon counting case) can be non-zero even though EF=0. On the other hand, calculation of the contextual entanglement in the spontaneously emitting qubit case shows that homodyne and heterodyne trajectories give a CE that are very close to the entanglement of formation.

In the little excursion mentioned earlier, it was shown that a photon transfer is possible in a linear cascaded cavity array, allowing a class of entangled states to be formed at given times.

The entanglement spectrum has also been computed for a resonantly driven qubit. It seems that the amplitude of the driving laser field affects the shape of the ES, because of the conditioning on the detection records. The entanglement spectrum behaves mostly as expected, but some peculiarities were found that are not very easy to account for. The dependence of ES(0) on η was shown to be as expected—ES(0) $\to 0$ as $\eta \to 0$ the dependence being more or less linear.

5.3 Future directions

Certainly not due to lack of interest, but due to a lack of time and ingenuity on the part of the author, some questions have remained untouched. The purpose of this section is to point them out to the reader.

One obvious extension that could be made to Ch. 1 would be to study higher-order correlation functions of the teleported field to see whether the restrictions

become more stringent.

It would be interesting to generalize the separability proof of Ch. 3 to a laser model that includes thermal photons, since it is not immediately obvious how the operators describing the creation of thermal photons in the laser cavity are to be taken care of. It is essential to consider this because the proof relies on the property of the coherent state as an eigenstate of the annihilation operator. Nevertheless, the driving of the qubit is still one-way and the conclusions are expected to hold.

There are quite a few paths to follow in the final chapter. Firstly, an analytical formula of the REE is now possible for bipartite systems so it could be computed and compared with the CE. Secondly, there are infinitely many types of CE available corresponding to the infinitely many ways of arranging detectors (and beam splitters). For a start, it would be interesting to calculate the CE with different combinations of homodyne, heterodyne, and photo-detectors for the resonance fluorescence system and see whether homodyne and heterodyne schemes give a CE that is close to the EF. Thirdly, answering the questions asked in the last part of the previous chapter would be interesting. The ES for different measurement schemes would be interesting also. However, for any scheme that includes a homodyne or heterodyne detector the Hilbert space grows very large and numerical simulations are that much harder to carry out. A more efficient way of finding the ES would be very helpful.

Appendix A

All-optical teleportation

The proposal of Ralph [34] is to replace Alice's homodyne measurements with a linear amplifier which takes in Alice's share of the EPR beam instead of a vacuum field. The scheme is depicted in Fig. A.1 (taken from Fig. 2 of [34]). $a_{\rm in}$ is the

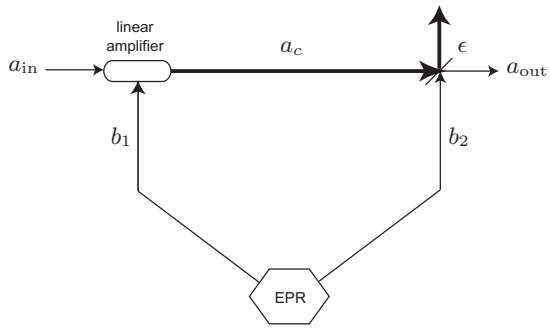

Figure A.1: Schematic of all-optical quantum teleportation.

input beam to be teleported, b_1 and b_2 are the correlated EPR beams, a_c is the classical signal, and $a_{\rm out}$ is the teleported field. Instead of making a displacement, Bob mixes the fields a_c and b_2 at a beam splitter of transmittivity ϵ. For an ideal phase-insensitive linear amplifier [77]

$$a_c = \sqrt{G}a_{\rm in} + \sqrt{G-1}b_1^\dagger, \tag{A.1}$$

where

$$\begin{aligned} b_1 &= \sqrt{H}v_1 + \sqrt{H-1}v_2^\dagger, \\ b_2 &= \sqrt{H}v_2 + \sqrt{H-1}v_1^\dagger, \end{aligned} \tag{A.2}$$

with independent vacuum inputs v_1 and v_2; G is the amplifier gain and H is the parametric gain. For large amplifier gain ($G >> 1$), $a_c \approx \sqrt{G}(a_{\rm in} + b_1^\dagger)$, and $a_{\rm out}$ is given by

$$\begin{aligned} a_{\rm out} &\approx \sqrt{\epsilon}a_c - \sqrt{1-\epsilon}b_2, \\ &= \sqrt{G\epsilon}(a_{\rm in} + \sqrt{H}v_1^\dagger + \sqrt{H-1}v_2) - \sqrt{1-\epsilon}(\sqrt{H}v_2 + \sqrt{H-1}v_1^\dagger). \end{aligned} \tag{A.3}$$

For $\epsilon = 1/G \approx 0$,

$$\begin{aligned} a_{\rm out} &\approx a_{\rm in} + b_1^\dagger - b_2, \\ &= a_{\rm in} + (\sqrt{H} - \sqrt{H-1})(v_1^\dagger - v_2), \end{aligned} \tag{A.4}$$

thus for infinite squeezing, i.e., $H \to \infty$, $a_{\rm out} \to a_{\rm in}$.

The point to note is that by writing $a_c = \sqrt{G}(a_{\rm in} + b_1^\dagger)$ one is ignoring the quantum nature of the field, because by doing so the commutator $[a_c, a_c^\dagger]$ becomes zero. This is what we mean by saying the measurement results are treated formally as operators but in the classical limit. Compare the first line of (A.3) with (2.16). a_c is equivalent to $(\mathcal{E}_{\rm in} + \mathcal{E}_A^\dagger)$ and $\mathcal{E}_B$ is equivalent to $(-)b_2$; classicality of the former means that the quantum nature of the output field comes from the latter fields (as it should be).

Appendix B

Four-time correlation functions

In this appendix we evaluate

$$\left\langle \mathcal{E}_{\rm in}^{\dagger}(t_1)\mathcal{E}_{\rm in}^{\dagger}(t_2)\mathcal{E}_{\rm in}(t_3)\mathcal{E}_{\rm in}(t_4)\right\rangle, \tag{B.1}$$

where $\mathcal{E}_{\rm in}$ is the scattered field of resonance fluorescence, i.e.,

$$\mathcal{E}_{\rm in} = \sqrt{\gamma_{\rm in}}\sigma_- + \xi_{\rm in}, \tag{B.2}$$

where σ_- is the lowering operator for a qubit driven by a laser, and $\xi_{\rm in}(t_1)$ is a vacuum field operator that commutes with $\sigma_-(t_2)$ if $t_2 \leq t_1$. Because $\mathcal{E}_{\rm in}$ is a free field operator and therefore commutes with itself, one needs consider the case of $t_2 > t_1$, $t_3 > t_4$ only; other cases are obtained by simply changing the time arguments. This means that all the $\xi_{\rm in}^{\dagger}$'s act to the left and all the $\xi_{\rm in}$'s act to the right, where they act on the vacuum state and can therefore be ignored. Thus (B.1) becomes

$$\gamma_{\rm in}^2 \left\langle \sigma_+(t_1)\sigma_+(t_2)\sigma_-(t_3)\sigma_-(t_4)\right\rangle. \tag{B.3}$$

The quantity (B.3) can be calculated from the quantum regression formula [50, 78], but time ordering has to be considered in order to use it. There are 6 different time

orderings, although not all of them are independent:

$$\begin{aligned} t_2 > t_3 > t_1 > t_4 &\xrightarrow{\dagger} t_3 > t_2 > t_4 > t_1 \\ t_2 > t_3 > t_4 > t_1 &\xrightarrow{\dagger} t_3 > t_2 > t_1 > t_4 \\ t_2 > t_1 > t_3 > t_4 &\xrightarrow{\dagger} t_3 > t_4 > t_2 > t_1 \end{aligned} \tag{B.4}$$

The arrows indicate that the two cases are related by an adjoint operation. Specifically, because of the relation

$$\langle \sigma_+(t_1)\sigma_+(t_2)\sigma_-(t_3)\sigma_-(t_4)\rangle^\dagger = \langle \sigma_+(t_4)\sigma_+(t_3)\sigma_-(t_2)\sigma_-(t_1)\rangle\,, \tag{B.5}$$

complex conjugation of the function for the case $t_2 > t_3 > t_1 > t_4$ is equal to the function for the case $t_3 > t_2 > t_4 > t_1$ upon relabeling the time arguments.

(B.3) needs to be evaluated for the 3 cases listed in (B.4). The quantum regression formula applied to the three cases gives

$$\mathrm{tr}\left\{\sigma_+ e^{\mathcal{L}(t_2-t_3)}\left[\sigma_- e^{\mathcal{L}(t_3-t_1)}\left[e^{\mathcal{L}(t_1-t_4)}\left[\sigma_-\rho(t_4)\right]\sigma_+\right]\right]\right\}, \tag{B.6a}$$

$$\mathrm{tr}\left\{\sigma_+ e^{\mathcal{L}(t_2-t_3)}\left[\sigma_- e^{\mathcal{L}(t_3-t_4)}\left[\sigma_- e^{\mathcal{L}(t_4-t_1)}\left[\rho(t_1)\sigma_+\right]\right]\right]\right\}, \tag{B.6b}$$

$$\mathrm{tr}\left\{\sigma_+ e^{\mathcal{L}(t_2-t_1)}\left[e^{\mathcal{L}(t_1-t_3)}\left[\sigma_- e^{\mathcal{L}(t_3-t_4)}\left[\sigma_-\rho(t_4)\right]\right]\sigma_+\right]\right\}, \tag{B.6c}$$

where $\mathcal{L}$ is the Liouville operator for the master equation of resonance fluorescence in a rotating frame[1]:

$$\dot{R} = \mathcal{L}R = i\frac{\Omega}{2}[\sigma_+ + \sigma_-, R] + \frac{\gamma}{2}(2\sigma_- R\sigma_+ - \sigma_+\sigma_- R - R\sigma_+\sigma_-), \tag{B.7}$$

where Ω is the Rabi frequency and γ is the natural linewidth of the qubit. Each $e^{\mathcal{L}(t_2-t_3)}$ acts on the term inside the square bracket to the right of it. R instead of ρ has been used to remind the reader that R is not a density operator in general; to evaluate the equations (B.6) we have to solve the master equation without the

[1] $\mathcal{L}$ should actually be the operator before going into the rotating frame. However, going into the rotating frame does not change the values of the four-time correlation function (B.3), so we work with the simpler form in this appendix.

assumption $\mathrm{tr}[R] = 1$. For this purpose we solve the optical Bloch equations:

$$\dot{R}_{+-}(t) = -i\frac{\Omega}{2}(R_{++}(t) - R_{--}(t)) - \frac{\gamma}{2}R_{+-}(t), \tag{B.8a}$$

$$\dot{R}_{-+}(t) = +i\frac{\Omega}{2}(R_{++}(t) - R_{--}(t)) - \frac{\gamma}{2}R_{-+}(t), \tag{B.8b}$$

$$\begin{aligned}\dot{R}_{++}(t) - \dot{R}_{++} &= i\Omega R_{+-}(t) - i\Omega R_{-+}(t) \\ &\quad - \gamma(R_{++}(t) - R_{--}(t) + R_{++}(0) + R_{--}(0)).\end{aligned} \tag{B.8c}$$

Of course the trace of R is preserved, where in matrix form we have

$$R = \begin{pmatrix} R_{--} & R_{-+} \\ R_{+-} & R_{++} \end{pmatrix}.$$

These equations are solved easily by Laplace transform. The solutions can be written as

$$R_{+-}(t) = R_{-+}(0)g_-(t) + R_{+-}(0)g_+(t) - R_{--}(0)f_-(t) - R_{++}(0)f_+(t), \tag{B.9a}$$

$$R_{-+}(t) = R_{-+}(0)g_+(t) + R_{+-}(0)g_-(t) + R_{--}(0)f_-(t) + R_{++}(0)f_+(t), \tag{B.9b}$$

$$R_{++}(t) - R_{--}(t) = R_{-+}(0)i(t) - R_{+-}(0)i(t) + R_{--}(0)h(t) + R_{++}(0)j(t), \tag{B.9c}$$

where

$$f_\pm(t) = -\frac{i}{\sqrt{2}}\frac{Y}{1+Y^2}\left[1 - e^{-\frac{3\gamma}{4}t}\left(\cosh(\delta t) + \frac{3\gamma}{4\delta}\sinh(\delta t)\right)\right] \pm \frac{iY}{\sqrt{2}}\frac{\gamma}{2\delta}\sinh(\delta t)e^{-\frac{3\gamma}{4}t}, \tag{B.10a}$$

$$g_\pm(t) = \frac{1}{2}e^{-\frac{\gamma}{2}t} \pm \frac{1}{2}e^{-\frac{3\gamma}{4}t}\left(\cosh(\delta t) + \frac{\gamma}{4\delta}\sinh(\delta t)\right), \tag{B.10b}$$

$$h(t) = -\frac{1}{1+Y^2}\left[1 + Y^2 e^{-\frac{3\gamma}{4}t}\left(\cosh(\delta t) + \frac{3\gamma}{4\delta}\sinh(\delta t)\right)\right], \tag{B.10c}$$

$$i(t) = \frac{iY}{\sqrt{2}}\frac{\gamma}{\delta}e^{-\frac{3\gamma}{4}t}\sinh(\delta t), \tag{B.10d}$$

$$\begin{aligned}j(t) = -\frac{1}{1+Y^2}\Bigg[&1 + 2e^{-\frac{3\gamma}{4}t}\left(\cosh(\delta t) + \frac{\gamma}{4\delta}\sinh(\delta t)\right) \\ &- Y^2 e^{-\frac{3\gamma}{4}t}\left(\cosh(\delta t) - \frac{5\gamma}{4\delta}\sinh(\delta t)\right)\Bigg],\end{aligned} \tag{B.10e}$$

with $Y = \sqrt{2}\Omega/\gamma$ and $\delta = \sqrt{1 - 8Y^2}\gamma/4$. All four values of $R(t)$ can be found from

(B.9) and $R_{++}(t) + R_{--}(t) = R_{++}(0) + R_{--}(0)$.

Having solved (B.7) we now show, as an example, how to evaluate (B.6a). The steady state density matrix

$$\rho_{\rm ss} = \begin{pmatrix} \frac{1}{2}\frac{2+Y^2}{1+Y^2} & -\frac{i}{\sqrt{2}}\frac{Y}{1+Y^2} \\ -\frac{i}{\sqrt{2}}\frac{Y}{1+Y^2} & \frac{1}{2}\frac{Y^2}{1+Y^2} \end{pmatrix} , \tag{B.11}$$

is substituted for $\rho(t_4)$, which gives

$$\sigma_-\rho(t_4) = \begin{pmatrix} \frac{i}{\sqrt{2}}\frac{Y}{1+Y^2} & \frac{1}{2}\frac{Y^2}{1+Y^2} \\ 0 & 0 \end{pmatrix} . \tag{B.12}$$

For convenience we define $R_1(\tau_1) \equiv e^{\mathcal{L}\tau_1}(\sigma_-\rho(t_4))$, where $\tau_1 = t_1 - t_4$. Then we need to evaluate $R_{1++}(\tau_1)$ and $R_{1-+}(\tau)$ only, because

$$R_1(\tau_1)\sigma_+ = \begin{pmatrix} R_{1-+}(\tau_1) & 0 \\ R_{1++}(\tau_1) & 0 \end{pmatrix} . \tag{B.13}$$

These can be evaluated from (B.9), giving

$$\begin{aligned} R_{1++}(\tau_1) &= \frac{1}{2}\left(R_{1++}(0) + R_{1--}(0) + R_{1++}(0) - R_{1--}(0)\rangle\right), \\ &= \frac{1}{2}\left(\frac{i}{\sqrt{2}}\frac{Y}{1+Y^2} + \frac{1}{2}\frac{Y^2}{1+Y^2}i(\tau_1) + \frac{i}{\sqrt{2}}\frac{Y}{1+Y^2}h(\tau_1)\right), \end{aligned} \tag{B.14}$$

and

$$R_{1-+}(\tau_1) = \left(\tfrac{1}{2}\frac{Y^2}{1+Y^2}g_+(\tau_1) + \frac{i}{\sqrt{2}}\frac{Y}{1+Y^2}f_-(\tau_1)\right). \tag{B.15}$$

Similarly, defining $R_2(\tau_2, \tau_1) \equiv e^{\mathcal{L}\tau_2}(R_1(\tau_1)\sigma_+)$, with $\tau_2 = t_3 - t_1$, we obtain

$$\sigma_- R_2(\tau_2, \tau_1) = \begin{pmatrix} R_{2+-}(\tau_2, \tau_1) & R_{2++}(\tau_2, \tau_1) \\ 0 & 0 \end{pmatrix} \tag{B.16}$$

where

$$R_{2++}(\tau_2, \tau_1) = \tfrac{1}{2}\left(R_{1-+}(\tau_1) - R_{1++}(\tau_1)i(\tau_2) + R_{1-+}h(\tau_2)\right), \tag{B.17}$$

and

$$R_{2+-}(\tau_2,\tau_1) = \left(R_{1++}(\tau_1)g_+(\tau_2) - R_{1-+}(\tau_1)f_-(\tau_2)\right). \tag{B.18}$$

Finally define $R_3(\tau_3,\tau_2,\tau_1) \equiv e^{\mathcal{L}\tau_3}\left(\sigma_- R_2(\tau_2,\tau_1)\right)$, with $\tau_3 = t_2 - t_3$. Then

$$\begin{aligned}\mathrm{tr}\left\{\sigma_+ R_3(\tau_3,\tau_2,\tau_1)\right\} &= R_{3-+}(\tau_3,\tau_2,\tau_1),\\ &= R_{2++}(\tau_2,\tau_1)g_+(\tau_3) + R_{2+-}f_-(\tau_3).\end{aligned} \tag{B.19}$$

Substituting (B.18), (B.17), (B.15), and (B.14) into (B.19), and making some rearrangements, Eqs. (B.6) can be written as

$$\begin{aligned}&\tfrac{1}{2}\Big(f_-(\tau_3)g_+(\tau_2) - \tfrac{1}{2}g_+(\tau_3)i(\tau_2)\Big)\Big(\tfrac{i}{\sqrt{2}}\tfrac{Y}{1+Y^2}(1+h(\tau_1)) + \tfrac{1}{2}\tfrac{Y^2}{1+Y^2}i(\tau_1)\Big)\\ &+\Big(\tfrac{1}{2}g_+(\tau_3)(1+h(\tau_2)) - f_-(\tau_3)f_-(\tau_2)\Big)\Big(\tfrac{i}{\sqrt{2}}\tfrac{Y}{1+Y^2}f_-(\tau_1) + \tfrac{1}{2}\tfrac{Y^2}{1+Y^2}g_+(\tau_1)\Big).\end{aligned} \tag{B.20a}$$

$$\begin{aligned}&-\tfrac{1}{2}\Big(f_-(\tau_3)g_-(\tau_2) + \tfrac{1}{2}g_+(\tau_3)i(\tau_2)\Big)\Big(\tfrac{i}{\sqrt{2}}\tfrac{Y}{1+Y^2}(1+h(\tau_1)) + \tfrac{1}{2}\tfrac{Y^2}{1+Y^2}i(\tau_1)\Big)\\ &+\Big(\tfrac{1}{2}g_+(\tau_3)(1+h(\tau_2)) - f_-(\tau_3)f_-(\tau_2)\Big)\Big(\tfrac{i}{\sqrt{2}}\tfrac{Y}{1+Y^2}f_-(\tau_1) + \tfrac{1}{2}\tfrac{Y^2}{1+Y^2}g_+(\tau_1)\Big),\end{aligned} \tag{B.20b}$$

$$\begin{aligned}&\tfrac{1}{2}\Big(f_-(\tau_3)g_+(\tau_2) + \tfrac{1}{2}g_-(\tau_3)i(\tau_2)\Big)\Big(\tfrac{i}{\sqrt{2}}\tfrac{Y}{1+Y^2}(1+h(\tau_1)) + \tfrac{1}{2}\tfrac{Y^2}{1+Y^2}i(\tau_1)\Big)\\ &+\Big(\tfrac{1}{2}g_+(\tau_3)(1+h(\tau_2)) + f_-(\tau_3)f_-(\tau_2)\Big)\Big(\tfrac{-i}{\sqrt{2}}\tfrac{Y}{1+Y^2}f_-(\tau_1) + \tfrac{1}{2}\tfrac{Y^2}{1+Y^2}g_-(\tau_1)\Big),\end{aligned} \tag{B.20c}$$

with appropriately defined τ_i.

chapterEvaluation of the four-time correlation functions We start by rewriting the equations (B.20a), (B.20b), and (B.20c). First we define

$$\{\gamma_i\} = \left\{0, \tfrac{\gamma_{\rm in}}{2}, \tfrac{3\gamma_{\rm in}}{4} - \delta, \tfrac{3\gamma_{\rm in}}{4} + \delta\right\}, \tag{B.21}$$

then $f_-(t)$ (equation (B.10a)) can be written as

$$f_-(t) = \sum_{i=0}^{3} f_i e^{-\gamma_i t}, \tag{B.22}$$

where

$$\begin{aligned} f_0 &= -\tfrac{i}{\sqrt{2}}\tfrac{Y}{1+Y^2}, & f_1 &= 0, \\ f_2 &= -\tfrac{f_0}{2}\left(1 + \tfrac{\gamma_{\rm in}}{4\delta}(1-2Y^2)\right), & f_3 &= -\tfrac{f_0}{2}\left(1 - \tfrac{\gamma_{\rm in}}{4\delta}(1-2Y^2)\right). \end{aligned} \tag{B.23}$$

Note that $f_+(t)$ is never used. The other functions in (B.10b)–(B.10d) can be similarly decomposed, giving definitions for $g_{\pm i}$, h'_i, and i_i, where we define $h'(t) = 1 + h(t)$ noting that $h(t)$ only appears in that combination. We write the four time correlation functions as $\sum_{i,j,k} P^l_{ijk} e^{-\gamma_i \tau_1} e^{-\gamma_j \tau_2} e^{-\gamma_k \tau_3}$ with appropriately defined P^l_{ijk}, where $l = 1, 2, 3$ denotes the cases $1, 2, 3$.

The most general integral for $S_1(0, \tau, \tau, 0)$ is then

$$\begin{aligned} \gamma_A^4 \gamma_B^4 \int_0^t \int_0^{t+\tau} \int_0^{t+\tau} \int_0^t dt_1 dt_2 dt_3 dt_4 e^{(\gamma_B - \gamma_A)(t_1+t_2+t_3+t_4)} \\ \underbrace{\int_0^{t_1} \int_0^{t_2} \int_0^{t_3} \int_0^{t_4} dt'_1 dt'_2 dt'_3 dt'_4}_{t'_2 > t'_3 > t'_1 > t'_4} e^{\gamma_A (t'_1 + t'_2 + t'_3 + t'_4)} e^{-\gamma_k \tau_1} e^{-\gamma_j \tau_2} e^{-\gamma_i \tau_3}, \end{aligned} \tag{B.24}$$

where $\tau_1 = t'_1 - t'_4$, $\tau_2 = t'_3 - t'_1$, and $\tau_3 = t'_2 - t'_3$, as defined in Appendix B. The second line of (B.24) can be written as

$$\begin{aligned} \int_0^{m_{1234}} \int_0^{m_{123} - t'_4} \int_0^{m_{23} - (\tau_1 + t'_4)} \int_0^{t2 - (\tau_1 + \tau_2 + t'_4)} dt'_4 d\tau_1 d\tau_2 d\tau_3 \\ e^{\gamma_A (4t'_4 + 3\tau_1 + 2\tau_2 + \tau_3)} e^{-\gamma_k \tau_1} e^{-\gamma_j \tau_2} e^{-\gamma_i \tau_3}, \end{aligned} \tag{B.25}$$

where m_{23} denotes the smaller of t_2 and t_3 etc. So in the case $t_3 > t_4 > t_1 > t_2$, the integral of t'_4 goes from 0 to t_2, because t'_4 has to be the smallest of the four. The integral of t'_1, which is the next smallest, goes from t'_4 to t_2 (up to t_2 because t'_1 has

to be smaller than t_2' and t_3'); thus $\tau_1 = t_1' - t_4'$ goes from 0 to $t_2 - t_4'$. For t_3' the integral goes from t_1' to t_2 and so on. Evaluating (B.25) gives

$$\begin{aligned}
&\frac{1}{\gamma_A-\gamma_i}\Bigg[-\left(e^{m_{1234}(4\gamma_A)}-1\right)\frac{1}{4\gamma_A}\frac{1}{2\gamma_A-\gamma_j}\frac{1}{3\gamma_A-\gamma_k}\\
&\left(e^{m_{1234}(\gamma_A+\gamma_k)}-1\right)e^{m_{123}(3\gamma_A-\gamma_k)}\frac{1}{\gamma_A+\gamma_k}\frac{1}{3\gamma_A-\gamma_k}\frac{1}{2\gamma_A-\gamma_j}\\
&+\left(e^{m_{1234}(3\gamma_A+\gamma_i)}-1\right)e^{t_2(\gamma_A-\gamma_i)}\frac{1}{3\gamma_A+\gamma_i}\frac{1}{\gamma_A+\gamma_i-\gamma_j}\frac{1}{2\gamma_A+\gamma_i-\gamma_k}\\
&-\left(e^{m_{1234}(\gamma_A+\gamma_k)}-1\right)e^{m_{123}(2\gamma_A+\gamma_i-\gamma_k)}e^{t_2(\gamma_A-\gamma_i)}\frac{1}{\gamma_A+\gamma_k}\frac{1}{2\gamma_A+\gamma_i-\gamma_k}\frac{1}{\gamma_A+\gamma_i-\gamma_j}\\
&+\left(e^{m_{1234}(2\gamma_A+\gamma_j)}-1\right)e^{m_{23}(2\gamma_A-\gamma_j)}\frac{1}{2\gamma_A+\gamma_j}\frac{1}{2\gamma_A-\gamma_j}\frac{1}{\gamma_A+\gamma_j-\gamma_k}\\
&-\left(e^{m_{1234}(2\gamma_A+\gamma_j)}-1\right)e^{m_{23}(\gamma_A+\gamma_i-\gamma_j)}e^{t_2(\gamma_A-\gamma_i)}\frac{1}{2\gamma_A+\gamma_j}\frac{1}{2\gamma_A+\gamma_i-\gamma_j}\frac{1}{\gamma_A+\gamma_j-\gamma_k}\\
&-\left(e^{m_{1234}(\gamma_A+\gamma_k)}-1\right)e^{m_{123}(\gamma_A+\gamma_j-\gamma_k)}e^{m_{23}(2\gamma_A-\gamma_j)}\frac{1}{\gamma_A+\gamma_k}\frac{1}{\gamma_A+\gamma_j-\gamma_k}\frac{1}{2\gamma_A-\gamma_j}\\
&+\left(e^{m_{1234}(\gamma_A+\gamma_k)}-1\right)e^{m_{123}(\gamma_A+\gamma_j-\gamma_k)}e^{m_{23}(\gamma_A-\gamma_j+\gamma_i)}e^{t_2(\gamma_A-\gamma_i)}\frac{1}{\gamma_A+\gamma_k}\frac{1}{\gamma_A+\gamma_j-\gamma_k}\frac{1}{\gamma_A+\gamma_i-\gamma_j}\Bigg].
\end{aligned} \tag{B.26}$$

We rewrite this as

$$\sum_{\alpha,\beta,\rho,\pi} C^1_{(\alpha,\beta,\rho,\pi)} e^{\alpha m_{1234}} e^{\beta m_{123}} e^{\rho m_{23}} e^{\pi t_2}, \tag{B.27}$$

where α, β, ρ, π, and $C^1_{(\alpha,\beta,\rho,\pi)}$ are constants that depend on γ_A and γ_i. The superscript 1 denotes the case 1. The final integral we evaluate is then

$$\int_0^t \int_0^{t+\tau} \int_0^{t+\tau} \int_0^t dt_1 dt_2 dt_3 dt_4 e^{(\gamma_B-\gamma_A)(t_1+t_2+t_3+t_4)} e^{\alpha m_{1234}} e^{\beta m_{123}} e^{\rho m_{23}} e^{\pi t_2}. \tag{B.28}$$

For $S_2(0,\tau,\tau,0)$ ($S_3(0,\tau,\tau,0)$), $e^{\alpha m_{1234}} e^{\beta m_{123}} e^{\rho m_{23}} e^{\pi t_2}$ in the integrand is replaced by $e^{\alpha m_{1234}} e^{\beta m_{234}} e^{\rho m_{23}} e^{\pi t_2}$ ($e^{\alpha m_{1234}} e^{\beta m_{123}} e^{\rho m_{12}} e^{\pi t_2}$), which is equivalent to exchanging the variables $t_1 \leftrightarrow t_4$ ($t_1 \leftrightarrow t_3$). This means the integrals (B.28) for the three cases are related to each other by changes of integration limits. Hence we calculate the integral

$$\int_0^x \int_0^{x'} \int_0^{z'} \int_0^z dt_1 dt_2 dt_3 dt_4 e^{(\gamma_B-\gamma_A)(t_1+t_2+t_3+t_4)} e^{\alpha m_{1234}} e^{\beta m_{123}} e^{\rho m_{23}} e^{\pi t_2}. \tag{B.29}$$

This expression, viewed as a function of $x, x', z, z', \alpha, \beta, \rho$, and π, can be used to

evaluate all the different terms in (2.44). To evaluate this integral we break it into different regions again; for example

$$\underbrace{\int_0^x \int_0^{x'} \int_0^{z'} \int_0^{z} dt_1 dt_2 dt_3 dt_4}_{t_1<t_2<t_3<t_4} = \int_0^{m_{xx'z'z}} \int_{t_1}^{m_{x'z'z}} \int_{t_2}^{m_{z'z}} \int_{t_3}^{z} dt_1 dt_2 dt_3 dt_4,$$

$$= \int_0^t \int_{t_1}^t \int_{t_2}^{m_{z'z}} \int_{t_3}^{z} dt_1 dt_2 dt_3 dt_4, \tag{B.30}$$

where the second line follows because two of the integration limits have to be t. All of these integrations have similar forms so we define yet another function

$$W(y_1, y_2, y_3, y_4, m, z) = \lim_{t\to\infty} e^{-\gamma_B(4t+2\tau)} \int_0^t dt_1 e^{t_1(\gamma_B-\gamma_A+y_1)} \int_{t_1}^t dt_2 e^{t_2(\gamma_B-\gamma_A+y_2)} \int_{t_2}^m dt_3 e^{t_3(\gamma_B-\gamma_A+y_3)} \int_{t_3}^z dt_4 e^{t_4(\gamma_B-\gamma_A+y_4)}. \tag{B.31}$$

The parameters y_i, m, and z depend on the integration region; for example, if $t_2 < t_1 < t_3 < t_4$, then $y_1 = y_3 = y_4 = 0$, $y_2 = \alpha + \beta + \rho + \pi$, and $m = m_{z'z}$. z differs for different cases. Note that in (B.26) the terms containing $e^{m_{1234}}$ give $\alpha + \beta + \rho + \pi = 4\gamma_A$, whereas the terms multiplied by the -1s in the brackets give $\alpha + \beta + \rho + \pi \neq 4\gamma_A$. Only the former terms survive after taking the limit $t \to \infty$, because of the term $\exp(-\gamma_A(\tau_1 + \tau_2 + \tau_3 + \tau_4))$ in the integrand. With this, the integral can be evaluated as

$$\begin{aligned} W(y_1, y_2, y_3, y_4, m, z) = {} & \frac{1}{\gamma_B-\gamma_A+y_1} \frac{1}{2(\gamma_B-\gamma_A)+y_3+y_4} \frac{1}{\gamma_B-\gamma_A+y_4} \frac{1}{4\gamma_B} e^{-2\gamma_B\tau} \\ & - \frac{1}{\gamma_B-\gamma_A+y_1} \frac{1}{\gamma_B-\gamma_A+y_3} \frac{1}{\gamma_B-\gamma_A+y_4} \frac{1}{3\gamma_B+y_1+y_2+y_3} e^{-2\gamma_B\tau} e^{z_0(\gamma_B-\gamma_A+y_4)} \\ & - \frac{1}{\gamma_B-\gamma_A+y_1} \frac{1}{2(\gamma_B-\gamma_A)+y_3+y_4} \frac{1}{\gamma_B-\gamma_A+y_4} \frac{1}{2(\gamma_B-\gamma_A)+y_1+y_2} e^{-2\gamma_B\tau} e^{m_0(2(\gamma_B-\gamma_A)+y_3+y_4)} \\ & - \frac{1}{\gamma_B-\gamma_A+y_1} \frac{1}{\gamma_B-\gamma_A+y_3} \frac{1}{\gamma_B-\gamma_A+y_4} \frac{1}{2(\gamma_B-\gamma_A)+y_1+y_2} e^{-2\gamma_B\tau} e^{z_0(\gamma_B-\gamma_A+y_4)} e^{m_0(2(\gamma_B-\gamma_A)+y_3)}, \end{aligned} \tag{B.32}$$

where $m_0 = m - t$ and $z_0 = z - t$ take one of the two values 0 and τ. There are 4! versions of W needed for each case, corresponding to the 4! time orderings which gives different y_i. As an example we have tabulated 6 different sets of arguments for W in Table B.1, where we have assumed t_1 to be the smallest in the terms m_{1234} and m_{123} in (B.29).

y_1	y_2	y_3	y_4	m	z
$\alpha+\beta$	$\rho+\pi$	0	0	$m_{z'z}$	z
$\alpha+\beta$	$\rho+\pi$	0	0	$m_{z'z}$	z'
$\alpha+\beta$	ρ	π	0	$m_{x'z}$	z
$\alpha+\beta$	ρ	0	π	$m_{x'z}$	x'
$\alpha+\beta$	0	$\rho+\pi$	0	$m_{x'z'}$	z'
$\alpha+\beta$	0	ρ	π	$m_{x'z'}$	x'

Table B.1: Sets of arguments for W contributing to (B.29) when t_1 is the smallest.

For $i=1$ the first four terms in (2.44) can be written as

$$\begin{aligned} &2\left(S_1(0,\tau,\tau,0)+S_1(\tau,0,0,\tau)+S_1(\tau,0,\tau,0)\right.\\ &\left.+S_1(0,\tau,0,\tau)+S_1(\tau,\tau,0,0)+S_1(0,0,\tau,\tau)\right), \end{aligned} \tag{B.33}$$

after converting S_2 and S_3 into S_1 by changing the integration limits as explained above. Each of the S_1's can be evaluated by summing first over the W's with appropriate factors determined from (B.26), (B.27) and then summing over these again with the factors P^1_{ijk} multiplied. For each i,j,k then, there are $8*24$ calculations of the W's. A fortran code for computing this function follows in Appendix C.

Appendix C

Fortran code

Below is a fortran code that computes the input contribution to the intensity correlation function of the teleported resonance fluorescence field.

```
Calculates the normalized intensity correlation function for teleported field
of resonance fluorescence.
To compare with the formulae in Appendix B, note that
S_1 = SW, SW1-SW3 do NOT refer to S_1-S_3, but different groupings of S_1.
and P_{ijk}^1 + p_{ijk}^{1*} =  2*P(i)*hgf(k,j)+Q(i)*(gfi(k,j)+gfi2(k,j))
Also gamma = \gamma_{in}, G = \gamma_A, and Gp = \gamma_B.

integer i,j,k,l,tlength
real*8 longt,gamma,Y,Y1,tau,G,Gp,dtau,lambda,lp,lm,ip,im,i4,const
real*8 t,corrEc,norm1,constcorrEc,const1,intcor,kappa
complex*16 f0,f2,f3,delta,P(0:3),Gmin(0:3),Gplus(0:3),Gpplus(0:3)
complex*16 Q(0:3),gfi(0:3,0:3),gfi1(0:3,0:3),gfi2(0:3,0:3),flu
complex*16 hgf(0:3,0:3),hgf1(0:3,0:3),gd,P1(0:3),h2,h3,g2,g3,z
      complex*16 gam(0:3),Gpigj,Gmigk,Gmigj,GmjG,GmiGpk,Gmi2G,eye
complex*16 GpjG,Gmjgk,Gpk2G,SW1,SW2,SW3,W,ans,v,imcorrEc,original
!!!!!!!!!!!!!!!statement function flu!!!!!!!!!!!!!!!!!!!!!!
flu(v,G,Gp,t) = G**2*Gp*(exp(-Gp*t)*v/Gp/(Gp**2-G**2)/(Gp**2-v**2)
     *            + exp(-v*t)/(G**2-v**2)/(Gp**2-v**2)
     *            - exp(-G*t)*v/G/(Gp**2-G**2)/(G**2-v**2));
!!!!!!!!!!!!!!!!!!!!!!!!!!!!!!!!!!!!!!!!!!!!!!!!!!!!!!!!!!!!!!!!
      z=dcmplx(0,0) !complex zero
x=0.0d0       !real zero
tlength = 200
G  = 5.0d0                    ! Alice's bandwidth
Gp = 0.101d0                    ! Victor's bandwidth
      gamma = 0.01d0                ! atomic linewidth(fullwidth)
Y = dsqrt(dfloat(2))*3.0        !*0.01/gamma/500.0d0;
lambda = 0.9d0               ! squeezing parameter
kappa = 1.0d0                 ! squeezing bandwidth
lp = 1.0d0+lambda
lm = 1.0d0-lambda
      dtau = 10.0d0/tlength/gamma

tau = 0.0d0

definition of constants
      Y1 = Y**2/(1+Y**2)
if ((8*Y**2 - 1) > 0.0d0) then
      delta = dcmplx(0,gamma/4*dsqrt(8*Y**2-1))
else
delta = dcmplx(gamma/4*dsqrt(1-8*Y**2),0)
endif
      gd = gamma/(4*delta)
g2 = 0.5*(1+gamma/(4*delta))
```

```
      g3 = 0.5*(1-gamma/(4*delta))

      f0 = dcmplx(0,-1/dsqrt(dfloat(2))*Y/(1+Y**2))
      f2 = -f0*(g2-gd*Y**2)
      f3 = -f0*(g3+gd*Y**2)

h2 = -0.5*Y1*(1+3*gd)
h3 = -0.5*Y1*(1-3*gd)

      eye2 = -f0*(1+Y**2)*2*gd;

      gam(0) = 0.0d0
gam(1) = gamma/2
gam(2) = 3*gamma/4-delta
gam(3) = 3*gamma/4+delta

do j=0,3
  Gmin(j) = G - gam(j)
  Gplus(j) = G + gam(j)
  Gpplus(j) = Gp + gam(j)
enddo

!!!!!!!!!     P     !!!!!!!
      P(0) = -f0**2
P(1) = 0.25*Y1
P(2) = 0.25*f0**2*((1-Y**2)+gamma/(4*delta)*(1-5*Y**2))
P(3) = 0.25*f0**2*((1-Y**2)-gamma/(4*delta)*(1-5*Y**2))
!!!!!!!!!     P1    !!!!!!!
      P1 = -P
      P1(1) = 0.25*Y1


!!!!!!!!!    hgf    !!!!!!!!
hgf(0,0) = -f0**2
hgf(:,1) = 0.0d0
hgf(0,2) = -f0*f2
hgf(0,3) = -f0*f3
hgf(1,0) = 0.25*Y1
hgf(1,2) = h2/4
hgf(1,3) = h3/4
hgf(2,0) = Y1*g2/4 - f0*f2
hgf(2,2) = h2*g2/4 - f2**2
hgf(2,3) = g2*h3/4-f2*f3
hgf(3,0) = Y1*g3/4-f0*f3
hgf(3,2) = g3*h2/4-f2*f3
hgf(3,3) = g3*h3/4-f3**2
!!!!!!!!!!   hgf1   !!!!!!!!!
      hgf1 = -hgf
hgf1(1,:) = hgf(1,:)

!!!!!!!!!!  Q    !!!!!!!!!!
      Q(0) = 0.5*Y1;
      Q(1) = 0;
Q(2) = -Y1/4*((1+3*gd)-(1+Y**2)*2*gd);
Q(3) = -Y1/4*((1-3*gd)+(1+Y**2)*2*gd);

!!!!!!!!! gfi  !!!!!!!!!!!!
      gfi(:,0) = 0.0d0
gfi(0,1) = -f0**2*0.5
gfi(0,2) = -f0**2*0.5*g2
gfi(0,3) = -f0**2*0.5*g3
gfi(1,1) = 0.0d0
gfi(1,2) = 0.25*f0*eye2
gfi(1,3) = -0.25*f0*eye2
      gfi(2,1) = -f0*(f2*0.5)
gfi(2,2) = -f0*(f2*0.5*g2 - 0.25*g2*eye2)
gfi(2,3) = -f0*(f2*0.5*g3 + 0.25*g2*eye2)
gfi(3,1) = -f0*(f3*0.5)
gfi(3,2) = -f0*(f3*0.5*g2 - 0.25*g3*eye2)
```

```
gfi(3,3) = -f0*(f3*0.5*g3 + 0.25*g3*eye2)


!!!!!!!!   gfi1  !!!!!!!!!!!!
      gfi1 = gfi
      gfi1(1,:) = -gfi(1,:)

!!!!!!!!!  gfi2  !!!!!!!!!!!
gfi2 = gfi
gfi2(:,1) = - gfi(:,1)


!!!!!!!!!!!!!!!!!!!!!!!!!!end of defining constants!!!!!!!!!!!!!!!!!!!!!!!!!

!!!!!!!!!!!!!!!!!!!!!!!!!!start of calculation!!!!!!!!!!!!!!!!!!!!!!!!!!!!!
      open(1,file='corrfn.dat')
open(2,file='test.dat')

      do l = 0,tlength+1

!!!!!!!!!!!!!!!!intensity correlation function for the vacuum input!!!!!!!!!!!!
      ip =  0.5d0*kappa*lambda/lp*(exp(-Gp*tau)*kappa*lp
     */(Gp**2-(kappa*lp)**2)*(Gp**2 - 4*G**2)/(Gp**2-G**2)
     *   + exp(-kappa*lp*tau)*Gp/(Gp**2-(kappa*lp)**2)
     *   *((kappa*lp)**2 -4*G**2)/(G**2-(kappa*lp)**2)
     *   +exp(-G*tau)*G*Gp*kappa*lp/(Gp**2-G**2)/(G**2-(kappa*lp)**2)*3)

      im = 0.5d0*kappa*lambda/lm*(exp(-Gp*tau)*kappa*lm
     * /(Gp**2-(kappa*lm)**2)*(-Gp**2)/(Gp**2-G**2)
     *     + exp(-kappa*lm*tau)*Gp/(Gp**2-(kappa*lm)**2)
     *     *(-(kappa*lm)**2)/(G**2-(kappa*lm)**2)
     *     +exp(-G*tau)*G*Gp*kappa*lm/(Gp**2-G**2)/(G**2-(kappa*lm)**2))

      i4 = 0.5*G*Gp/(Gp**2-G**2)*(exp(-G*tau) - exp(-Gp*tau)*G/Gp)

if(Gp == kappa*lm)then
      im = 0.5d0*kappa*lambda/lm*(exp(-Gp*tau)/(Gp+kappa*lm)
     *  /(G**2-(kappa*lm)**2)/(Gp**2-G**2)
     *    *(-Gp*kappa*lm*(Gp*kappa*lm+G**2))
     *    +exp(-G*tau)*G*Gp*kappa*lm/(Gp**2-G**2)/(G**2-(kappa*lm)**2))
print *,im
endif

if(l == 0)then
 const = im+ip+i4
endif
!!!!!!!!!!!!!!!!!!!end of calculation for vacuum input!!!!!!!!!!!!!!!!!!!!!!

!!!!!!!!!!!!!!!!!!<E_{in}^\daggerE_{in}> part!!!!!!!!!!!!!!!!!!!!!!!!!!!!!!!!!!
      imcorrEc = gamma*Y1/(1+Y**2)/8*(2*flu(gamma/2,G,Gp,tau)
     * *(1+Y**2)     +4/Gp
     *        -(1-Y**2)*(flu(3*gamma/4-delta,G,Gp,tau)
     *                + flu(3*gamma/4+delta,G,Gp,tau))
     *        -(1-5*Y**2)*gd*(flu(3*gamma/4-delta,G,Gp,tau)
     *                     - flu(3*gamma/4+delta,G,Gp,tau)))
      corrEc = dreal(imcorrEc)
if(l == 0)then
 constcorrEc = corrEc
endif

!!!!!!!!!!!!end of calculation for <Ec^daggerEc> part!!!!!!!!!!!!!!!!!!!!!!!


!!!!!!!!!!!!!!!!!!original intensity correlation function!!!!!!!!!!!!!!!!!
      original = 1-0.5*exp(-gam(2)*tau)*(1+3*gd)
     *         -0.5*exp(-gam(3)*tau)*(1-3*gd)
!!!!!!!!!!!!!!!!!!!!!!!!!!!!!!!!!!!!!!!!!!!!!!!!!!!!!!!!!!!!!!!!!!!!!!!!!!!!
```

```
!!!!!!!!!contribution from the second order resonance fluorescence!!!!!!!!!
  ans = 0.0d0
  do k=0,3
          do i=0,3
      do j =0,3
        Gpigj = Gplus(i)+gam(j)
        Gmigk = Gmin(i)+gam(k)
        Gmigj = Gmin(i)+gam(j)
        GmjG = Gmin(j)+G
        GmiGpk = Gmin(i)+Gplus(k)
        Gmi2G  = Gmin(i)+2*G
GpjG = Gplus(j) + G
Gmjgk = Gmin(j)+gam(k)
        Gpk2G = Gplus(k) + 2*G
! this part calculates (0,tau,tau,0) and (tau,0,0,tau) contributions

 ans=ans+(2*P(i)*hgf(k,j)+Q(i)*(gfi(k,j)+gfi2(k,j)))/(Gmin(k))*(
     *SW1(Gplus(i),Gmigj,Gmjgk,Gmin(k),G,Gp,tau)/(Gplus(i)*Gmigj*Gmjgk)
     *  -SW1(Gplus(i),Gmigj,GmjG,z,G,Gp,tau)/(Gplus(i)*Gmigj*GmjG)
     *  -SW1(Gplus(i),GmiGpk,z,Gmin(k),G,Gp,tau)/(Gplus(i)*GmiGpk*Gmjgk)
     *  +SW1(Gplus(i),Gmi2G,z,z,G,Gp,tau)/(Gplus(i)*Gmi2G*GmjG)
     *  -SW1(GpjG,z,Gmjgk,Gmin(k),G,Gp,tau)/(GpjG*Gmigj*Gmjgk)
     *  +SW1(GpjG,z,GmjG,z,G,Gp,tau)/(GpjG*Gmigj*GmjG)
     *  +SW1(Gpk2G,z,z,Gmin(k),G,Gp,tau)/(Gpk2G*GmiGpk*Gmjgk)
     *  -SW1(dcmplx(4*G,0),z,z,z,G,Gp,tau)/(4*G*Gmi2G*GmjG))
!calculates (0,tau,0,tau) and (tau,0,tau,0)
     *  +(P(i)*hgf(k,j)+P1(i)*hgf1(k,j)+Q(i)*(gfi(k,j)+gfi1(k,j)))
     *   /(Gmin(k))*(
     * SW2(Gplus(i),Gmigj,Gmjgk,Gmin(k),G,Gp,tau)/(Gplus(i)*Gmigj*Gmjgk)
     *  -SW2(Gplus(i),Gmigj,GmjG,z,G,Gp,tau)/(Gplus(i)*Gmigj*GmjG)
     *  -SW2(Gplus(i),GmiGpk,z,Gmin(k),G,Gp,tau)/(Gplus(i)*GmiGpk*Gmjgk)
     *  +SW2(Gplus(i),Gmi2G,z,z,G,Gp,tau)/(Gplus(i)*Gmi2G*GmjG)
     *  -SW2(GpjG,z,Gmjgk,Gmin(k),G,Gp,tau)/(GpjG*Gmigj*Gmjgk)
     *  +SW2(GpjG,z,GmjG,z,G,Gp,tau)/(GpjG*Gmigj*GmjG)
     *  +SW2(Gpk2G,z,z,Gmin(k),G,Gp,tau)/(Gpk2G*GmiGpk*Gmjgk)
     *  -SW2(dcmplx(4*G,0),z,z,z,G,Gp,tau)/(4*G*Gmi2G*GmjG))
!calculates (0,0,tau,tau) and (tau,tau,0,0)
     *  +(P(i)*hgf(k,j)+P1(i)*hgf1(k,j)+Q(i)*(gfi1(k,j)+gfi2(k,j)))
     * /(Gmin(k))*(
     * SW3(Gplus(i),Gmigj,Gmjgk,Gmin(k),G,Gp,tau)/(Gplus(i)*Gmigj*Gmjgk)
     *  -SW3(Gplus(i),Gmigj,GmjG,z,G,Gp,tau)/(Gplus(i)*Gmigj*GmjG)
     *  -SW3(Gplus(i),GmiGpk,z,Gmin(k),G,Gp,tau)/(Gplus(i)*GmiGpk*Gmjgk)
     *  +SW3(Gplus(i),Gmi2G,z,z,G,Gp,tau)/(Gplus(i)*Gmi2G*GmjG)
     *  -SW3(GpjG,z,Gmjgk,Gmin(k),G,Gp,tau)/(GpjG*Gmigj*Gmjgk)
     *  +SW3(GpjG,z,GmjG,z,G,Gp,tau)/(GpjG*Gmigj*GmjG)
     *  +SW3(Gpk2G,z,z,Gmin(k),G,Gp,tau)/(Gpk2G*GmiGpk*Gmjgk)
     *  -SW3(dcmplx(4*G,0),z,z,z,G,Gp,tau)/(4*G*Gmi2G*GmjG))

  enddo
enddo
        enddo

!!!!!!!!!!!!normalizations!!!!!!!!!!!!!!!!
      norm1 = (const+constcorrEc)**2
const1 = const*(2*constcorrEc + const)
intcor = ((Ip + Im + I4)*(2*corrEc + (Ip+Im+I4))
     * + const1 + gamma**2*G**4*Gp**2*2*dreal(ans))/norm1;
write (2,200) gamma*tau,(Ip+Im+I4)**2/const**2 +1
write (1,300) gamma*tau,intcor,dreal(original)
      print 100,l
tau = tau + dtau
print *,intcor,dreal(original)
enddo
```

```
100   format($,I6)
200   format( 2g15.8)
300   format( 3g15.8)
      end



      Function SW1(a,b,r,p,G,Gp,tau)
      complex*16 a,b,r,p,SW1,z,ya,yb,yc,yd,W
real*8 G,Gp,tau,x,m0,z0

      W(ya,yb,yc,yd,m0,z0,G,Gp,tau) =
     *  exp(-2*Gp*tau)/(4*Gp*(Gp-G+yd)*(2*(Gp-G)+yc+yd)*(Gp-G+ya))
     *    -exp(z0*(Gp-G+yd)-2*Gp*tau)/((Gp-G+yd)*(Gp-G+yc)*(Gp-G+ya)
     * *(3*(Gp-G)+ya+yb+yc))
     *    +exp(m0*(Gp-G+yc)+z0*(Gp-G+yd)-2*Gp*tau)/((Gp-G+yd)*(Gp-G+yc)
     *     *(Gp-G+ya)*(2*(Gp-G)+ya+yb))
     *    -exp(m0*(2*(Gp-G)+yc+yd)-2*Gp*tau)/((2*(Gp-G)+yc+yd)
     *      *(Gp-G+yd)*(Gp-G+ya)*(2*(Gp-G)+ya+yb))
z = dcmplx(0,0)
x = 0.0d0

      !(0,tau,tau,0) + (tau,0,0,tau)
      SW1 =W(a+b,p+r,z,z,x,tau,G,Gp,tau) + W(a+b,p+r,z,z,x,x,G,Gp,tau)
     *   + W(a+b,z,p+r,z,tau,tau,G,Gp,tau)+W(a+b,r,p,z,x,x,G,Gp,tau)
     *   + W(a+b,r,z,p,x,tau,G,Gp,tau)+W(a+b,z,r,p,tau,tau,G,Gp,tau)
     * + W(a+b+p+r,z,z,z,x,x,G,Gp,tau)+W(a+b+p+r,z,z,z,x,tau,G,Gp,tau)
     * + W(a+b+p+r,z,z,z,x,x,G,Gp,tau)+W(a+b+p+r,z,z,z,x,x,G,Gp,tau)
     * + W(a+b+p+r,z,z,z,x,x,G,Gp,tau)+W(a+b+p+r,z,z,z,x,tau,G,Gp,tau)
     *   + W(a+b+r,p,z,z,x,x,G,Gp,tau) + W(a+b+r,p,z,z,x,x,G,Gp,tau)
     *   + W(a+b+r,z,p,z,x,x,G,Gp,tau) + W(a+b+r,z,p,z,x,x,G,Gp,tau)
     *   + W(a+b+r,z,z,p,x,tau,G,Gp,tau)+W(a+b+r,z,z,p,x,tau,G,Gp,tau)
     * + W(a,b,p+r,z,tau,tau,G,Gp,tau) + W(a,b,r,p,tau,tau,G,Gp,tau)
     * + W(a,b+p+r,z,z,x,tau,G,Gp,tau) + W(a,b+r+p,z,z,x,x,G,Gp,tau)
     * + W(a,b+r,p,z,x,x,G,Gp,tau) + W(a,b+r,z,p,x,tau,G,Gp,tau)

     *   + W(a+b,p+r,z,z,x,x,G,Gp,tau) + W(a+b,p+r,z,z,x,tau,G,Gp,tau)
     *   + W(a+b,z,p+r,z,x,x,G,Gp,tau) + W(a+b,r,p,z,x,tau,G,Gp,tau)
     *   + W(a+b,r,z,p,x,x,G,Gp,tau) + W(a+b,z,r,p,x,x,G,Gp,tau)
     * + W(a+b+p+r,z,z,z,x,tau,G,Gp,tau)+W(a+b+p+r,z,z,z,x,x,G,Gp,tau)
     * + W(a+b+p+r,z,z,z,tau,tau,G,Gp,tau)
     * + W(a+b+p+r,z,z,z,tau,tau,G,Gp,tau)
     * + W(a+b+p+r,z,z,z,x,tau,G,Gp,tau)+W(a+b+p+r,z,z,z,x,x,G,Gp,tau)
     *   + W(a+b+r,p,z,z,tau,tau,G,Gp,tau)
     *   + W(a+b+r,p,z,z,tau,tau,G,Gp,tau)
     *   + W(a+b+r,z,p,z,x,tau,G,Gp,tau)+W(a+b+r,z,p,z,x,tau,G,Gp,tau)
     *   + W(a+b+r,z,z,p,x,x,G,Gp,tau) + W(a+b+r,z,z,p,x,x,G,Gp,tau)
     * + W(a,b,p+r,z,x,x,G,Gp,tau) + W(a,b,r,p,x,x,G,Gp,tau)
     * + W(a,b+p+r,z,z,x,x,G,Gp,tau) + W(a,b+r+p,z,z,x,tau,G,Gp,tau)
     * + W(a,b+r,p,z,x,tau,G,Gp,tau) + W(a,b+r,z,p,x,x,G,Gp,tau)
return
end

Function SW2(a,b,r,p,G,Gp,tau)
      complex*16 a,b,r,p
real*8 G,Gp,tau
      complex*16 z,SW2,ya,yb,yc,yd,W
real*8 x

W(ya,yb,yc,yd,m0,z0,G,Gp,tau) =
     *  exp(-2*Gp*tau)/(4*Gp*(Gp-G+yd)*(2*(Gp-G)+yc+yd)*(Gp-G+ya))
     * -exp(z0*(Gp-G+yd)-2*Gp*tau)/((Gp-G+yd)*(Gp-G+yc)*(Gp-G+ya)
     * *(3*(Gp-G)+ya+yb+yc))
     * +exp(m0*(Gp-G+yc)+z0*(Gp-G+yd)-2*Gp*tau)/((Gp-G+yd)*(Gp-G+yc)
     *     *(Gp-G+ya)*(2*(Gp-G)+ya+yb))
     * -exp(m0*(2*(Gp-G)+yc+yd)-2*Gp*tau)/((2*(Gp-G)+yc+yd)
     *      *(Gp-G+yd)*(Gp-G+ya)*(2*(Gp-G)+ya+yb))

z = dcmplx(0,0)
```

```
x = 0.0d0
      !(0,tau,0,tau) + (tau,0,tau,0)
      SW2 =W(a+b,p+r,z,z,x,x,G,Gp,tau) + W(a+b,p+r,z,z,x,tau,G,Gp,tau)
     *   + W(a+b,z,p+r,z,x,x,G,Gp,tau) + W(a+b,r,p,z,tau,tau,G,Gp,tau)
     *   + W(a+b,r,z,p,tau,tau,G,Gp,tau) + W(a+b,z,r,p,x,tau,G,Gp,tau)
     * + W(a+b+p+r,z,z,z,x,tau,G,Gp,tau)+W(a+b+p+r,z,z,z,x,x,G,Gp,tau)
     * + W(a+b+p+r,z,z,z,x,tau,G,Gp,tau)+W(a+b+p+r,z,z,z,x,x,G,Gp,tau)
     * + W(a+b+p+r,z,z,z,x,x,G,Gp,tau) + W(a+b+p+r,z,z,z,x,x,G,Gp,tau)
     *   + W(a+b+r,p,z,z,x,tau,G,Gp,tau) + W(a+b+r,p,z,z,x,x,G,Gp,tau)
     *   + W(a+b+r,z,p,z,tau,tau,G,Gp,tau)+W(a+b+r,z,p,z,x,x,G,Gp,tau)
     *   + W(a+b+r,z,z,p,tau,tau,G,Gp,tau)+W(a+b+r,z,z,p,x,tau,G,Gp,tau)
     * + W(a,b,p+r,z,x,x,G,Gp,tau) + W(a,b,r,p,x,tau,G,Gp,tau)
     * + W(a,b+p+r,z,z,x,x,G,Gp,tau) + W(a,b+r+p,z,z,x,x,G,Gp,tau)
     * + W(a,b+r,p,z,x,x,G,Gp,tau) + W(a,b+r,z,p,x,tau,G,Gp,tau)

     *   + W(a+b,p+r,z,z,x,tau,G,Gp,tau) + W(a+b,p+r,z,z,x,x,G,Gp,tau)
     *   + W(a+b,z,p+r,z,x,tau,G,Gp,tau) + W(a+b,r,p,z,x,x,G,Gp,tau)
     *   + W(a+b,r,z,p,x,x,G,Gp,tau) + W(a+b,z,r,p,x,x,G,Gp,tau)
     * + W(a+b+p+r,z,z,z,x,x,G,Gp,tau)+W(a+b+p+r,z,z,z,x,tau,G,Gp,tau)
     * + W(a+b+p+r,z,z,z,x,x,G,Gp,tau)+W(a+b+p+r,z,z,z,x,tau,G,Gp,tau)
     * + W(a+b+p+r,z,z,z,tau,tau,G,Gp,tau)
     *  + W(a+b+p+r,z,z,z,tau,tau,G,Gp,tau)
     *   + W(a+b+r,p,z,z,x,x,G,Gp,tau) + W(a+b+r,p,z,z,x,tau,G,Gp,tau)
     *   + W(a+b+r,z,p,z,x,x,G,Gp,tau) + W(a+b+r,z,p,z,x,tau,G,Gp,tau)
     *   + W(a+b+r,z,z,p,x,x,G,Gp,tau) + W(a+b+r,z,z,p,x,x,G,Gp,tau)
     * + W(a,b,p+r,z,x,tau,G,Gp,tau) + W(a,b,r,p,x,x,G,Gp,tau)
     *+W(a,b+p+r,z,z,tau,tau,G,Gp,tau)+W(a,b+r+p,z,z,tau,tau,G,Gp,tau)
     * + W(a,b+r,p,z,x,tau,G,Gp,tau) + W(a,b+r,z,p,x,x,G,Gp,tau)
      return
end

Function SW3(a,b,r,p,G,Gp,tau)
      complex*16 a,b,r,p
real*8 G,Gp,tau
complex*16 z,SW3,ya,yb,yc,yd,W
real*8 x
W(ya,yb,yc,yd,m0,z0,G,Gp,tau) =
     *  exp(-2*Gp*tau)/(4*Gp*(Gp-G+yd)*(2*(Gp-G)+yc+yd)*(Gp-G+ya))
     * -exp(z0*(Gp-G+yd)-2*Gp*tau)/((Gp-G+yd)*(Gp-G+yc)*(Gp-G+ya)
     * *(3*(Gp-G)+ya+yb+yc))
     * +exp(m0*(Gp-G+yc)+z0*(Gp-G+yd)-2*Gp*tau)/((Gp-G+yd)*(Gp-G+yc)
     *     *(Gp-G+ya)*(2*(Gp-G)+ya+yb))
     * -exp(m0*(2*(Gp-G)+yc+yd)-2*Gp*tau)/((2*(Gp-G)+yc+yd)
     *      *(Gp-G+yd)*(Gp-G+ya)*(2*(Gp-G)+ya+yb))
z = dcmplx(0,0)
x = 0.0d0
      !  (0,0,tau,tau) + (tau,tau,0,0)
      SW3 =W(a+b,p+r,z,z,tau,tau,G,Gp,tau)
     *   + W(a+b,p+r,z,z,tau,tau,G,Gp,tau)
     *   + W(a+b,z,p+r,z,x,tau,G,Gp,tau) + W(a+b,r,p,z,x,tau,G,Gp,tau)
     *   + W(a+b,r,z,p,x,x,G,Gp,tau) + W(a+b,z,r,p,x,x,G,Gp,tau)
     * + W(a+b+p+r,z,z,z,tau,tau,G,Gp,tau)
     * + W(a+b+p+r,z,z,z,tau,tau,G,Gp,tau)
     * + W(a+b+p+r,z,z,z,x,tau,G,Gp,tau)+W(a+b+p+r,z,z,z,x,x,G,Gp,tau)
     * + W(a+b+p+r,z,z,z,x,x,G,Gp,tau)+W(a+b+p+r,z,z,z,x,tau,G,Gp,tau)
     *   + W(a+b+r,p,z,z,x,tau,G,Gp,tau) + W(a+b+r,p,z,z,x,x,G,Gp,tau)
     *   + W(a+b+r,z,p,z,x,tau,G,Gp,tau) + W(a+b+r,z,p,z,x,x,G,Gp,tau)
     *   + W(a+b+r,z,z,p,x,x,G,Gp,tau) + W(a+b+r,z,z,p,x,x,G,Gp,tau)
     * + W(a,b,p+r,z,x,tau,G,Gp,tau) + W(a,b,r,p,x,x,G,Gp,tau)
     * + W(a,b+p+r,z,z,x,tau,G,Gp,tau) + W(a,b+r+p,z,z,x,x,G,Gp,tau)
     * + W(a,b+r,p,z,x,x,G,Gp,tau) + W(a,b+r,z,p,x,x,G,Gp,tau)

     *   + W(a+b,p+r,z,z,x,x,G,Gp,tau) + W(a+b,p+r,z,z,x,x,G,Gp,tau)
     *   + W(a+b,z,p+r,z,x,x,G,Gp,tau) + W(a+b,r,p,z,x,x,G,Gp,tau)
     *   + W(a+b,r,z,p,x,tau,G,Gp,tau) + W(a+b,z,r,p,x,tau,G,Gp,tau)
     * + W(a+b+p+r,z,z,z,x,x,G,Gp,tau) + W(a+b+p+r,z,z,z,x,x,G,Gp,tau)
     * + W(a+b+p+r,z,z,z,x,x,G,Gp,tau)+W(a+b+p+r,z,z,z,x,tau,G,Gp,tau)
     * + W(a+b+p+r,z,z,z,x,tau,G,Gp,tau)+W(a+b+p+r,z,z,z,x,x,G,Gp,tau)
     *   + W(a+b+r,p,z,z,x,x,G,Gp,tau) + W(a+b+r,p,z,z,x,tau,G,Gp,tau)
```

```
     *    + W(a+b+r,z,p,z,x,x,G,Gp,tau)+W(a+b+r,z,p,z,tau,tau,G,Gp,tau)
     *   +W(a+b+r,z,z,p,x,tau,G,Gp,tau)+W(a+b+r,z,z,p,tau,tau,G,Gp,tau)
     * + W(a,b,p+r,z,x,x,G,Gp,tau) + W(a,b,r,p,x,tau,G,Gp,tau)
     * + W(a,b+p+r,z,z,x,x,G,Gp,tau)+W(a,b+r+p,z,z,x,tau,G,Gp,tau)
     * + W(a,b+r,p,z,tau,tau,G,Gp,tau)
     * + W(a,b+r,z,p,tau,tau,G,Gp,tau)
      return
end
```

Bibliography

[1] A. Furusawa, J. L. Sorensen, S. L. Braunstein, C. A. Fuchs, H. J. Kimble, and E. S. Polzik, "Unconditional quantum teleportation" Science **282**, 706 (1998).

[2] John. S. Bell, *Speakable and unspeakable in quantum mechanics* (Cambridge university press, 1987).

[3] A. Aspect, J. Dalibard, and G. Roger, "Experimental test of Bell's inequalities using time-varying analyzers" Phys. Rev. Lett. **49**, 1804 (1982).

[4] G. Weihs, T. Jennewein, C. Simon, H. Weinfurter, and A. Zeilinger, "Violation of Bell's inequality under strict Einstein locality conditions" Phys. Rev. Lett. **81**, 5039 (1998).

[5] C. H. Bennett, G. Brassard, C. Crepeau, R. Jozsa, A. Peres, and W. K. Wootters, "Teleporting an Unknown Quantum State via Dual Classical and Einstein-Podolsky-Rosen Channels" Phys. Rev. Lett. **70**, 1895 (1993).

[6] L. Vaidman, "Teleportation of quantum states" Phy. Rev. A **49**, 1473 (1994).

[7] S. L. Braunstein and H. J. Kimble, "Teleportation of Continuous Quantum Variables" Phys. Rev. Lett. **80**, 869 (1998).

[8] D. Bouwmeester, J. Pan, K. Mattle, M. Eibl, H. Weinfurter, and A. Zeilinger, "Experimental quantum teleportation" Nature **390**, 575 (1997).

[9] W. P. Bowen, N. Treps, B. C. Buchler, R. Schnabel, T. C. Ralph, H. Bachor, T. Symul, and P. K. Lam, "Experimental investigation of continuous-variable quantum teleportation" Phys. Rev. A **67**, 032302 (2003).

[10] H. J. Carmichael, *Statistical Methods in Quantum Optics*, Vol. 1, 2nd ed. (Springer, 2002).

[11] Marlan O. Scully and M. Suhail Zubairy, *Quantum Optics* (Cambridge university press, 1997).

[12] D. F. Walls and G. J. Milburn, *Quantum Optics* (Springer-Verlag, 1994).

[13] H. J. Carmichael, *An Open Systems Approach to Quantum Optics* (Springer, 1993).

[14] J. Dalibard, Y. Castin, and K. Mølmer, "Wave-Function Approach to Dissipative Processes in Quantum Optics" Phys. Rev. Lett. **68**, 580 (1992).

[15] R. Dum, P. Zoller, and H. Ritsch, "Monte Carlo simulation of the atomic master equation for spontaneous emission" Phys. Rev. A **45**, 4879 (1992).

[16] R. Dum, A. S. Parkins, P. Zoller, and C. W. Gardiner, "Monte Carlo simulation of master equations in quantum optics for vacuum, thermal, and squezed reservoirs" Phys. Rev. A **46**, 4382 (1992).

[17] H. J. Carmichael, *Statistical Methods in Quantum Optics*, Vol. 2 (Springer, 2008).

[18] A. Einstien, B. Podolsky, and N. Rosen, "Can Quantum-Mechanical Description of Physical Reality Be Considered Complete?" Phys. Rev. **47**, 777 (1935).

[19] A. J. Ekert, "Quantum Cryptography Based on Bell's Theorem" Phys. Rev. Lett. **67**, 661 (1991).

[20] C. H. Bennett and S. J. Wiesner, "Communication via One- and Two-Particle Operators on Einstein-Podolsky-Rosen States" **69**, 2881 (1992).

[21] P. W. Shor, "Algorithm for quantum computation: discrete logarithms and factoring" in *Proceedings,* 35^{th} *Annual Symposium on Foundations of Computer Science* (IEEE Press, Los Alamitos, CA, 1994).

[22] A. J. Ekert, "Quantum Mechanics Helps in Searching for a Needle in a Haystack" Phys. Rev. Lett. **79**, 325 (1997).

[23] H. Nha and H. J. Carmichael, "Entanglement within the Quantum Trajectory Description of Open Quantum Systems" Phys. Rev. Lett. **93**, 120408 (2004).

[24] P. van Loock, Samuel L. Braunstein, and H. J. Kimble, "Broadband teleportation" Phys. Rev. A **62**, 022309 (2000).

[25] H. Yonezawa, S. L. Braunstein, and A. Furusawa, "Entanglement Demonstration of Quantum Teleportation of Broadband Squeezing" Phys. Rev. Lett. **99**, 110503 (2007).

[26] C Noh, A. Chia, H. Nha, M. J. Collett, and H. J. Carmichael, "Quantum Teleportation of the Temporal Fluctuations of Light" Phys. Rev. Lett. **102**, 230501 (2009).

[27] G. Lindblad, "On the Generators of Quantum Dynamical Semigroups" Commun. Math. Phys. **48**, 119 (1976).

[28] H. J. Carmichael, "Continuous Variable Teleportation of Quantum Fields" in C. Soo and W. Zhang, eds. *Proceedings of the 1st Asia-pacific Conference Quantum Information Science*, pages pp11–25 (World Scientific, 2004).

[29] T. W. Marshall, "Random Electrodynamics" Proc. R. Soc. London **276**, 475 (1963).

[30] E. P. Wigner, "On the Quantum Correction for Thermodynamic Equilibrium" Phys. Rev. **40**, 746 (1932).

[31] H. J. Carmichael and H. Nha, "Continuous variable teleportation within stochastic electrodynamics" in P. Hannaford, A. Sidorov, H. Bachor, and K. Baldwin, eds. *Proceedings of the XVI international conference laser spectroscopy*, pages 324–333 (World Scientific, 2003).

[32] Andy Chia, "A Stochastic Electrodynamics Description of Quantum Teleportation with Continuous Variables," Master's Thesis (University of Auckland, April 2005).

[33] C. W. Gardiner, *Handbook of Stochastic Methods*, 3rd ed. (Springer, 2003).

[34] T. C. Ralph, "All-optical quantum teleportation" Opt. Lett. **24**, 348 (1999).

[35] T. C. Ralph, "Interferometric tests of teleportation" Phys. Rev. A **65**, 012319 (2001).

[36] C. W. Gardiner, "Inhibition of Atomic Phase Decays by Squeezed Light: A Direct Effect of Squeezing" Phys. Rev. Lett. **56**, 1917 (1986).

[37] M. Dagenais and L. Mandel, "Investigation of two-time correlations in photon emissions from a single atom" Phys. Rev. A **18**, 2217 (1978).

[38] R. Short and L. Mandel, "Observation of Sub-Poissonian Photon Statistics" Phys. Rev. Lett. **51**, 384 (1983).

[39] J. Gea-Banacloche, "Some implications of the quantum nature of laser fields for quantum computations" Phys. Rev. A **65**, 022308 (2002).

[40] S. J. van Enk and H. J. Kimble, "On the classical character of control fields in quantum information processing" Quantum Inf. Comput. **2**, 1 (2002).

[41] W. M. Itano, "Comment on "Some implications of the quantum nature of laser fields for quantum computations"" Phys. Rev. A **68**, 046301 (2003).

[42] S. J. van Enk and H. J. Kimble, "Reply I to "Comment on 'Some implications of the quantum nature of laser fields for quantum computations' "" Phys. Rev. A **68**, 046302 (2003).

[43] Julio Gea-Banacloche, "Reply II to "Comment on 'Some implications of the quantum nature of laser fields for quantum computations' "" Phys. Rev. A **68**, 046303 (2003).

[44] A. Silberfarb and I. H. Deutsch, "Continuous measurement with traveling-wave probes" Phys. Rev. A **68**, 013817 (2003).

[45] H. Nha and H. J. Carmichael, "Decoherence of a two-state atom driven by coherent light" Phys. Rev. A **71**, 013805 (2005).

[46] H. J. Carmichael, "Quantum Trajectory Theory for Cascaded Open Systems" Phys. Rev. Lett. **70**, 2273 (1993).

[47] C. W. Gardiner, "Driving a quantum system with the output field from another driven quantum system" Phys. Rev. Lett. **70**, 2269 (1993).

[48] K. Mølmer, "Optical coherence: A convenient fiction" Phy. Rev. A **55**, 3195 (1997).

[49] M. Scully and W. E. Lamb, "Quantum Theory of an Optical Maser. I. General Theory" Phys. Rev. **159**, 208 (1967).

[50] M. Lax, "Quantum Noise.X.Density-Matrix Treatment of Field and Population-Difference Fluctuations" Phys. Rev. **157**, 213 (1967).

[51] R. Graham and H. Haken, "Laserlight– First Example of a Second-Order Phase Transition Far Away from Thermal Equilibrium" Z. Phys. **237**, 31 (1970).

[52] T. Rudolph and B. C. Sanders, "Requirement of Optical Coherence for Continuous-Variable Quantum Teleportation" Phy. Rev. Lett. **87**, 077903 (2001).

[53] S. J. van Enk and C. A. Fuchs, "Quantum State of an Ideal Propagating Laser Field" Phy. Rev. Lett. **88**, 027902 (2002).

[54] H. M. Wiseman, "Optical coherence and teleportation: Why a laser is a clock, not a quantum channel." arXiv:quant-ph/0303116v1 (2003).

[55] S. D. Bartlett, T. Rudolph, and R. W. Spekkens, "Dialogue Concerning Two Views on Quantum Coherence: Factist and Fictionist" arXiv:quant-ph/0507214v2 (2005).

[56] C. Noh and H. J. Carmichael, "Disentanglement of Source and Target and the Laser Quantum State" Phy. Rev. Lett. **100**, 120405 (2008).

[57] J. Gea-Banacloche, "Collapse and Recreation of the State Vector in Quantum Mechanics" in A. O. Barut, ed. *New Frontiers in Quantum Electrodynamics and Quantum Optics*, pages 531–540 (Plenum, New York, 1990).

[58] J. Gea-Banacloche, "Emergence of Classical Radiation Fields through Decoherence in the Scully-Lamb Laser Model" Found. Phys. **28**, 531 (1998).

[59] R. B. Griffiths, "Consistent Interpretation of Quantum Mechanics Using Quantum Trajectories" Phys. Rev. Lett. **70**, 2201 (1993).

[60] P. R. Rice and H. J. Carmichael, "Photon statistics of a cavity-QED laser: A comment on the laser-phase-transition analogy" Phys. Rev. A **50**, 4318 (1994).

[61] S. J. van Enk, "Atoms, dipole waves, and strongly focused light beams" Phys. Rev. A **69**, 043813 (2004).

[62] H. J. Carmichael and C. Noh, "Open systementanglement and the laser quantum state" Physica E (2009), doi:10.1016/j.physe.2009.06.019 (2009).

[63] A. L. Schawlow and C. H. Townes, "Infrared and Optical Masers" Phys. Rev. **112**, 1940 (1958).

[64] C. H. Bennett, "Mixed-state entanglement and quantum error correction" Physics Today **48**, 24 (1995).

[65] C. H. Bennett, "Quantum Information" Physica Scripta **T76**, 210 (1998).

[66] C. H. Bennett, H. J. Bernstein, S. Popescu, and B. Schumacher, "Concentrating partial entanglement by local operations" Phys. Rev. A **53**, 2046 (1996).

[67] M. B. Plenio and S. Virmani, "An introduction to entanglement measures." arXiv:quant-ph/0504163v3 (2006).

[68] C. H. Bennett, D. P. DiVincenzo, J. A. Smolin, and W. K. Wootters, "Mixed-state entanglement and quantum error correction" Phys. Rev. A **54**, 3824 (1996).

[69] V. Vedral, M. B. Plenio, M. A. Rippin, and P. L. Knight, "Quantifying Entanglement" Phys. Rev. Lett. **78**, 2275 (1997).

[70] S. Hill and W. K. Wootters, "Entanglement of a Pair of Quantum Bits" Phys. Rev. Lett. **78**, 5022 (1997).

[71] W. K. Wootters, "Entanglement of Formation of an Arbitrary State of Two Qubits" Phys. Rev. Lett. **80**, 2245 (1998).

[72] A. Miranowicz and S. Ishizaka, "Closed formula for the relative entropy of entanglement" Phys. Rev. A **78**, 032310 (2008).

[73] M. Gu, A. S. Parkins, and H. J. Carmichael, "Entangled-state cycles from conditional quantum evolution" Phys. Rev. A **73**, 043813 (2006).

[74] A. Chia and A. S. Parkins, "Entangled-state cycles of atomic collective-spin states" Phys. Rev. A **77**, 033810 (2008).

[75] J. I. Cirac, P. Zoller, H. J. Kimble, and H. Mabuchi, "Quantum State Transfer and Entanglement Distribution among Distant Nodes in a Quantum Network" Phys. Rev. Lett. **78**, 3221 (1997).

[76] A. S. Parkins and H. J. Kimble, "Quantum State Transfer between motion and light" J. Opt. B **1**, 496 (1999).

[77] C. M. Caves, "Quantum limits on noise in linear amplifiers" Phys. Rev. D **26**, 1817 (1982).

[78] M. Lax, "Formal Theory of Quantum Fluctuations from a Driven State" Phys. Rev. **129**, 2342 (1963).